

2937

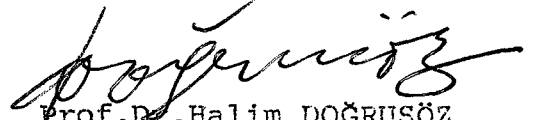
BEARING CAPACITY ANALYSIS OF LAYERED
ROCK FOR AN UNDERGROUND MINE

A MASTER'S THESIS
in
Mining Engineering
Middle East Technical University

By
Mehmet Kemal GÖKAY
February, 1988

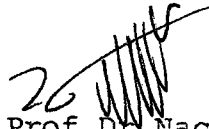
T. C.
Yükseköğretim Kurulu
Dokümantasyon Merkezi

Approval of the Graduate School of Natural and Applied
Sciences

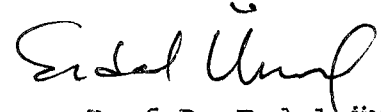

Prof. Dr. Halim DOĞRUSÖZ

Director

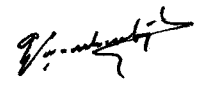
I certify that this thesis satisfies all the requirements
as a thesis for the degree of Master of Science in Mining
Engineering



Assoc. Prof. Dr. Naci BÖLÜKBAŞI
Chairman of the Department


We certify that we have read this thesis and that in our
opinion it is fully adequate in scope and quality, as a
thesis for the degree of Master of Science in Mining
Engineering



Assoc. Prof. Dr. Erdal ÜNAL
Supervisor


Examining Committee in Charge

Assoc. Prof. Dr. A. Günhan PAŞAMEHMETOĞLU (Chairman) 

Assoc. Prof. Dr. Erdal ÜNAL 

Assoc. Prof. Dr. Levent TUTLUOĞLU 

Assoc. Prof. Dr. Seyfi KULAKSIZ 

Dr. Gürel ŞENYUR 

ABSTRACT

BEARING CAPACITY ANALYSIS OF LAYERED ROCK FOR AN UNDERGROUND MINE

GÖKAY, Mehmet Kemal

M.S. in Mining Eng.

Supervisor : Assoc. Prof.. Dr. Erdal Ünal

February 1988, 135 pages

A series of plate bearing tests was carried out on sedimentary rock units in an underground borax mine. Square section loading plates with different sizes were used in order to investigate the size effect on the plate bearing capacity. Major rock types tested in the field included ulexite, colemanite, and a bedded and laminated limestone with claystone. It was observed that this limestone showed large variations for bearing capacity depending upon the spacing of bedding and laminations. Based on the field results, alternative designs for base plates of individual hydraulic props to be used in the mine were suggested.

In order to estimate in-situ bearing capacity values from laboratory test results empirical approaches suggested in Foundation Engineering and Soil Mechanics were used. It was found however that these values were higher than in-situ measured values. When proper rock failure criteria, especially Hoek & Brown's empirical failure criterion were

used with corrected strength parameters for in-situ condition, better estimates of field bearing capacity were obtained.

A theoretical analysis was conducted in order to investigate the effect of discontinuity properties, i.e. normal and shear stiffnesses and the spacing on the initiation of bearing capacity failures. Stress distribution in a bedded or cross-anisotropic rock under plate loading was studied. A failure analysis based on the Mohr-Coulomb failure criterion was conducted to estimate the reductions in the bearing capacity with spacing and stiffness parameters of the beds.

Key words : bearing capacity, laminated rock, size effect,

ÖZET

YERALTI OCAGINDA TABAKALI KAYALARIN TAŞIMA KAPASİTELERİNİN ANALİZİ

GÖKAY, Mehmet Kemal

Yüksek Lisans Tezi, Maden Müh. Bölümü

Tez Yöneticisi: Doc.Dr. Erdal Ünal

Şubat 1988, 135 sahife

Simav yeraltı boraks madeninde bulunan sedimenter kayalarda birçok plaka-yükleme deneyi yapılmıştır. Taşıma kapasitesinde ki boyut etkisini bulmak için değişik boyuttaki kare kesitli plakalar kullanılmıştır. Arazi çalışmalarında, üzerinde deney yapılan önemli kayaçların; üleksit, kolemanit ve kiltası laminalı kireçtaşı olduğu gözlenmiş ayrıca kiltası laminalı kireçtaşının taşıma kapasitesinin lamina kalınlığına göre büyük farklılıklar gösterdiği görülmüştür. Arazi çalışmaları sonucu elde edilen bilgilerden yola çıkarak yeraltı ocağında kullanılacak bireysel hidrolik direk altlıkları, değişik tabakalar için alternatif tasarımlar şeklinde verilmiştir.

Labaratuvar deney sonuçlarını kullanarak arazi taşıma kapasitesine, zemin mekanigi formülleri kullanılarak ulaşılmaya çalışılmış fakat hasaplar sonucu elde edilen değerlerin ölçülen arazi taşıma değerlerinden yüksek olduğu görülmüştür. Bununla birlikte özellikle Hoek & Brown'nun empirik yenilme kriteri, kayaçların düzenlenmiş mekanik

degerleri kullanıldığında, arazi taşıma kapasitelerine yakın sonuçlar verdiği gözlenmiştir.

Süreksizlik özelliklerinin yük plakası altındaki kayaç yenilmesine etkisi teorik olarak analiz edilmiş, tabakalı ve kross-anizotropik kayaçlarda; yükleme plakası altında oluşan gerilme-deformasyon dağılımları incelenmiştir. Yenilme analizlerinde Mohr-Coulomb yenilme kriteri kullanılarak, süreksizlikler arası uzaklığın ve süreksizlik pekliginin taşıma kapasitesine etkisi analiz edilmiştir.

Anahtar kelimeler : taşıma kapasitesi, laminalı kayaç, boyut etkisi.

ACKNOWLEDGEMENTS

The author would like to express his gratitude to Assoc. Prof. Dr. Levent Tutluođlu and Assoc. Prof. Dr. Erdal Ünal for their kind supervision, valuable suggestions and discussions throuhout this research.

The author would also like to express his sincere appreciation to Assoc. Prof. Dr. A. Günhan Pasamehmetođlu for his suggestions and discussions on the thesis.

Thanks are also due to many others who helped in various ways.

TABLE OF CONTENTS

	<u>Pages</u>
ABSTRACT	iii
ÖZET	iv
ACKNOWLEDGEMENTS	vii
LIST OF TABLES	xi
LIST OF FIGURES	xiii
LIST OF SYMBOLS	xv
1. INTRODUCTION	1
1.1. Introduction	1
1.2. Background	2
1.2.1. General Review of Literature	2
1.2.2. Theoretical Approaches of Foundation Engineering	4
1.2.3. Rock Failure Criteria and Bearing Capacity Analysis	11
1.3. Factor Controlling the Bearing Capacity	16
2. GENERAL DESCRIPTION OF THE TEST SITE	17
2.1. Mine Location	17
2.2. Geology	17
2.2.1. Geology of Bigadic Borax Basin	17
2.2.2. Regional Tectonic	19
2.2.3. Description of Seam	19
2.3. Mining Method	23
2.4. Laboratory and Site Investigation	25
2.4.1. Sampling	25
2.4.2. General Description of Samples and Rock Types Rock Types	25

TABLE OF CONTENTS (Cont'd)

	<u>Pages</u>
2.4.3. Results of Laboratory Tests	27
2.5. Classification of rocks around the seams . . .	29
3. EXPERIMENTAL WORK	36
3.1. Test Location	36
3.2. Test Set-up	37
3.3. Measuring System	37
3.3.1. Load Measurements	37
3.3.2. Displacement Measurements	38
3.4. Test Procedure	38
3.4.1. Preparation of Test Place	38
3.4.2. Instalation of Test Frame	39
3.4.3. Testing	40
4. RESULTS OF PLATE LOADING TESTS	47
4.1. Introduction	47
4.2. Test Results	48
4.2.1. Clay Banded Limestone Under Seam 2	49
4.2.2. Clay Banded Limestone Under Seam 4	53
4.2.3. Colemanite	53
4.2.4. Ulexite	55
4.3. Variation of Bearing Capacity With Plate Size .	56
4.4. Failure Mechanisms Observed in the Tests . . .	58
4.5. Comparison of Results With Theoretical Estimation of Bearing Capacity	68
4.6. Comparison of Field Results With Theoretical Estimations	73

TABLE OF CONTENTS (Cont'd)

	<u>Pages</u>
5. FLOOR PENETRATION OF HYDRAULIC PROPS	78
5.1. Design of Base Plate With Respect to the Penetration Load	78
5.1.1. Failure Loads For Clay Banded Limestone . . .	79
5.1.2. Failure Loads For Colemanite	81
5.1.3. Failure Loads For Ulexite	83
5.1.4. Suggested Base Plate Design For Hydraulic Props	85
5.1.5. Alternative Precautions For Exceptionally Weak Floors	89
6. ANALYSIS OF STRESSES AND FAILURE FOR LAYERED ROCK UNDER THE LOADING PLATE	92
6.1. Introduction	92
6.2. General Approach and Assumptions	92
6.3. Solution Technigue and Input Parameters	97
6.4. Results of Stress Analysis	99
6.4.1. General Interpretation of Results	99
6.4.2. Discussion of Results of Stress Analysis . . .	101
6.5. Failure Analysis	104
6.5.1. Failure Analysis For Isotropic Rock Under a Circular Loading Area	117
6.5.2. Failure Analysis For Cross-Anisotropic Rock Under a Circular Loading Area	119
6.6. Effect of Spacing on Critical Depth	122
7. CONCLUSIONS	126
REFERENCES	128
APPENDIXES	130

LIST OF TABLES

<u>Table</u>	<u>Pages</u>
1. Bearing Capacity Factors	9
2. Thickness of Seams and Inter-seam Strata in Simav Underground Mine	21
3. Density & Porosity Test Results	30
4. Uniaxial Compressive Strength Test Results	30
5. Indirect (Brazilian) Tensile Strength Test Results.	31
6. Laboratory Deformability Test Results	31
7. Triaxial Test Results	32
8. Shear Strength Test Results	32
9. Slake Durability Index Test Results	33
10. Clay Analysis Results	33
11. RMR and Q Values Around the Seams Determined From Rock Mass Classification Systems.	34
12 _a . Rock Mass Class of RMR System	35
12 _b . Rock Mass Class of Q System	35
13. Plate Loading Test Results For Clay Banded Limest.	50
14. " " " " " Colemanite	51
15. " " " " " Ulexite	52
16 _a . Bearing Capacity Coefficients as Determined by Various Investigators	70
16 _b . Bearing Capacity Coefficients, Determined at Simav Mine	70
17 _a . Coefficients of Bearing Capacity With Respect to Base Area by Using Linear Regression.	71

LIST OF TABLES (Cont'd)

<u>Tables</u>	<u>Pages</u>
17 _b . Coefficients of Bearing Capacity With Respect to Base Area by Using Power Regression.	71
18. Coefficients of Bearing Capacity With Respect to Base Periphery/ Base Area	72
19. Calculated Bearing Capacity Values by Using Analytical Approaches of Foundation Engineering . .	76
20. Calculated Bearing Capacity Values by Using Mohr- Coulomb and Hoek-Brown Failure Criteria	77
21. Penetration loads For Clay Banded Limestone	82
22. " " " Colemanite	82
23. " " " Ulexite	84
24. Summary of Existing Solutions	94
25. Input Parameters of Computer Programs	102

LIST OF FIGURES

<u>Figures</u>	<u>Pages</u>
1. Failure Zones Under Shallow Footing	6
2. Zones Underneath the Loading Plate	12
3. A General Section Through out the Seams of Simav Mine	22
4. Layout of Representative longwall Panel in Simav Mine	24
5. Plate Loading test Set-up and it's Position in an Inclined Longwall Mine	41
5. Picture of Main Rock Types at Simav Mine	27
6. Plate Loading Test Set-up for Testing the Roof Strata	42
7. Picture of Test Set-up Showing Optical Displacement Measuring System	43
8. Picture of Test Set-up Showing Optical and Mechanical Displace. Measuring System	44
9. Typical Floor Strata Under Seam 4	54
10. Variation of Bearing Capacity With Plate Size for Clay Banded Limestone	59
11. Variation of Bearing Capacity With Plate Size for Colemanite	60
12. Variation of Bearing Capacity With Plate Size for Ulexite	61
13. Typical Load- Displacement Curves for Plate Loading of Clay Banded Limestone	63
14. Typical Load -Disp. Curves of Ulexite	64

LIST OF FIGURES (Cont'd)

<u>Figures</u>	<u>Pages</u>
15 _a . Failure Modes of Clay Banded Limestone Under Seam 4 . . .	65
15 _b . " " " " " " " " . . .	66
16. " " " " " " " Seam 2 . . .	67
17. Punching Failure Mode for Ulexite and Colemanite . . .	67
18. Typical Suggested Base plates and Their Weight . . .	87
19. Penetration and Failure Mode Under Hydraulic Props With the Special Expanding Cross-Section Base plates	88
20. U-Shaped Steel Bar Plate	91
21. Representation of Layered Rock as Homogeneous Equivalent Rock Mass	100
22. Presentation of Input Parameters for Computer Prog.	100
23. Tangential Stress Distribution at the Edge of the Loading Plate Along Radial Distance	105
24. Radial Stress Distribution on Surface Along the Radial Distance	107
25. Vertical Displacement Variation at the Surface Along the Radial Distance	109
26. Radial Displ. Variation at the Surface Along the Radial Distance.	111
27. Vertical Stress Distribution Underneath the plate Along r=0 Line	113
28. Radial Stress Distr. Beneath the Center of Plate	115
29. Effect of Spacing, Plate size, k_s/k_n Ratios on Z_{cr}	124
30. " " " " " " " P/Co.	125

LIST OF SYMBOLS

- γ : Unit Weight
- ϕ : Internal Friction Angle (deg)
- q_u : Ultimate Bearing Capacity (Foundation Engineering Cons.)
- C : Material Cohesion
- N_c, N_q, N_γ : Dimensionless Bearing Capacity Factors
- D : Embedment thickness, Depth
- τ_f : Shear Stress on Failure Plane
- σ_f : Normal Stress " " "
- B : Width of Plate, or Footing
- L : Length of Plate, or Footing
- σ_1 : Major Principle Stress
- σ_3 : Minor " "
- C_o : Uniaxial Compressive Strength
- m, s : Rock Constants
- P_b : Bearing Capacity
- k, m, n, K : Constants for size effect relations
- P_{max} : Max. Load on Plate

1. INTRODUCTION

1.1. General

After the development of self advancing hydraulic supports or chocks, having design load capacities of up to 600-1000 tons, there is a great need for engineering information that will help the operator to select his longwall support equipment for their effectiveness. All systems of face support depend upon the stability of the floors on which they are erected. Loss of control of the roof may immediately follow the failure of the floor, and if productivity is to increase, sufficient information about the nature and behaviour of the floor must be acquired to permit the design of support system which will at least effectively minimize the possibility of the floor fracturing and failure, after underground support installation. If the mine roof and floor strata are weak in bearing strength large bearing pressures can cause the supports to penetrate into the strata and cause operational difficulties.

Bearing capacity of roof and floor can be determined by the bearing capacity tests. Especially plate loading test is a rapid and less expensive means for assessing the bearing capacity as well as the rock mass deformability of the mine roof and floor strata.

As a result of plate loading tests, base plates for hydraulic props can be designed properly to prevent failure of the floor at the load levels applied by these props. Also, by averaging the displacement measurements over the loaded area, and recording the load levels with the

corresponding average displacements during a test, it is possible to obtain a measure of deformability of the roof and floor strata.

1.2. Background

1.2.1. General Review of Literature

The floor is commonly the weakest member in the structural system of a longwall mine, and any failure or weakness in it that causes downward movement of the support base will result in reduced support efficiency and greater number of roof control problems. The existence of floor stability problems in mines and tunnels has been recognized for many years; Knowledge of the bearing capacity of mine floors is particularly important when designing face supports in longwall mining. Considering the use of plate loading tests in determination of bearing capacity of floor strata, the following work is worth reviewing here in short paragraphs before going into the subject in detail.

Jenkins (1955-1958) observed that bearing capacity of the floor loaded by hydraulic supports was a function of perimeter length and shape of the base. He stated that round plates yield lower stress concentrations in the rock under the loading plate than square plates of equal area. Lee (1961) found similar results with Jenkins and added that failure of floor or roof strata which were supported with props also depends on stratigraphy and characteristics of rock types involved. White (1956) proposed that the

effect of moisture and water content on the clay, especially montmorillonite, bearing floor is significant on bearing capacity. Dulaney (1960), after testing the floor strata of six coal mines, supported White's findings and suggested that laboratory samples should be tested for in-situ water content in order to evaluate the bearing capacity correctly. Holland (1962), using Dulaney's data, reasoned that the allowable load on floor strata should be $1/2$ to $2/3$ the unconfined compressive strength of underclay under conditions of in-situ water content. Chlumecky (1968) and Singh et. al. (1974) confirmed Jenkins's findings and they added that ultimate bearing strength decreased with increasing plate bearing area. Platt (1956), modelling the movements beneath mine support units, found that bearing plates with flat bases produced the classical bearing capacity failure profiles predicted by the plasticity approach of Prandtl (1921). Nair and Barry (1970) proposed a practical method for in-situ plate loading tests in order to determine bearing capacities of mine roof and floor strata. Afrouz (1975) combined theoretical studies with in-situ tests and noted that doubling the base area would decrease bearing capacity of coal mine floors by 16-35 percent, and this ratio is around 5-20 percent for underclays. He also confirmed that the perimeter length of base plates was a significant factor on bearing capacity as Jenkins stated. In addition, he observed that strength of floor decreased from the mid-face towards the face ends

due to cracking and fracturing of the rock in the face area.

Plate bearing tests are also used in evaluating the deformability of the roof and floor strata. Heuze and Salem (1977) determined the critical parameters affecting the plate loading tests by means of finite element method. They showed how the ratio of plate to rock modulus, the rock anisotropy and the plate geometry influence the deformation under the loading plate. Heuze (1980) stated that field elasticity moduli determined by plate loading tests generally appear to be between 20-60 percent of laboratory values. He gave specific suggestions for the interpretation of deformation moduli values. Salomon in 1968 presented a theoretical analysis for computing elastic moduli of a stratified rock mass with the use of an equivalent isotropic medium approach. In 1982, Gerrard proposed a theoretical approach for determination of the equivalent elastic moduli of a rock mass consisting of orthorhombic layers with individually different elastic properties. Although the last two approaches for the deformability of a layered rock are not directly concerned with the bearing capacity of this rock, they provide a method to estimate an equivalent deformation modulus which is an input parameter for a theoretical analysis of stress distribution and failure under the loaded area.

1.2.2. Theoretical Approaches of Foundation Engineering

The bearing capacity approaches of soil mechanics and foundation engineering are applicable for soft and

plastic rocks in general. Considering, the failure mechanisms for rock under the loading or base plates and using the proper failure criteria for rock, some modifications are necessary in the bearing capacity approaches, and examples of these are given in the next section.

In the soil mechanic sense, bearing capacity in general, is defined as maximum load at failure divided by the area under a footing. The term " bearing capacity " used here will be defined as the maximum contact pressure applied by loading plates or base plates of props to the underlying strata without any failure.

Prandtl's Approach For Bearing Capacity :

Prandtl (1921) combined the solutions described by Nadai (1913) which were based on the limit equilibrium principles for metal punching problems. In his approach; failure zone is divided into three regions as shown in Figure 1. Region I is an active zone which pushes region II radially and region III upwards. In Figure, region I is bounded by the line AC which is inclined at $\beta = 45 + (\phi/2)$ degrees from the horizontal. Failure line DE under region III is inclined at $45 - (\phi/2)$ from the horizontal.

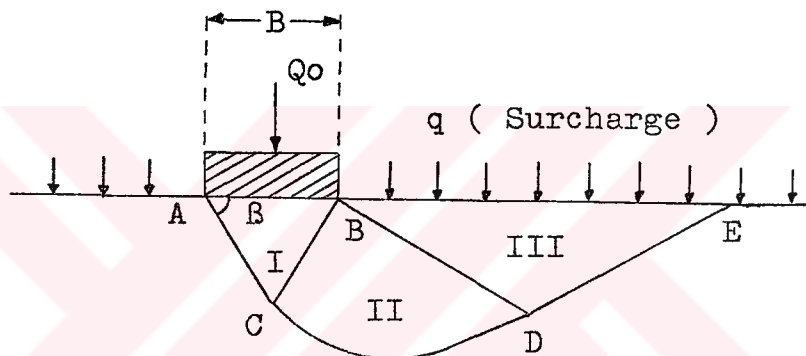
Protection of failure surface of region II in Figure 1 changes from an arc for $\phi=0$ (frictionless) condition to a logarithmic spiral for $\gamma=0$ (weightless) condition, (Dee Beer, 1965). For a weightless material, $\gamma=0$, the ultimate bearing capacity q_u is :

$$q_u = C \cdot N_c + q \cdot N_q \quad (1.1)$$

where ; C : Material cohesion

q : Surcharge load ($q = D \cdot \gamma$ where D is depth of embedment, and note that q is zero for the plate loading test.)

N_c and N_q : Dimensionless bearing capacity factors.



Active Zone : Region I

Radial Zone : Region II and III

Figure 1. Failure zones under a shallow footing ,
(After Prandtl, 1921)

Nadai's limit equilibrium or plasticity approach assumes that the material exhibits no deformation prior to shear failure and the failure is characterized by the plastic flow of clay bearing weak floor strata under the

footing at a constant stress. Therefore, the usual stress strain relations of elasticity and material properties such as Young's modulus and Poisson's ratio are not used in this plasticity approach. In formulating the initial theory, the model is assumed to contain on infinitely long foundation so that plane strain assumptions and simplifications can be utilized. Yield condition used is the Mohr-Coulomb criterion given by :

$$\tau_f = C + \sigma_f \cdot \tan \phi \quad (1.2)$$

where ; τ_f : Shear stress on failure plane

σ_f : Normal stress on failure plane

Cohesion, C, and the friction angle, ϕ , are the strength parameters for the failure plane.

Modification on Prandtl's Approach :

Terzaghi (1943) followed by Meyerhof (1955) and Terzaghi and Peak (1966) computed the bearing capacity due to the weight and the friction of the overlying material for a failure surface different from that of Prandtl. The angle β , in region I, is not fixed at $45 + (\phi/2)$, but takes on whatever value minimizes the bearing capacity. The weight effect depends on ϕ and β only and results in the bearing capacity component.

$$q_u = (0.5) \cdot B \cdot \gamma \cdot N_\gamma \quad (1.3)$$

where ; $N_\gamma = 2 \cdot (N_q + 1) \cdot \tan \phi$

B : Width of the loading area

N_c , N_q and N_γ values were tabulated for ϕ values. These bearing capacity components are combined for the most general case where $C \neq 0$, $\phi \neq 0$ and $\gamma \neq 0$ to yield the equation :

$$q_u = C.N_c + q.N_q + (0.5).\gamma.B.N_\gamma \quad (1.4)$$

Meyerhof (1963), Dee Beer (1965), and Vesic (1975) modified the general equation semi-empirically to include shape effects since the original derivation assumes an infinite foundation length. The equation applicable for the ultimate bearing capacity q_u for a rectangular footing is ,

$$q_u = C.N_c.(1+0.3 B/L) + \gamma.D.N_q + (1-0.2 B/L).N_\gamma.B/2.\gamma \quad (1.5)$$

where ; C : Cohesion

B : Width of footing

L : Length of footing

D : Depth of surcharge

For mining purpose, Brady and Brown (1985) quoted the work by Brich Hansen (1975) who derived the following expressions for a cohesive frictional material such as a soft rock

$$q_u = (0.5).\gamma.B.N_\gamma + C.N_c \quad (1.6)$$

Table 1. Bearing capacity factors (after Bieniawski(1987))

ϕ	N_c	N_q	N_γ
0	5.14	1.00	0.00
1	5.38	1.09	0.07
2	5.63	1.20	0.15
3	5.90	1.31	0.24
4	6.19	1.43	0.34
5	6.49	1.57	0.45
6	6.81	1.72	0.57
7	7.16	1.88	0.71
8	7.53	2.06	0.86
9	7.92	2.25	1.03
10	8.35	2.47	1.22
11	8.80	2.71	1.44
12	9.28	2.97	1.69
13	9.81	3.26	1.97
14	10.37	3.59	2.29
15	10.98	3.94	2.65
16	11.63	4.34	3.06
17	12.34	4.77	3.53
18	13.10	5.26	4.07
19	13.93	5.80	4.68
20	14.83	6.40	5.39
21	15.82	7.07	6.20
22	16.88	7.82	7.13
23	18.05	8.66	8.20
24	19.32	9.60	9.44
25	20.72	10.66	10.88
26	22.25	11.85	12.54
27	23.94	13.20	14.47
28	25.80	14.72	16.72
29	27.86	16.44	19.34
30	30.14	18.40	22.40
31	32.67	20.63	25.99
32	35.49	23.18	30.22
33	38.64	26.09	35.19
34	42.16	29.44	41.06
35	46.12	33.30	48.03
36	50.59	37.75	56.31
37	55.63	42.92	66.19
38	61.35	48.93	78.03
39	67.87	55.96	92.25
40	75.31	64.20	109.41
41	83.86	73.90	130.22
42	93.71	85.38	155.55
43	105.11	99.02	186.54
44	118.37	115.31	226.64
45	133.38	134.88	271.76

$$\text{where ; } N_c = (N_q - 1) \cdot \cot \phi \quad (1.7)$$

$$N_\gamma = 1.5 (N_q + 1) \cdot \tan \phi \quad (1.8)$$

$$N_q = e^{\pi \cdot \tan \phi} \cdot \tan^2 (\pi/4 + \phi/2) \quad (1.9)$$

The above equation (1.6) is only applicable for the determination of bearing capacity developed under a long rib pillar. For pillars of finite length L , the bearing capacity is given by :

$$q_u = (0.5) \cdot \gamma \cdot B \cdot N_\gamma \cdot S_\gamma + C \cdot N_q \cdot S_q \cdot \cot \phi - C \cdot \cot \phi \quad (1.10)$$

where ; S_γ and S_q are shape factors defined as ;

$$S_\gamma = 1.0 - 0.4(B/L) \quad (1.11)$$

$$S_q = 1.0 - (B/L) \cdot \sin \phi \quad (1.12)$$

Skempton's Approach :

Skempton in (1942) developed an equation for ultimate bearing capacity for footings in cohesive clays

$$q_u = 5 \cdot C \cdot (1 + 0.2 B/L) \cdot (1 + 0.2 D/B) \quad (1.13)$$

In order to use this formula for the determination of bearing capacities for hydraulic props, surcharge depth D is eliminated and the formula becomes

$$q_u = 5 \cdot C \cdot (1 + 0.2 B/L) \quad (1.14)$$

finally, for a square base plate where $B=L$ or $B/L = 1$

$$q_u = 6.C \quad (1.15)$$

1.2.3. Rock Failure Criteria and Bearing Capacity Analysis

For studying bearing capacity, failure of the rock under plate loading, a mechanism of crack propagation, breaking and final failure under the loaded area is considered first. Based on this failure mechanism, two rock failure criteria, namely Mohr-Coulomb and Hoek & Brawn failure criteria are used to develop expressions for bearing capacity of the rock type under the plate.

Mohr-Coulomb Failure Underneath the Bearing Plate :

When the rock under the plate is loaded, cracing usually starts around corners of the loaded area, regions of very high stress cocentration and propagates down with increasing load.

Broken zone contains fractured rock which has passed beyond the peak of the stress-strain curve and it is the post failure stage of the stress-strain behaviour. Therefore failure criterion for zone A can be written as;

$$\sigma_1 = Co_R + q_R \cdot \sigma_3 \quad (1.16)$$

where ; Co_R : Residual unconfined coperative strength
 q_R : Residual friction factor

A radial side pressure, P_h , is applied to the surrounding rock in zone B due to the dilatency of failed

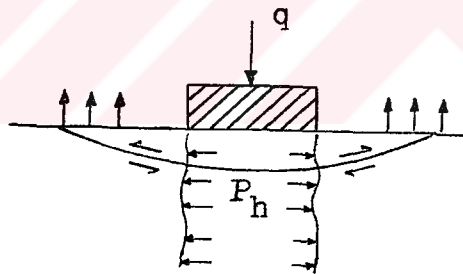
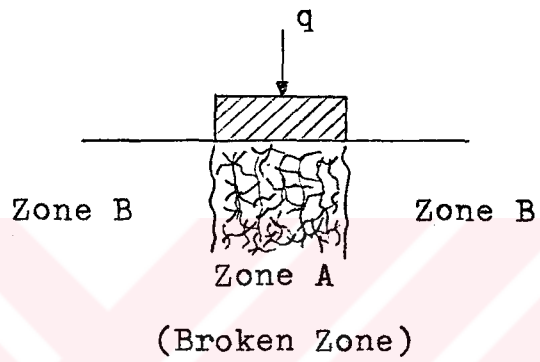
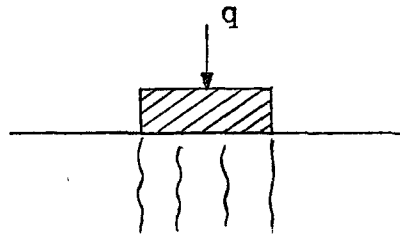


Figure 2. Zones underneath the loading plate.

rock in zone A. As a result of this effect radial cracking and final compressive failure occurs in zone B where failure criteria is expressed in terms of peak strength parameters.

$$\sigma_1 = C_{o_p} + q_p \cdot \sigma_3 \quad (1.17)$$

where ; $\sigma_1 = P_h$ and for $\sigma_3 = 0$, $P_h = C_{o_p}$

The radial pressure at the interface of zone A and B acts as a confining pressure for zone A, therefore, for zone A using $\sigma_3 = P_h$, $\sigma_1 = q_f$

$$q_f = C_{o_r} + q_r \cdot C_{o_p} \quad (1.18)$$

where ; q_f : Bearing capacity

q_r : Residual friction factor

C_{o_r} : Residual compressive strength, in zone A

C_{o_p} : Uniaxial compressive strength for zone B, intact rock.

In terms of cohesion and friction angles ϕ_p and ϕ_r for peak and residual cases.

$$q_f = 2 \cdot S_r \cdot \tan(45 + \phi_r/2) + P_h \cdot \tan^2(45 + \phi_r/2) \quad (1.19)$$

$$\text{where ; } P_h = 2 \cdot S_p \cdot \tan(45 + \phi_p/2) \quad (1.20)$$

If bearing capacity is to be determined conservatively then using $C_{o_r} = 0$, $q_r = 1$, lower limit of bearing capacity is equal to the compressive strength of rock.

$$q_f = C_{o_p} \quad (1.21)$$

Upper limit of bearing capacity can be determined as follows ; $C_{o_r} = C_{o_p}$ and $q_p = q_r$ then, (Goodman, 1980),

$$q_f = C_{o_p}(q_p + 1) \quad (1.22)$$

where ; $q_p = \tan^2 (45 + \phi_p / 2)$ (1.23)

Hoek and Brown's Empirical Failure Criterion :

This failure criterion was developed due to lack of extension of other failure criteria beyond a limited range. The authors used their experiences for both theoretical and experimental aspects of rock behaviour to develop following empirical relationship between the principal stresses associated with the failure of rock. They reached this resultant formulas by a process of trial and error.

$$\sigma_1 = \sigma_3 + (m \cdot C_o \cdot \sigma_3 + s \cdot C_o^2)^{1/2} \quad (1.24)$$

where ; σ_1 : Major principal stress of failure

σ_3 : Minor principal stress applied to the specimen

C_o : Uniaxial compressive strength of the intact rock material in the specimen.

m and s : Constants, which depend upon the properties of the rock.

Considering the failure mechanism used with Mohr - Coulomb failure criteria again, a bearing capacity expression can be developed using Hoek and Brown failure criterion.

For zone A, where $\sigma_1 = q_f$ and $\sigma_3 = P_h$, using residual strength parameters m_r and s_r ;

$$q_f = P_h + (m_r \cdot Co \cdot P_h + s_r \cdot Co^2)^{1/2} \quad (1.25)$$

For zone B, where $\sigma_1 = P_h$ and $\sigma_3 = 0$, using peak parameters m and s ;

$$P_h = Co \cdot (s)^{1/2} \quad (1.26)$$

Finally, bearing capacity q_f with the use of Hoek and Brown's empirical failure criterion is ;

$$q_f = Co \cdot \left((s)^{1/2} + (m_r \cdot (s)^{1/2} + s_r)^{1/2} \right) \quad (1.27)$$

Availability of rock mass equivalents of parameters m and s offers an advantage in using this expression for bearing capacity estimation. Hoek and Brown (1980) provides values of m and s to be used for different rock masses based on the results of rock mass classifications. For example ; for the fair rock considered in next sections these parameters are $s=0.04$, $m_r=0.15$ and $s_r=0.01$

Equation (1.27) in terms of Hoek and Brown equation is equivalent to equation (1.18) for Mohr-Coulomb analysis. This equation again gives an estimation of bearing capacity value between upper and lower limits which are predicted by substituting $m_r=m$, $s_r=s$ and $m_r=0$, $s_r=0$ respectively for upper and lower bound.

1.3. Factor Controlling the Bearing Capacity

Eccentric Loading :

If the floor is not uniformly loaded, the bearing capacity will be reduced by substituting B' for B

$$B' = B - 2e \quad (1.28)$$

where ; e is the distance between the location at which the resultant force of uniform loading acts. Obviously for uniform loading $e=0$ and $B'=B$. If there is eccentricity in two direction, both the width and length should be reduced by the amount shown in equation.

Water :

Water is known to reduce considerably the strength of soft and plastic rock. If the rock is saturated with water, γ is replaced by γ' in bearing capacity equations of soil mechanics and foundation engineering.

$$\gamma' = \gamma - \gamma_w \quad (1.29)$$

where ; γ_w is the weight per unit volume of water. That means, the bearing capacity of the saturated soft rock will be reduced by almost 50 % because γ_w is approximately 1/2 of the γ . For plate bearing tests described in next sections the effect of water is neglected since the tested rock surface are dry or moist only.

2. GENERAL DESCRIPTION OF THE TEST SITE

2.1. Mine Location

Bigadiç Colemanite Mines are located in northern part of west Turkey. Administration buildings of mines are near Osmanca village which is located at NE of Bigadiç. These buildings are 12 km away from Bigadiç. Simav underground mine which plate loading tests were conducted is located at the south of administration buildings and distance between them is about 2 km.

2.2. Geology

2.2.1. Geology of Bigadiç Borax Basin

Bigadiç borax basin is in the Pontid tectonic system. Paleozoic aged rock, metamorphosed metamorphites, recrystallized limestones, serpentinites and mesozoic aged ophiolites form the base of Bigadiç borax basin.

Neocene aged volcanic, volcanosedimentary, and sedimentary rocks were situated discordantly on that basin. These formations contain basalt, andesite, agglomerate and tuffs. Mineable colemanite and ulexite seams were also deposited between these formations.

Paleoquarterner and quarterner formations are the youngest ones in the region. They are located at the upper part of this basin.

Lower limestone formation is a kind of volcanosediment and contains carbonates and tuffs. It was deposited

with pyroclastic rocks which were originated from volcanic activities.

Lower ore zone was formed in pannonien era when volcanic activity rate was relatively slow and volcanic eruptions continued with irregular time intervals. Therefore, precipitation of carbonates was sometimes interrupted with volcanic materials. Carbonates and volcanic materials were deposited as a stratified rock mass. Lower ore zone contains colemanite and ulexite bearing seams at the bottom part. However this zone mainly consist of limestone, marl, claystone and tuffs. Lower ore zone is about 100 m thick.

Upper tuff zone is situated at the slope of hills in this region. It was deposited after deposition of lower ore zone. Volcanic activities were increased during deposition of upper tuff zone.

Upper ore zone contains mineable colemanite seams, claystones, carbonates and tuffs in a stratified manner. Its thickness is also about 100 m and it was deposited at the end of the volcanic activities which formed the upper tuff zone. Tuff interbands in this zone show that volcanic activities continued with time intervals while sedimentation was going on.

Paleoquarterner formation contains fine sand interbanded conglomerate and tuff. They formed horizontal morphology which was covered with soil.

Quarterner basalt rock is black in color and it shows flow type structure. Quarterner aged rocks in the region can be seen at the side of river banks. They are

generally circular and edged sand size clastic materials which have not been sedimented yet.

Bigadiç borax basin contains major part of colemanite and ulexite reserve of Turkey. These minerals are economically extracted in the region.

2.2.2. Regional Tectonics

Tectonical feature of Bigadiç volcanosedimentary basin can be summarized as follows ;

Neocene aged formations which contains mineable seams have NE-SW strike direction. General dip of stratified rocks changes in the range of 0-30 degrees with the exception of local irregularities. Direction of dip is commonly NW-SE . Dip of the stratified rocks increases especially in Avsar, Simav and Kadiköy regions.

Main tectonic structures include folds, faults and discordants in Bigadiç borax basin. Güney fault, Simav fault, Dombaydere fault form the main fault system and Avsar-Simav syncline is the main fold system in the region of mining activity.

2.2.3. Description of Seam

Colemanite and ulexite were deposited with a closed lake in Bigadiç borax basin. Therefore, mineable seams were precipitated from lake's water. Country rocks around the seams are stratified limestone-claystone, their thicknesses changed due to ancient precipitation rate which was

interrupted by sediments transported from surrounding regions. This kind of deposition conditions affected the deposition of boron minerals as a seams. Consequently some part of seams contain regular clay beds and bands (2-3 cm thick). Some parts were deposited with clay , as a result clay bearing seams were formed.

Part of seams which was deposited in good geological conditions without any interruption, so colemanite and ulexite minerals formed massive crystalline layers in these parts of seams. Seams were seperated with 1-2 m thick laminated limestone-claystone strata. Thickness of these inter-seam strata can be changed due to ancient climatic conditions.

Mineable colemanite and ulexite seams in Simav mine have a N 55° E strike direction. Their dip direction and dip are SE and 20° respectively. There are four major seams in Simav mine, and these are parallel to eachother. First and second seams mainly contain colemanite minerals. Third seam contains colemanite and ulexite minerals, colemanite generally being at the top of the seam. Fourth seam contains ulexite minerals.

Claystone and limestone beds and bands with varying thicknesses form the strata between these seams. Table 2 shows minimum, average, and maximum thicknesses of seams and inter-seam strata.

Table 2. Thickness of seams and inter-seam strata in Simav underground mine

Formations	Thickness (m)		
	Minimum	Average	Maximum
Seam 1 (colemanite)	2.00	3.50	5.75
Inter-seam Strata	2.00	2.70	5.50
Seam 2 (colemanite)	3.00	4.75	7.00
Inter-seam Strata	2.20	3.95	5.70
Seam 3 (colemanite and ulexite)	4.80	7.00	9.00
Inter-seam Strata	3.80	4.75	6.50
Seam 4 (ulexite)	3.50	4.50	6.50

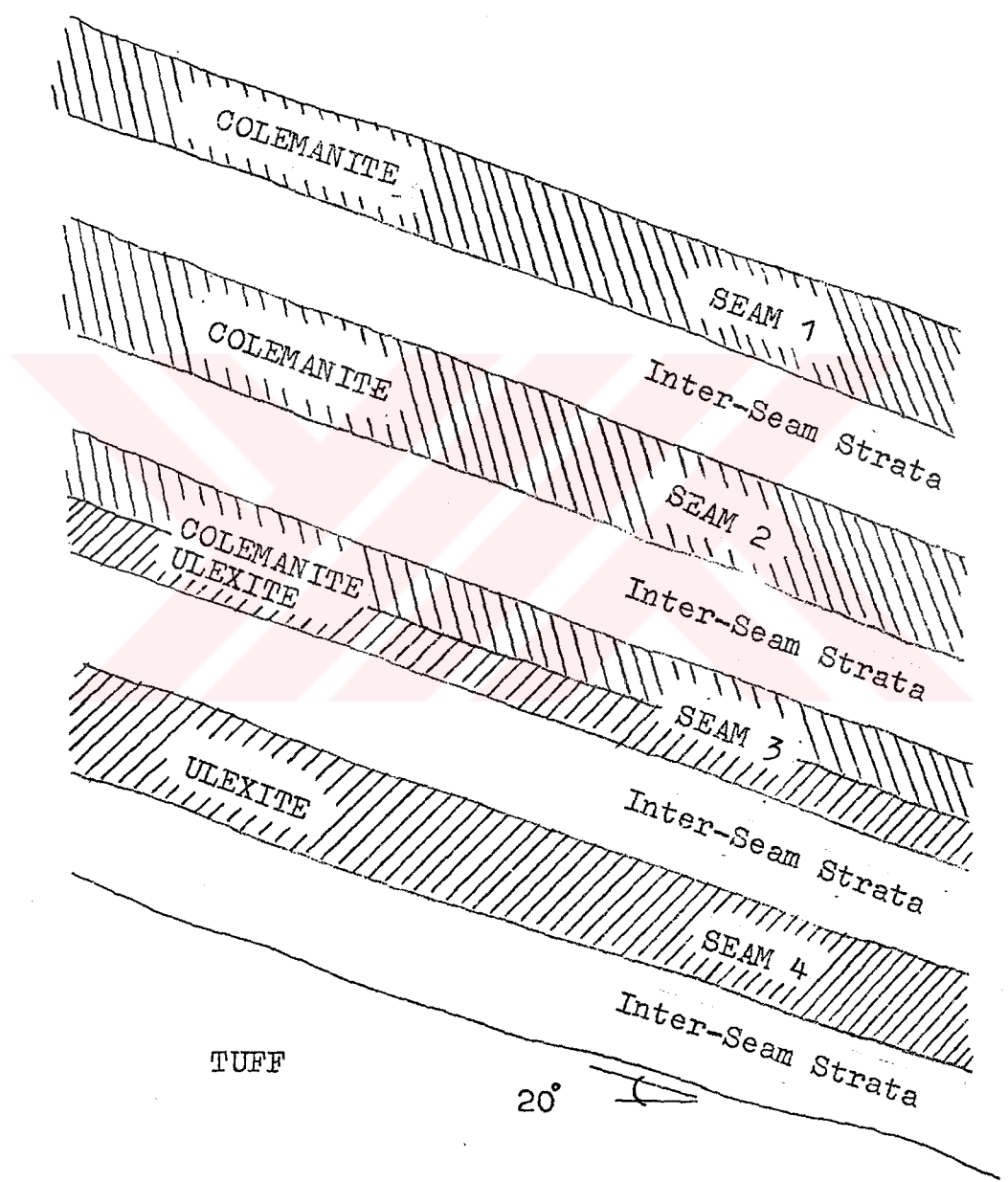


Figure 3. A general section through the seams of Simav mine.

2.3. Mining Method

In Simav underground mine, mining is generally done by the method of retreat longwall mining with caving.

In order to excavate nearly horizontal (20 degrees) seam with 6 to 8 m thicknesses, simultaneous slicing with retreat longwall method is applied. Thick seams are divided into three parts. Upper part (thickness = 2-2.5 m), middle part (thickness = 0.5-1 m) and lower part (thickness= 2-3 m). First the upper then the lower part is excavated. Middle part which is thinner than the other two part, and it is recovered from the back of the longwall used for extracting the lower part.

On the other hand, if the seam thickness is about 3-5 meters, retreat longwall with sublevel caving method is applied to extract such a seam. The seam is undermined with longwall mining method, and upper part of the seam is recovered by caving the roof in a controlled manner.

Current mining activity is about 120 m deep below the surface. Access is provided by two inclines and a vertical shaft. Main galleries are positioned parallel to the strike of the seam at a certain level, vertical distance between levels is 20 m. Longwall panels in seams are connected to main galleries with cross-cuts. Tail gate of every longwall panel is connected to the cross-cut at the upper level. Ore is drilled and blasted then it is loaded to the conveyors at the main gate by hand shovel and mining is conducted by conventional methods.

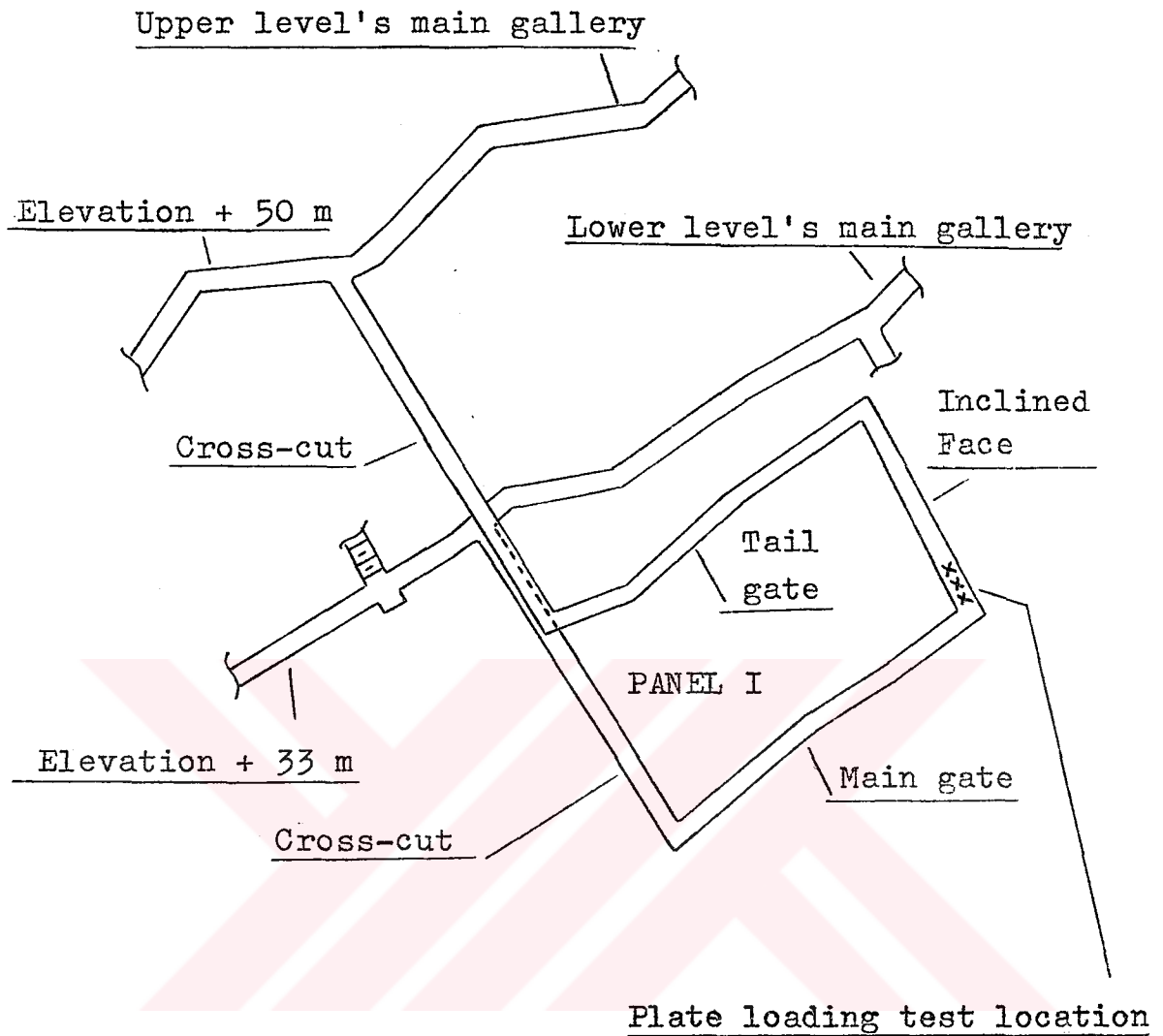


Figure 4. Layout of representative longwall panel in Simav underground mine.

2.4. Laboratory and Site Investigation

In order to determine mechanical properties of rocks a series of laboratory tests were carried out. Specimens were prepared according to ISRM standards suggested by ISRM and average properties were determined from a large number of test results.

2.4.1. Sampling

One way of taking specimens from underground strata is drilling. Drilling was carried out at 5 locations which were chosen in a way that regional variations of underground strata would be reflected in the core samples. Core samples were covered with nylon bags for preserving them in their natural moisture content.

A second way of specimen collection was to take rock blocks around working longwalls in Simav mine. Blocks chosen were taken out of the mine with care. Then, they are covered with concrete to prevent damage during transportation. Specimens were taken in different directions from the blocks and this way directional effect of stratification on the mechanical properties could also be investigated.

2.4.2. General Description of Samples and Rock Types

Result of laboratory tests showed that observed standard deviations, in general were quite high. This was believed to be due to the sedimentary origin of samples.

Sometimes samples were named as clay bearing since crystals of colemanite and ulexite were surrounded by thin layers of clay, however, had a pure crystalline structure without any clay fillings.

Observations in the mine showed that water affected the sedimentary strata significantly, and it sometimes turns the clay bearing strata to mud for the extreme cases. Slake durability and density test results show this fact. Clay bearing ulexite, for example disintegrated in water, so it's saturated density could not be measured.

Samples chosen from blocks and drill holes always represented the strongest part of strata, since weaker parts of block and core samples were cracked and damaged during drilling or sample preparation. Therefore, laboratory test results usually gived upper limits of strength values.

Laboratory samples that were also tested in the field by plate loading can be divided into three groups mainly, colemanite, ulexite and clay banded limestone.

i) Colemanite : Colemanite samples were taken from the longwall face of seam 2, and cores from exploration boreholes. Drill cores were enough to provide samples which represent all colemanite seams including Seam 1 and upper part of Seam 3. Crystalline colemanite samples and clay bearing ones were tested and if test results were significantly different than each other, they were noted differtly. However, test results did not change too much

and remained usually in a common range.

ii) Ulexite : Ulexite samples which were taken mostly from blocks and a few from boreholes often contained clay. However, there were also massive crystallized ulexite samples. Although test results showed variations depending on the clay content, they usually remained in a common range.

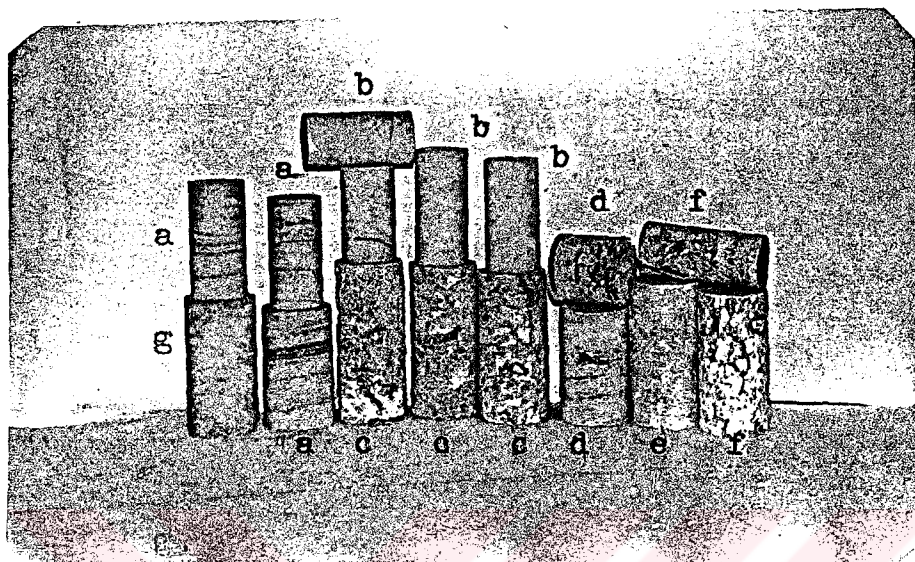
iii) Clay banded limestone : This is the general name used here for laminated and bedded limestone with clay and claystone. Individual clay and claystone bed thicknesses changed in the range of 1 mm - 3 cm, and this constitutes the weaker part. When the limestone thickness is more, clay banded limestone yields higher strength values. On the contrary, strength values are lower for samples having thick claystone beds. Thickness of limestone layers usually between 0.1 - 10 cm, and on the average it is about 3 - 5 cm.

A picture of main rock types in the region can be seen in Figure 5.

2.4.3. Results of Laboratory Tests

Results of laboratory tests are given in following tables. Laboratory tests were performed and results were evaluated according to I.S.R.M.'s suggested standard test procedures.

According to laboratory test result ulexite has the lowest strength values, and clay banded limestone has the highest values among these there major rock types.



- where;
- a) Clay banded limestone (thinly bedded)
 - b) Clay banded limestone
 - c) Weathered limestone
 - d) Colemanite
 - e) Ulexite
 - f) Ulexite with clay fillings
 - g) Tuff

Figure 5. Picture of main rock types at Simav underground mine.

In order to obtain discontinuities stiffness values which will be used in next sections, special shear strength tests were conducted on resultant values are listed in Table 8.

2.5. Classification of Rocks Around the Seams

Following the core logging and geotechnical investigations on samples taken from drill holes, standard procedures were employed to classify the strata in the region. RMR and Q values for two different rock classification systems given in Table 11 for rocks around the seams. Classification was performed for each drill hole separately, then their values were averaged to get a single classification value for each of structurally different rock units. Table 11 shows also minimum and maximum values for RMR and Q determined from 5 drill holes.

Classification limits of RMR and Q systems and rock mass descriptions are given below in Table 12a and 12b.

According to RMR system and the values found here, strata which are located at top and bottom of the seams are classified as poor rock, and seams themselves are classified as poor and fair rock. According to Q system, strata under and above the seams are classified as very poor rock, and seams are classified as very poor and poor rock.

Table 3. Density & Porosity test results

Rock Type	Number of Spec.	Porosity (%)	Dry Density (g/cm ³) ρ_d	Saturated Density (g/cm ³) ρ_s
Colemanite	30	2.22 ± 1.3	2.16 ± 0.12	2.23 ± 0.17
Ulexite	33	-	1.81 ± 0.11	-
Clay Banded Limestone	48	10.7 ± 0.99	1.84 ± 0.02	1.94 ± 0.03

Table 4. Uniaxial compressive strength test results

Rock Type	Number of Spec.	Unconfined (uniaxial) Compressive Strength (MPa) , Co
Colemanite	38	17.33 ± 10.38
Ulexite	41	14.78 ± 6.31
Clay Banded Limestone	44	19.43 ± 7.49

Table 5. Indirect (Brazilian) tensile strength test results

Rock Type	Number of Spec.	Indirect (Brazilian) Tensile Strength (MPa) , T_o
Colemanite	62	1.39 ± 0.89
Ulexite	16	0.79 ± 0.45
Clay Banded Limestone	15	2.69 ± 1.88

Table 6. Laboratory deformability test results

Rock Type	Number of Spec.	Modulus of Elasticity (GPa) , E_t	Poisson's Ratio (ν_t)
Colemanite	7	47.28 ± 17.00	0.18 ± 0.06
Ulexite	9	20.47 ± 15.54	0.17 ± 0.89
Clay Banded Limestone	19	9.37 ± 4.90	0.26 ± 0.10

Table 7. Triaxial test results (Applied confining pressure series; 0, 4.9, 9.8, and 14.7 MPa)

Rock Type	Number of Spec.	Relationship Between $\sigma_1 - \sigma_3$ (MPa)
Colemanite	4-1	$\sigma_1 = 17.33 \pm 4.89 \sigma_3$
Ulexite	4-3	$\sigma_1 = 14.28 \pm 3.13 \sigma_3$
Clay Banded Limestone	4-5	$\sigma_1 = 19.43 \pm 2.36 \sigma_3$

Table 8. Shear strength test results

Rock Type	Normal Stiff. (MPa/m) k_n	Normal Stiff. (MPa/m) k_s	Relationship Between $\tau - \sigma$ (kPa)
Clay Banded Limestone (Thinly Laminated)	320	1254	$\tau \geq 25 + 0.40 \sigma ; \sigma < 250$ $\tau \geq 70 + 0.24 \sigma ; \sigma > 250$
Clay Banded Limestone	2651	5700	with irregularities : $\tau \geq 160 + 0.75 \sigma$ slickensided : Peak values ; $\tau_p \geq 40 + 0.55 \sigma ; \sigma < 625$ $\tau_p \geq 180 + 0.38 \sigma ; \sigma > 625$ Residual values ; $\tau_r \geq 80 + 0.36 \sigma$

Table 9. Slake-Durability Index test results

Rock Type	Number of Spec.	Slake Durability Index , I_d (%)		Suggested Durability Classifi. (Gamble 1971)
		First Cycle I_{d-1} (%)	Second Cycle I_{d-2} (%)	
Colemanite	6	89 ± 4	79 ± 7	Medium
Ulexite	4	61 ± 13	31 ± 7	Low
	1	37	3	Very Low
Clay Banded Limestone	5	97 ± 3	93 ± 5	Medium & Med. High

Table 10. Clay analysis results (X-Ray Diffraction)

Rock Type	Number of Spec.	Clay Content Ratio , (%)	Clay Type
Colemanite	1	10	Montmorillonite
	5	60-80	"
Ulexite	1	5	"
	1	90	"
Clay Banded Limestone	9	78 (50-90)	"

Table 11. RMR and Q values around the seams determined from rock mass classification systems.

	According to RMR system		According to Q system	
	Average RMR	Limit Values RMR	Average Q	Limit Values Q
~5 m ↑↓	30	29 - 33	0.650	0.495-0.832
SEAM 1	36	27 - 46	0.725	0.152-2.459
	24	21 - 30	0.213	0.151-0.694
SEAM 2	35	25 - 44	1.097	0.198-1.561
	23	14 - 48	0.471	0.039-1.199
SEAM 3	29	16 - 33	0.325	0.058-1.126
	28	14 - 33	0.341	0.015-0.407
SEAM 4	44	21 - 50	0.978	0.304-2.451
~5 m ↑↓	30	23 - 34	0.692	0.495-1.119

Table 12a. Rock mass classes of RMR system.

RMR	Rock Mass Class
0 - 20	Very Poor Rock
21 - 40	Poor Rock
41 - 60	Fair Rock
61 - 80	Good Rock
81 - 100	Very Good Rock

Table 12b. Rock mass classes of Q system.

Q Values	Rock Mass Class
0.001 - 0.01	Exceptionally Poor Rock
0.01 - 0.1	Extremelly Poor Rock
0.1 - 1.0	Very Poor Rock
1.0 - 4.0	Poor Rock
4.0 - 10.0	Fair Rock
10.0 - 40.0	Good Rock
40.0 - 100.0	Very Good Rock
100.0 - 400.0	Extremelly Good Rock
400.0 - 1000.0	Exceptionally Good Rock

3. EXPERIMENTAL WORK

3.1. Test Location

In order to prevent penetration of hydraulic props into the floor and roof strata bearing capacities had to be determined. Therefore a series of plate loading tests was performed at the face area of the longwalls in Simav mine. Tests were conducted on the floor and roof strata in the immediate vicinity of the retreating longwall face. Longwall panels in which the testing was carried out were Panel I, II and III in Seam 2 and Panel U-1 in Seam 4, Fig. 4 shows general test locations at a representative panel.

Strata which are disturbed by mining operation gives lower bearing capacity values. Shotfiring and use of timber or hydraulic props in longwalls usually develop secondary and tertiary fractures in the longwall roof and floor strata. The magnitude and concentration of these fractures and the state of stress within the floor of the face ends differ from the mid-face. This is mainly due to the pressure and time influence on the gate roads leading to their prospective faces. Afrouz (1975) showed that generally average bearing capacity and modulus of deformation decreased from the mid-face towards the face ends.

Purpose of the tests was to determine the minimum value of ultimate bearing capacity of roof and floor strata because new support design was to be based on this minimum bearing capacity value. Therefore, most of the tests were

performed around face ends in Simav mine.

3.2. Test Set-up

Bearing capacity of strata around longwall faces of Simav mine was measured by using the test set-up shown in Figure 6,7 and 8. Test set-up consist of mainly of a hydraulic ram, a pump, and steel reaction boxes.

The hydraulic ram driven by a hand pump provided the loading on the surface of the rock under the test plate. When one end of the test frame was loading the surface to be tested, steel boxes were used to transfer the reaction force to the other end equipped with a wide reaction plate in contact with the rock at this end.

3.3. Measuring System

3.3.1. Load Measurements

Hydraulic ram had a load capacity of 200 tons and a stroke of 18 cm. During a test, hydraulic ram pressure was measured with a pressure gage in the hydraulic line. Hydraulic ram and pump used in the tests were calibrated in the Rock Mechanic Laboratory of M.E.T.U. where a hydraulic press with a pre-calibrated load measuring system was available. Resulting calibration factor, 1.968 , was obtained to convert pressure gage readings recorded during the field tests to desired values of the load.

3.3.2. Displacement Measurements

Measuring of displacement was performed with two separate systems. These systems could be used together or individually depending on the accuracy required from the displacement measuring system.

i) Optical System : A viewing system with a theodolite was used in this system. Two steel meters were attached to the test set-up as seen in Figure 6_a. These meters responded to relative movements of roof and floor strata while test plate was being forced to penetrate into the tested strata. Theodolite was located 2-3 m away from the test set-up. During a test, it acted as a fixed reference point so that relative movements of meters could be viewed through the theodolite with respect to this fixed point.

ii) Mechanical System : Dial gages were used in this displacement measuring system. Dial gages can measure displacements very accurately. In one end they were attached to a plate which moves together with loading plates. In the other hand they were in contact with a reference bar fixed through its end points which are positioned away from the loading area.

3.4. Test Procedure

3.4.1. Preparation of Test Place

By cleaning the debris and weak surface layers on undisturbed surface layer was tried to be exposed before

each test. Surface of the strata which would be tested was chosen as smooth as possible. It did not contain any visible cracks, fissure joints, and other discontinuities which were created during mining operations. Test surface was flattened and prepared by a hand hammer when it was rough.

3.4.2. Installation of Test Frame

Timber supports around the testing place were rearranged after choosing the test place. Special shaped timber post (with a dimension of 10×20×250 cm) was installed between roof and floor of longwall. This post helped to prevent overturning of test set-up during mounting. In addition, it prevented any possible sliding of the test frame, because of 20° inclination of longwall face. Then, the test frame was installed by taking necessary safety precautions.

Following procedure is applied to prepare the test set-up for typical plate loading test at the roof

(Figure 6_b):

i) Plate A with a 0.5 m² area (dimension 70×70×2.5 cm) was put on floor strata. This plate transferred the reaction force to the floor.

ii) Plate B (dimension 30×30×6 cm) was put on plate A to distribute the ram force over plate A .

iii) Plate C (dimension 30×30×1 cm), in other words reference plate was put on plate B. There were two screw

holes at the side of this plate for attaching the steel meter.

iv) The hydraulic ram was seated on plate C.

v) Plate D (dimension 30×30×6 cm) and steel boxes were placed on the ram. Steel boxes with dimensions 20×20×50 cm were bolted together.

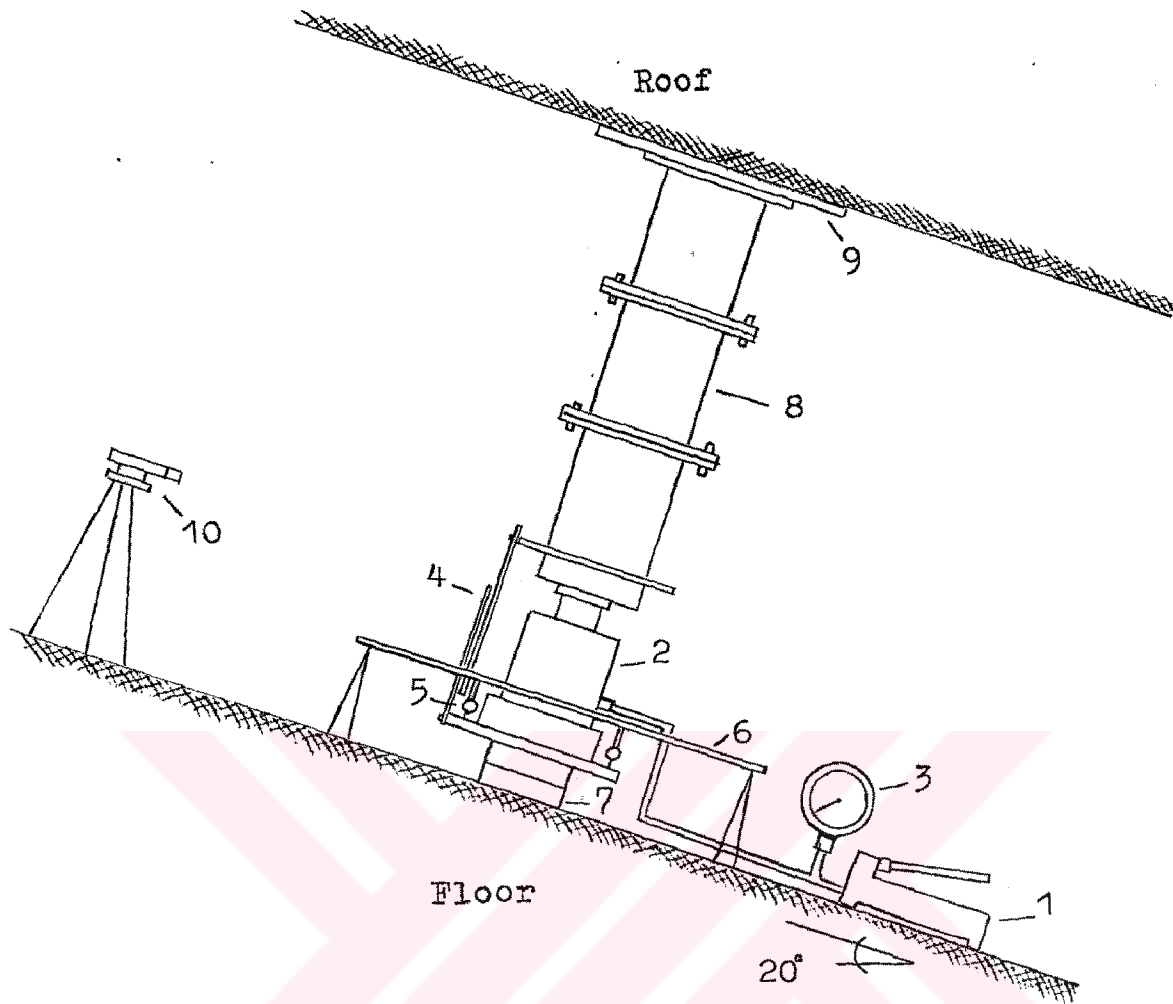
vi) At the end, square section test plate was inserted between the test frame and the test surface. Different sizes of loading plates were used depending on the test purpose; However, thickness of the loading plate was kept at a minimum 6 cm enough to distribute applied load uniformly over the rock surface.

For plate loading tests on the floor, test set-up was installed in a similar way. However, in this case loading plate was put on the floor surface and reaction plate A was inserted between the frame and the roof.

3.4.3. Testing

After installing the test frame, measuring systems were attached to the system. It was noticed that neither theodolite nor dial gages would be shaken after their adjusting. Measured quantities were recorded at certain intervals while the test was going on.

Plate loading test was started by actuating the ram and loading plate perpendicular to the strata. Hydraulic ram force was increased step by step while quantity of force on the loading plate and average displacement over



- | | |
|------------------|-------------------|
| 1- Hand Pump | 6- Reference Bar |
| 2- Hydraulic Ram | 7- Loading Plate |
| 3- Pressure Gage | 8- Steel Boxes |
| 4- Steel Meters | 9- Reaction Plate |
| 5- Dial Gage | 10- Theodolite |

Figure 6_a. Plate loading test set-up and its position in an inclined longwall face.

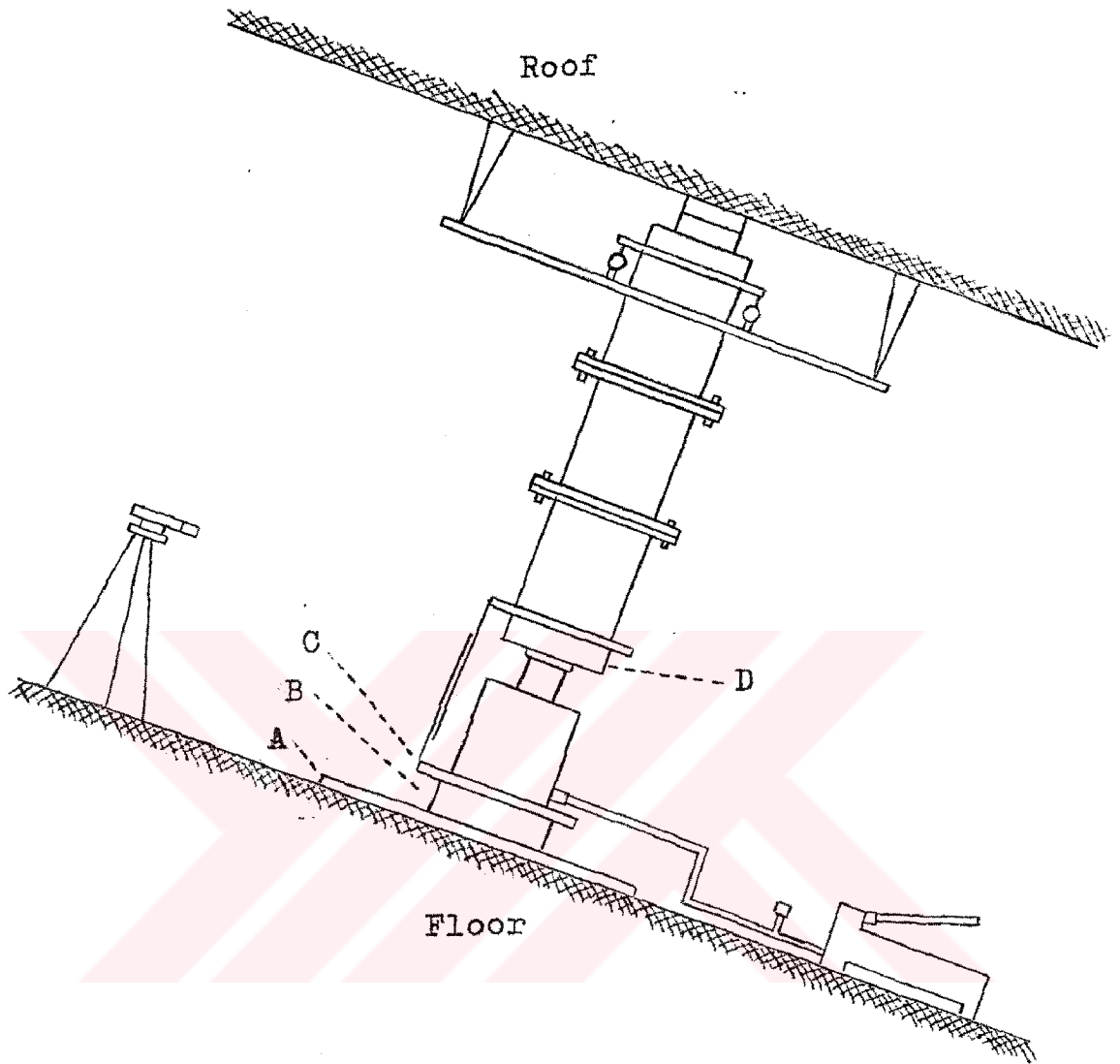


Figure 6_b. Plate loading test set-up for testing the roof strata (A,B,C, and D are specially prepared steel plates)



Figure 7. Picture of test set-up, showing optical displacement measuring system.

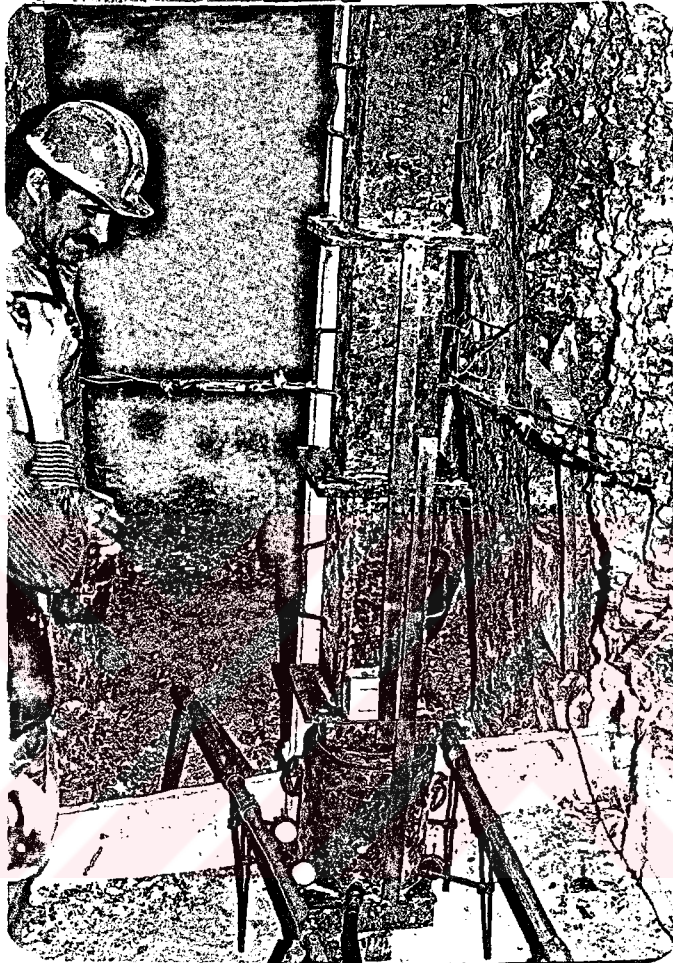


Figure 8. Picture of test set-up, showing optical and mechanical displacement measuring systems.

the loaded area recorded at certain intervals. Increasing the force was no longer possible when bearing capacity of strata was exceeded. After this force level, vertical displacement rate increased and with increasing displacement force level either remained constant or started dropping down as pumping continued. Failure point of the strata was determined by that bearing pressure between the plate and the rock at which the penetration rate increased noticeably while being accompanied by a drop in the recorded fluid pressure. This force was recorded as the maximum force to which strata could be subjected without failure for the loading plate area.

In addition, in order to study deformation response of the strata perpendicular to bedding and to determine in-situ modulus of deformation, loading and unloading cycles were carried out for some tests. Fissures, joint closing, and other fractures that existed in the rock mass caused high irreversible deformations during first loading cycle of the test. As a result, displacement levels were high in the first loading cycle and for displacement measurements, viewing the steel meters through the theodolite was accurate enough. Sensitivity of the system was about 0.5 mm. On the other hand, displacement data from first unloading cycle and second loading-unloading cycle were obtained by using dial gages.

After collecting enough data, loading plate was pushed into the strata to get about 3-4 cm plate penetra-

tion. This was necessary to see if there is any hardening or stronger strata underneath the failed region.



4. RESULTS OF PLATE LOADING TESTS

4.1. Introduction

A special testing program was employed to study the effect of base size on the ultimate bearing capacity and so plate loading tests were carried out. Longwall operations were going on in Seam 2 and 4 during testing period (1986-1987) in Simav mine. Therefore, all of the plate loading tests were carried out in longwalls of these two seams.

Bearing capacity of strata at the roof and floor depended on type of strata and mining condition around it. During the mining of upper slice and lower slice roof and floor conditions were different. When taking the upper slice, the floor consisted of ore seam itself, and the roof was inter-seam strata with bedded and laminated limestone and claystone. However, roof strata consisted of ore seam itself, and floor rock was the same inter-seam strata during lower slice mining. Therefore, sufficient number of plate loading tests were carried out to take different mining conditions into account.

Observations showed that floor heaving was a major result of time lapse during preparation of longwall face. Floor heaving was observed to increase when the longwall face advance rate decreased. Strata disturbed by mining operations and interaction gived lower bearing capacity values. All these factors were belived to effect the result

to some extent and to reflect variations of these factors in the results, a large number of tests was conducted at different stages of operations.

Stability and bearing capacity of the floor are affected by the presence of water. It was observed that moisture content of tested rock was about the same for all tests.

4.2. Test Results

Result of bearing capacity test which were conducted in Simav mine are tabulated in Table 13, 14, and 15. They are tabulated under separate rock names. Observations in the test site supplied enough data to identify the major rock types in the test site as colemanite, ulexite and clay banded limestone. These were the rock names used in tabulating and discussing the results.

Bearing capacity values of colemanite tabulated in Table 14 were determined when colemanite was located at both roof and floor of the longwalls. Table 15 shows resultant bearing capacity values of ulexite which was tested only at the roof of longwalls. Therefore, these results were treated accordingly. Table 13 shows bearing capacity values of clay banded limestone tested in the longwalls of Seam 2 and 4.

Test places are given together with the results in the tables. Therefore, any difference between test results could be interpreted with respect to the test place as well

as interpretation based on the plate size.

4.2.1. Clay Banded Limestone Under Seam 2

Result of tests performed in the clay banded limestone under Seam 2, were tabulated in Table 13. Thickness of this seam was about 3-6 meters and it was mined by retreat longwall mining method with downward slicing. Floor strata under this seam consist of clay banded limestone. Tests performed in Panel I and III showed that average bearing capacity of floor strata including all test results was $P_b = 6.74 \pm 3.16$ MPa without taking the size effect into account.

On the other hand during preparation of Panel III, it was observed that the same floor strata were in a heaved and broken condition and it didn't give any measurable bearing capacity values. Floor strata under Panel I gave higher average bearing capacities, $P_b = 23.0 \pm 11.9$ MPa for clay banded limestone, compared to Panel III's floor strata which had an average bearing capacity of about $P_b = 6.31 \pm 2.6$ MPa. Observation in the tested rocks showed that ; floor strata under Panel I had a thicker stratum compared to Panel III. In addition, the normal stiffness of the strata was believed to be higher in Panel I, since fractures in the strata had been filled with crystalline colemanite. Therefore cementation effect of the filling material increased bearing capacity of this rock.

Table 13. Plate loading results for clay banded limestone

Plate Dimen. (cm)	Bearing Capacity (MPa)	Average Bear. Cap. (MPa)	Test Place
10 x 10	10.43 6.49 8.85 7.28	12.20 ± 6.9	Panel III Seam 2
	10.82 6.89 7.87 10.03 5.91		Panel U.1 Seam 4 (Thinly Bedded)
	11.81 15.74 29.52 24.60		Panel U.1 Seam 4
	14.60		Panel I Seam 2
15 x 15	31.40	11.83 ± 6.7	Panel I Seam 2
	10.44 7.87 8.31 2.60 9.53 7.87		Panel III Seam 2
	14.17 6.99 8.74 13.99 8.31		Panel U.1 Seam 4 (Thinly Bedded)
	29.74 19.24 17.49 18.36		Panel U.1 Seam 4
20 x 20	2.71 5.16 4.43 5.41	7.88 ± 3.9	Panel III Seam 2
	6.89 6.39 6.89 4.82		Panel U.1 Seam 4 (Thinly Bedded)
	16.04 10.33 14.27 9.35 9.84		Panel U.1 Seam 4
25 x 25	4.72 3.94 4.41 3.15	5.87 ± 2.7	Panel III Seam 2
	10.71 5.66 8.51		Panel U.1 Seam 4

Table 14. Plate loading test results; Colemanite, Seam 2

Plate Dimen. (cm)	Bearing Capacity (MPa)		Average Bear. Cap. (MPa)	Test Place
10 x 10	26.70		24.46 ± 1.9	Panel III (Longwall Raise) ROOF
	23.10			
10 x 10	23.60		12.34 ± 1.7	Panel III ROOF
	13.38	3.94		
	13.40	9.80		
15 x 15	12.79		9.97 ± 3.9	Panel I ROOF
	17.20	6.80		
	13.10	7.87		
	15.70	6.99		
15 x 15	10.20	7.00	7.76 ± 4.8	Panel III ROOF
	8.50	6.30		
	4.60	5.20		
20 x 20	11.80	4.92	7.76 ± 4.8	Panel II FLOOR
	15.70	4.33		
20 x 20	4.60	5.20	4.52 ± 1.1	Panel III ROOF
	3.46	5.98		
25 x 25	4.25	4.41	4.52 ± 1.1	Panel III ROOF

Table 15. Plate loading test results for ulexite, Seam 4

Plate Dimen. (cm)	Bearing Capacity (MPa)	Average Bear. Cap. (MPa)	Test Place
10 x 10	5.91 5.91	5.91	Panel U.1 Seam 4 ROOF
15 x 15	4.54 4.11	4.32 ± 0.3	"
20 x 20	3.94 3.94 4.04 5.91 2.71	4.10 ± 1.1	"
25 x 25	2.52 2.45	2.48 ± 0.04	"

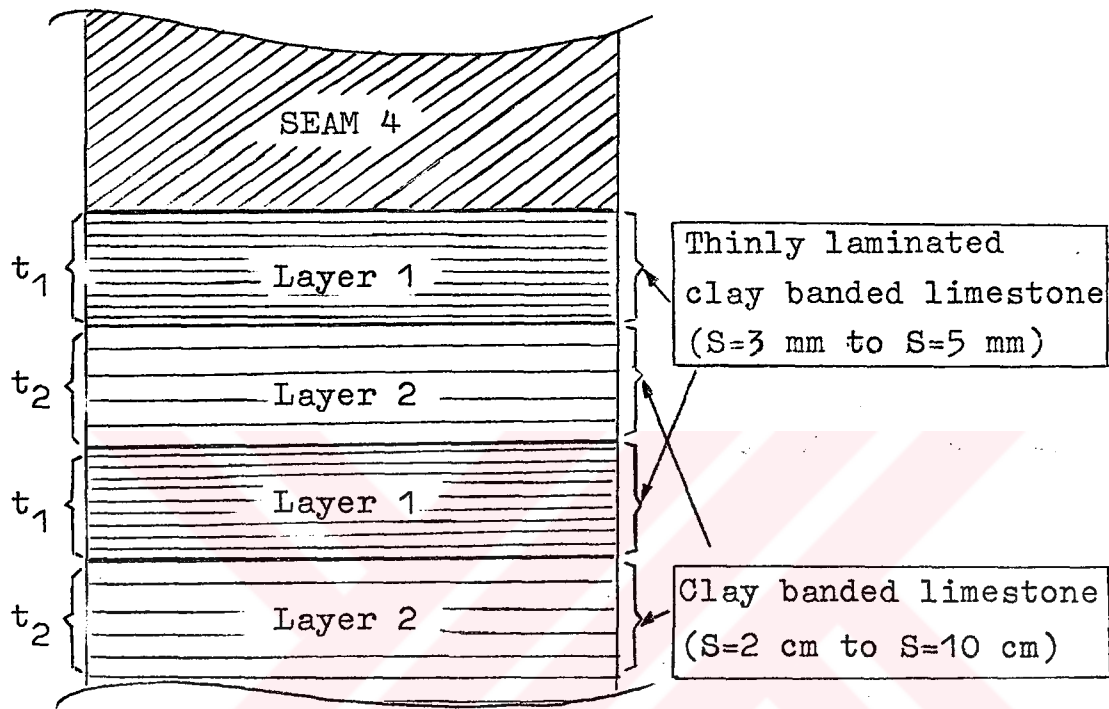
4.2.2. Clay Banded Limestone Under Seam 4

Table 13 also shows plate bearing test results of Seam 4. Average bearing capacity of floor strata under Seam 4 was determined as $P_b = 11.09 \pm 4.9$ MPa which is an average for all plate sizes. However, floor strata of Seam 4 usually seemed to have two types of layering. First layer, as seen in Figure 9, was located just under the seam. Thickness of the individual beds for this layer was about 1 mm - 5 mm, and this was called thinly laminated and laminated clay banded limestone. Average bearing capacity value was about $P_b = 8.29 \pm 2.83$ MPa for tests conducted on this layer.

Second layer was also clay banded limestone but this layer had wider spacing and beds. Thickness of stratum was observed to be between 2-3 cm for this case. This layer is similar to clay banded limestone under Seam 2. Average bearing capacity for tests having the second layer under the loading plate was determined as $P_b = 15.7 \pm 7.25$ MPa.

4.2.3. Colemanite

Roof strata tested during mining of Panel II and III also floor strata tested during mining of lower slice for Panel II were colemanite. Test results obtained at the roof colemanite of Seam 2 were tabulated in Table 14. Average bearing capacity value without considering size effect was calculated as about $P_b = 11.32 \pm 6.89$ MPa for all roof strata tested. However, the average was about



where ; t_1 is the thickness of Layer 1, which is about 10-18 cm .

t_2 is the thickness of Layer 2, which is about 20-30 cm .

S is the spacing between bedding plane.

Figure 9. Typical floor strata under Seam 4

$P_b = 24.5 \pm 1.9$ MPa for tests in the starter raise of Panel III. Moreover after advancing about 8-10 m away from the starter raise of Panel III cracking and fracturing in the roof strata started to be effective, and therefore the bearing capacity of the roof colemanite in this case was measured as $P_b = 13.2$ MPa which was lower than the values obtained in the raise. Additional test results obtained when the face front reached the mid-point of Panel III, yielded even a lower average value, a bearing capacity at the floor of a longwall $P_b = 9.14 \pm 4.17$ MPa.

Colemanite was also tested during the mining of upper slice in Panel II. These test results showed that bearing capacity of the colemanite tested at the floor was about $P_b = 6.96 \pm 2.1$ MPa. This value, which was slightly lower than the bearing capacity values found for the roof, showed that roof and floor values for colemanite could be treated together, also showed that if there was any structural weakening at the colemanite roof due to the longwall operation this was also effective at the colemanite floor.

4.2.4. Ulexite

Fourth seam was mined in a way that roof strata were always ulexite. The average bearing capacity for this ulexite was determined as $P_b = 4.18 \pm 1.3$ MPa which was the lowest value among the main rock types tested. Results of plate loading tests for the roof ulexite were tabulated in Table 15. Ulexite at the roof of Seam 4 was quite thick

due to the mining method. Therefore, roof was not fractured and cracked into blocks during longwall operations as it occurred at the roof of Seam 2. As a result, as far as the block movements were considered, roof strata in Seam 4 were stable in spite of low bearing capacity values. In fact, main reason for these low values was the high clay content of the ulexite left as the roof, and this also led to the plastic flow or punching type failure under the loading plate as opposed to failure types with brittle crack formation and propagation usually observed in clay banded limestone.

4.3. Variation of Bearing Capacity With Plate Size

The result of experiments indicated that there is a significant variation in bearing capacity values with plate size for similar mining conditions and the same rock types. This variation is to be believed to depend on numerous factors such as presence of different geological features in the floor or roof tested and their random distribution with respect to the size of the loaded area.

Table 13 shows average bearing capacity values found for clay banded limestone for different plate sizes. If standard deviation of test results for the same plate size are examined, it is seen that standard deviation value for the smallest plate size is higher than the others. In fact, standard deviation value decreased with increasing plate size. The reason for this can be explained as follows,

according to the observations at the test side with a small loading plate, if the discontinuities are widely spaced, no discontinuity may exist under the plate in which case a higher value of bearing capacity is obtained. On the other hand, for some tests, there may be closely spaced discontinuities and beds under the loaded area, and this situation yields lower values for bearing capacity. A larger plate, almost all the representative beds and discontinuities exist under the loaded area, the resulting bearing capacity values reflect the weakening effect of these weaknesses for all tests at different locations, and therefore standard deviations are smaller for larger plate sizes. In addition, when tables giving the results are examined, it is seen that strata tested in Simav mine yielded decreasing bearing capacity values with increasing plate size. Rate of decrease of bearing capacity with increasing plate size for different rock types was different. Ulexite and colemanite showed lower rates of decrease compared to the clay banded limestone. When the size effect and rock's failure types were interpreted together ; rocks with plastic type failure mechanisms showed a weaker size effect compared to rocks that had brittle type failure mechanisms.

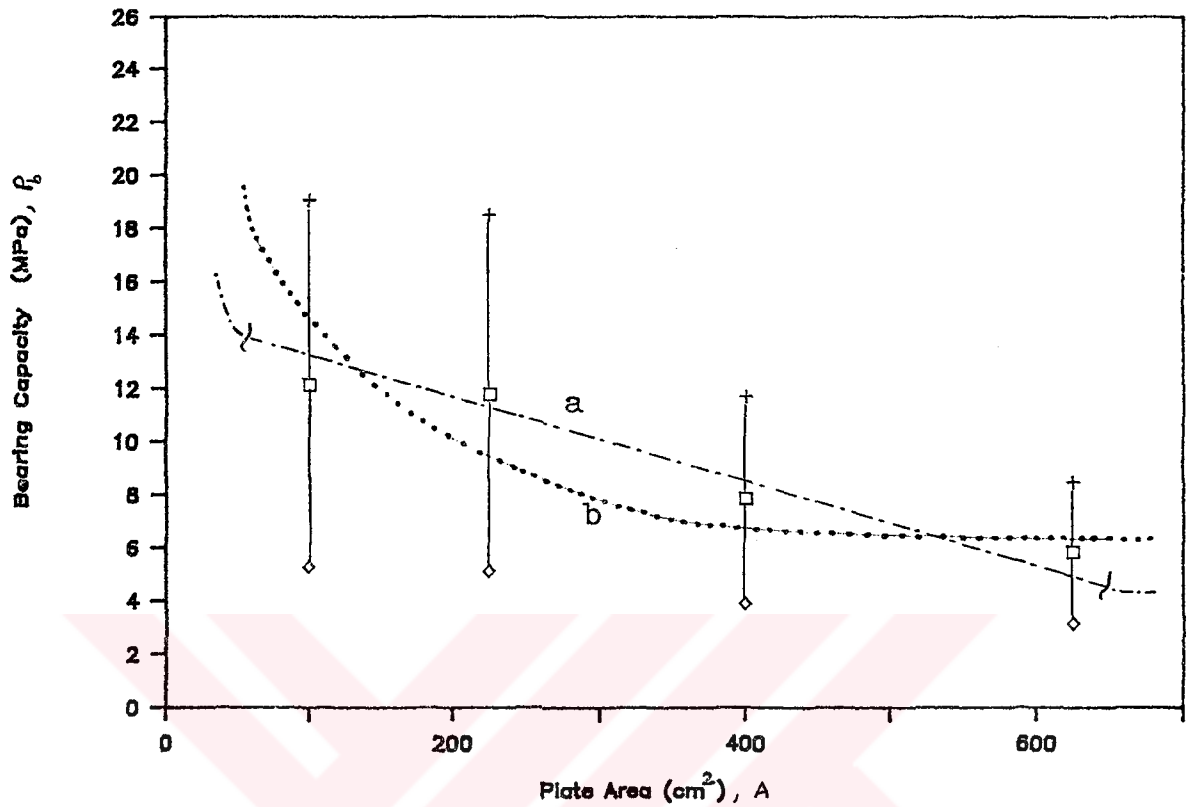
This concept was also investigated by Wagner and Schumann (1971) during their research on the stamp-load bearing strength of rock. They found that size effect is more dominant in brittle rocks than in ductile rocks. So

it was believed that the size dependence of the bearing strength was closely related to the brittleness of the material. Figures 10, 11 and 12 show the variation of plate bearing capacities with the plate area for different rock types in the test site. Here, it is interesting to note that the ulexite which had the highest clay content among the tested rocks shows the lowest size effect. As a matter of fact, for this ulexite with high clay content, failure mechanism was always plastic or punching type with no visible signs of brittle crack formation and propagation under the loading plate.

4.4. Failure Mechanisms Observed in the Tests

Load-deformation curve of test results showed that ulexite had the type of curves, which indicated plastic type of failures. Slopes of the first loading cycles were small for these rocks. Moreover these rocks could be loaded again up to about maximum bearing load with increasing displacement rates during second loading cycle of tests. However, clay banded limestone strata had different load deformation curves. They had brittle type failure mechanisms. After reaching failure load they were fractured and the bearing load decreased suddenly. During the second loading cycle bearing load could be increased only to $2/3$ of maximum bearing load, and it never reached the maximum bearing load attained in the first cycle.

Typical load-displacement curves for different rock



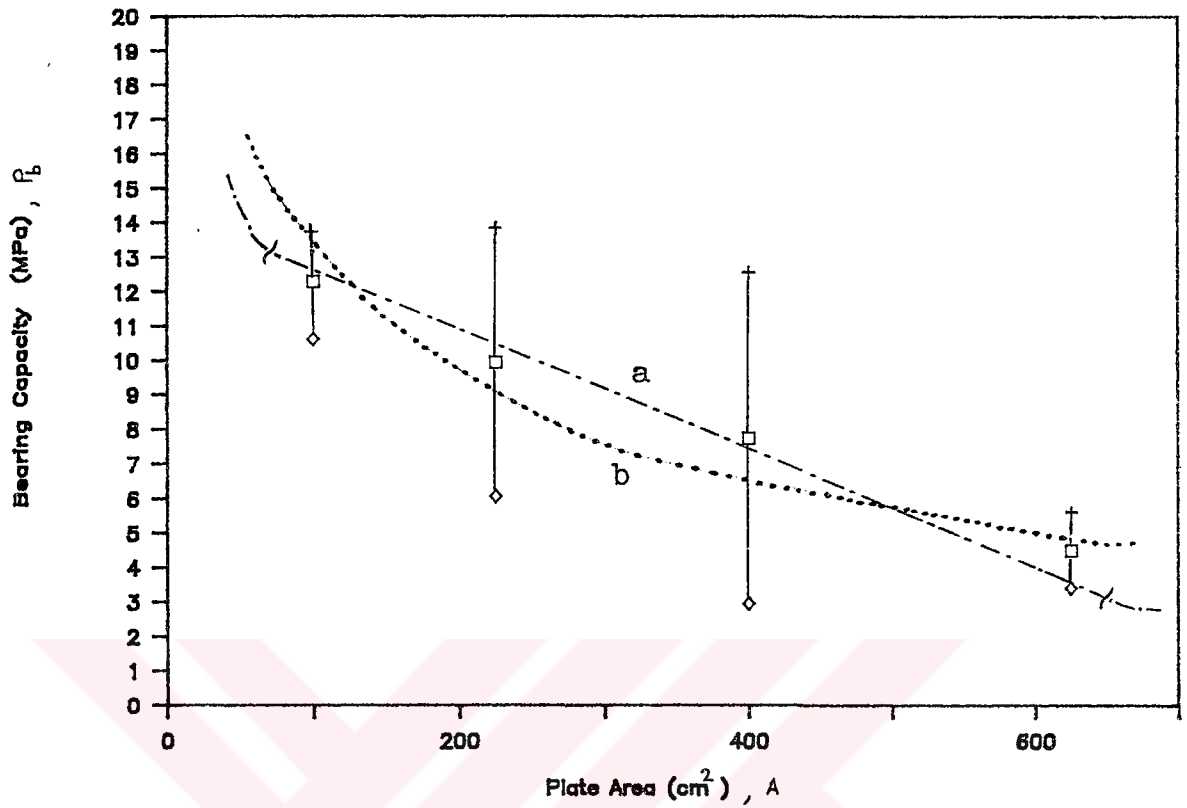
□ : Average bearing capacity values.

+, ◇ : Limits of values, \pm standard deviation

a) Linear regression ($P_b = 14.44 + (-0.0160) \cdot A$)

b) Power regression ($P_b = 97.2 A^{(-0.426)}$)

Figure 10. Variation of bearing capacity with plate size for clay banded limestone.



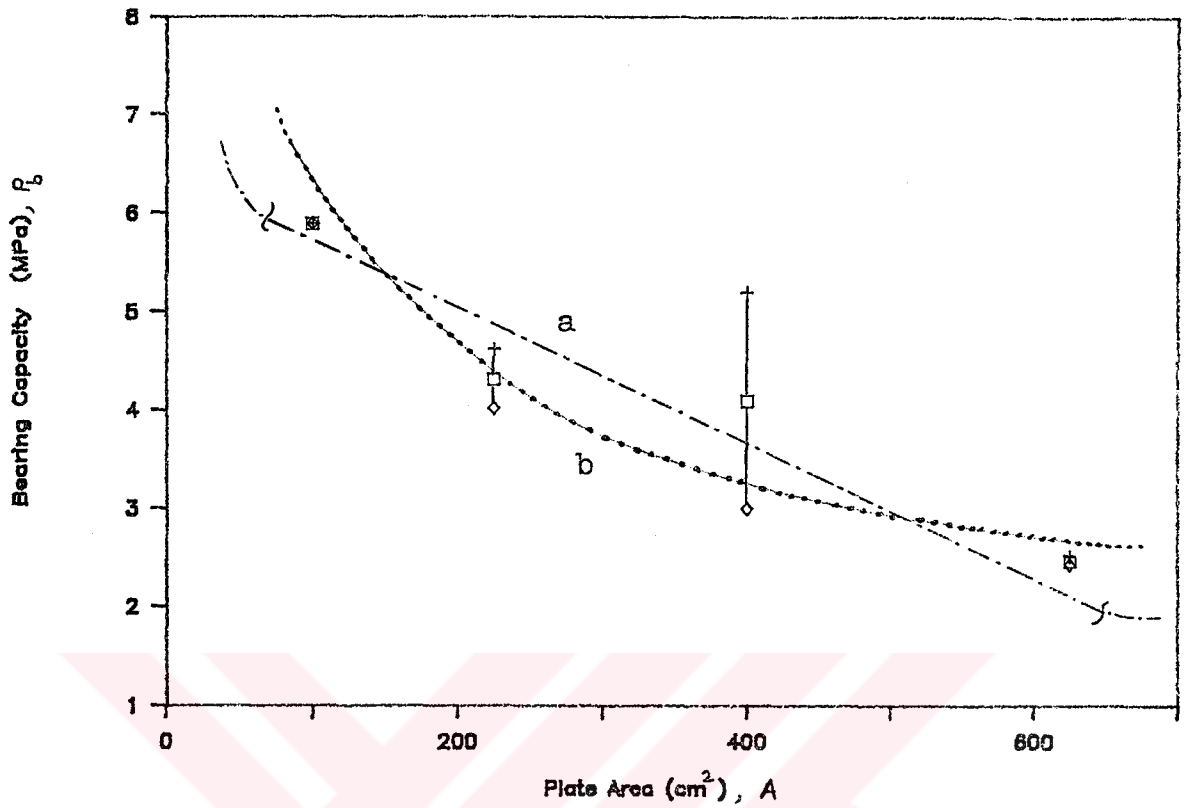
□ : Average bearing capacity values

+, ◇ : Limits of values , ± standard deviation

a) Linear regression ($P_b = 14.13 + (-0.017) \cdot A$)

b) Power regression ($P_b = 158.2 A^{(-0.533)}$)

Figure 11. Variation of bearing capacity with plate size for colemanite.



□ : Average bearing capacity values

+, ◇ : Limit values, \pm standard deviation

a) Linear regression ($P_b = 6.42 + (-0.0071) \cdot A$)

b) Power regression ($P_b = 46.49 A^{(-0.439)}$)

Figure 12. Variation of bearing capacity capacity with plate size for ulexite.

types can be seen in Figures 13, and 14. These curves usually give us very good indications about the failure mechanism, that is, if the failure mode is punching type or brittle cracking type under the load plate. Generally floor failure initiated from the periphery of the base plates and propagated mainly outwards with abrupt surfaces of fracture in nearly all tests, on clay banded limestone. The mode of fracture beneath the base plates, tended to propagate outwards from the corners with 5-25 cm extension along each stratum. In Seam 4, on clay banded limestone, vertical cracks propagated into next stratum when the upper one was crushed away. After cracking and crushing of all thinly bedded, laminated, clay banded limestone stratum, applied load started to affect Layer 2, clay banded limestone. However, crushed material of Layer 1 acted as a cushion above the layer 2. So applied load was not fully affected by this strata, some part of it was used for further crushing and compaction of pre-crushed Layer 1 of Seam 4 floor strata. After compaction of that material applied load started to affect Layer 2 directly.

As seen in Figure 16 failure modes of clay banded limestone under Seam 2 was different. It was observed that clay banded limestone under Seam 2 was divided into layers in addition vertical cracks divided it into midsize blocks. Therefore, fractures propagated both vertically and horizontally. Failure mode of second layer of clay banded limestone under Seam 4 was different than other clay banded

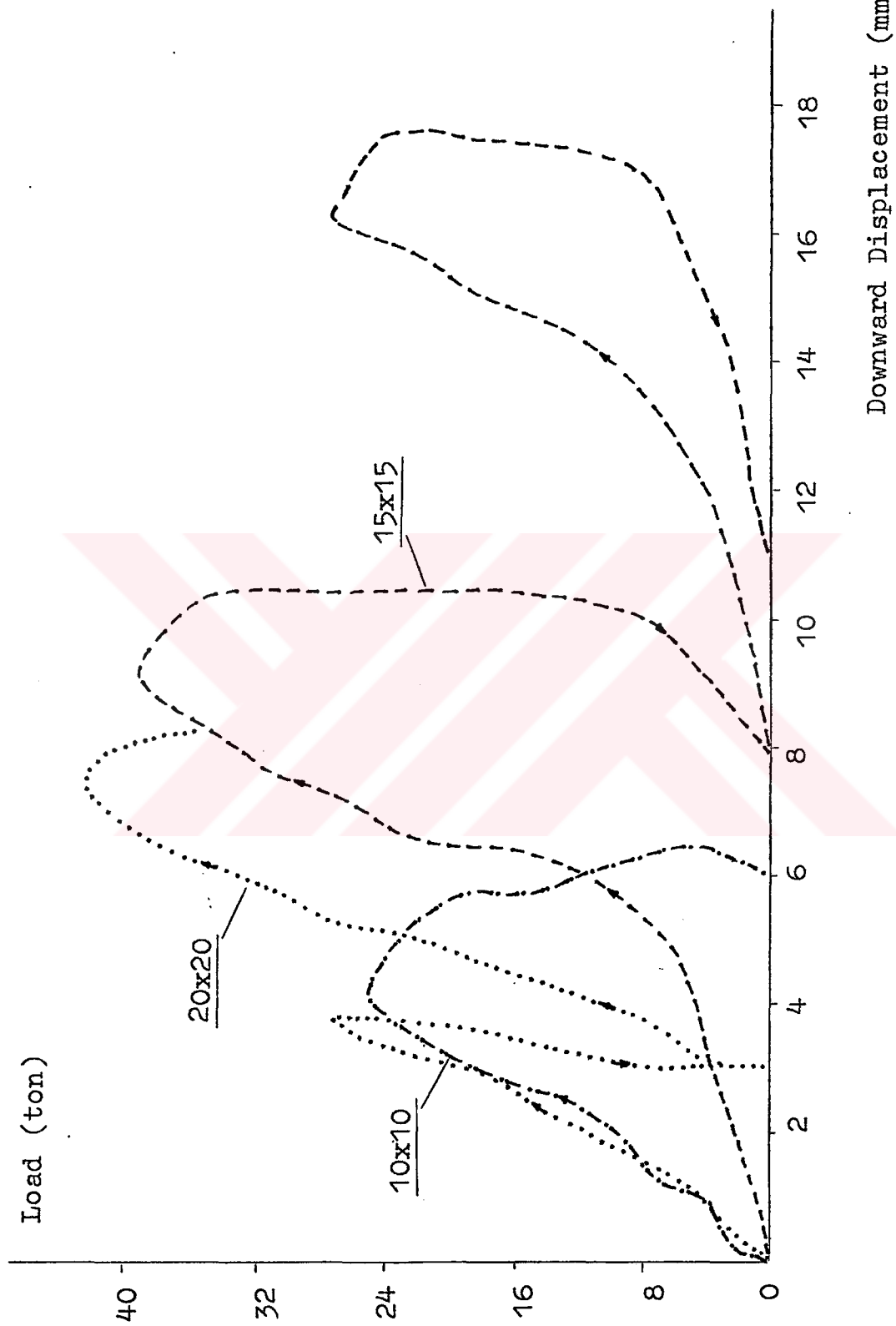


Figure 13. Typical Load-displacement curves for plate loading of clay banded limestone
 (Plate size ; cm x cm)

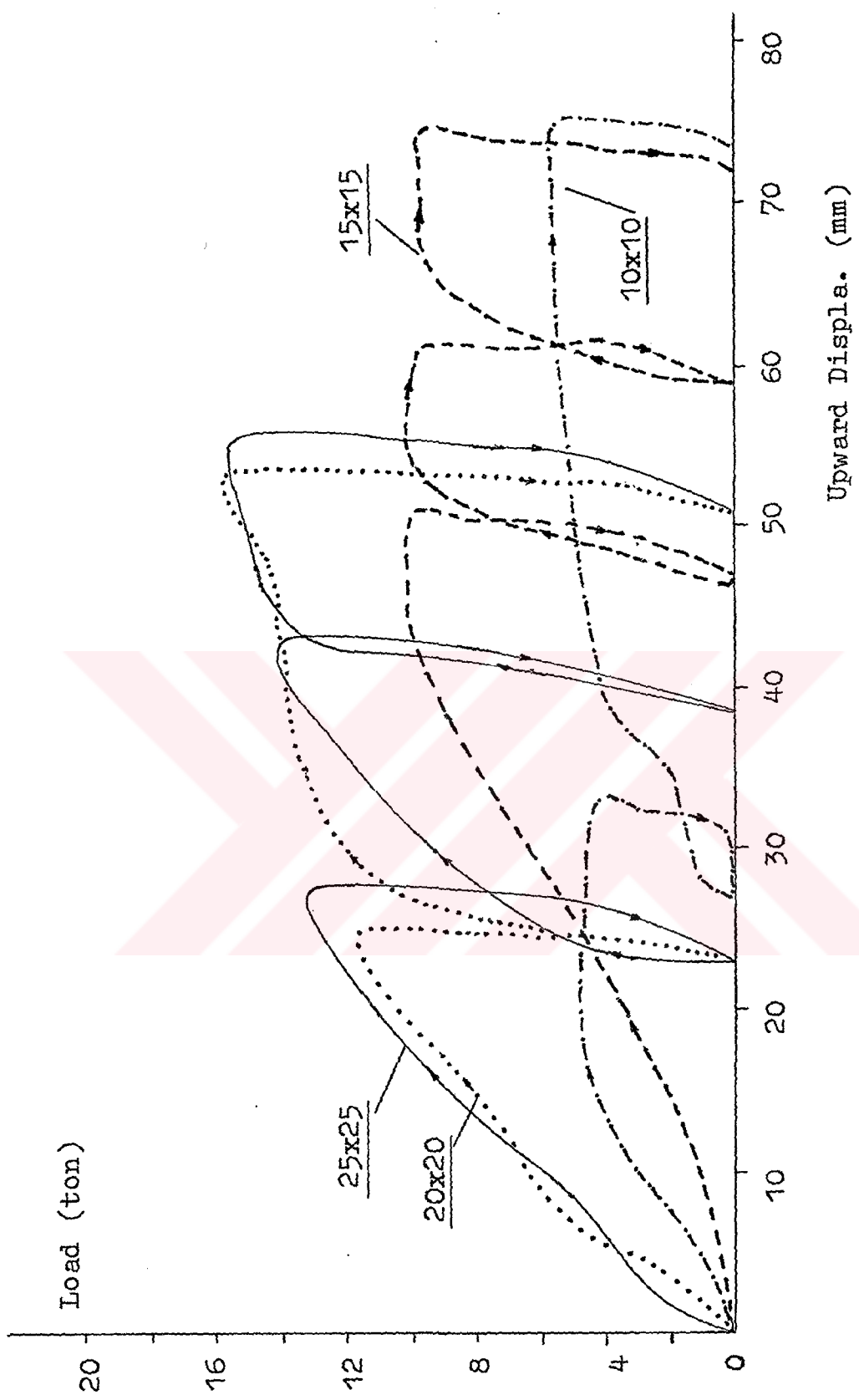


Figure 14. Typical Load- Displa. curves for plate loading of ulexite
 (Plate size ; cm x cm)

limestone strata. When the applied load reached strata's maximum bearing load; strata suddenly cracked into blocks around the periphery of plate. It was observed that there was no visible cracks around base periphery before the final failure of strata, at the maximum load point.

Bearing capacity tests showed that colemanite with high clay content and especially ulexite had punching type of failure modes under plate loading as shown in Figure 17. When loading plate was penetrating into the strata continuously with increasing load, there was no visible cracking around the plate. This was because clay material under the load plate was compacted, and colemanite and ulexite crystals in this clay material were crushed under the plate load. Generally ulexite and colemanite with high clay content showed plastic type (punching type) failure mechanism, especially when they were in a disturbed condition by the longwall operation. However, tests performed at the starter raise of Panel III showed that undisturbed colemanite strata with a very little clay content had typical brittle failure mechanisms. But, when the face started advancing cracking and crushing weakened the strata, and thus the strata started showing plastic or punching type failure mechanisms under plate loading.

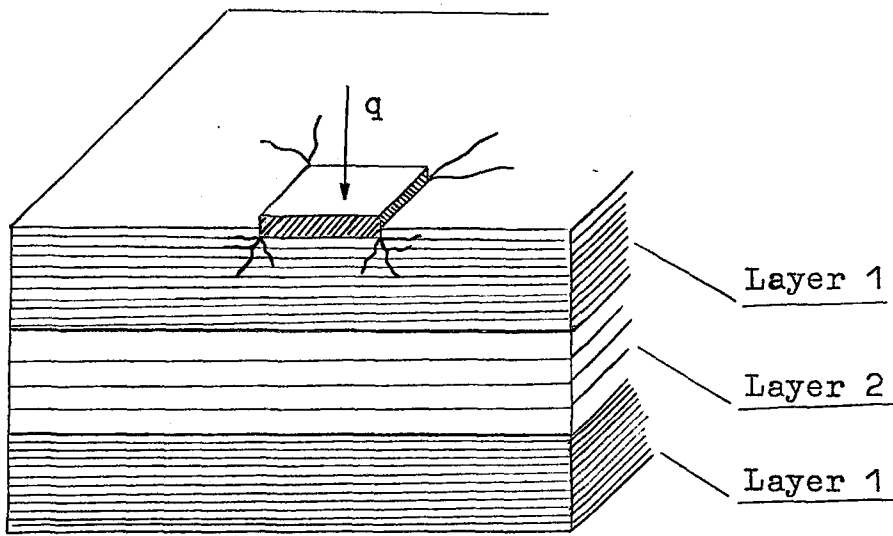


Figure 15a. Failure mode of clay banded limestone (thinly bedded) under Seam 4

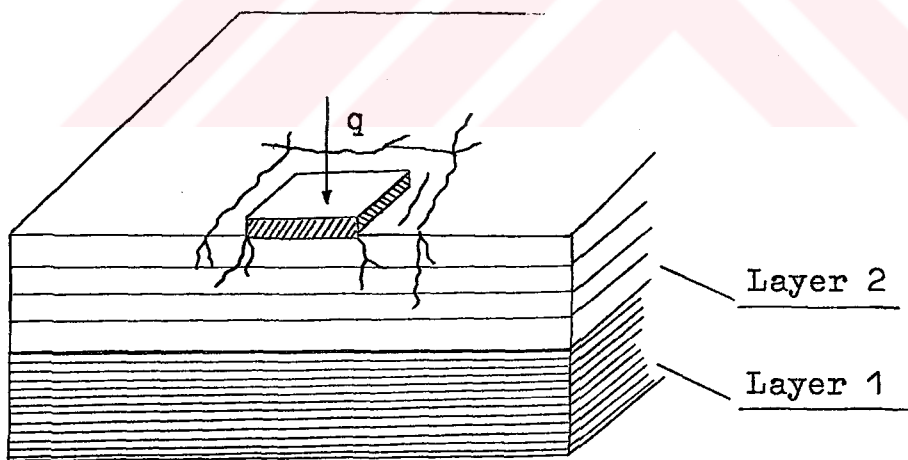


Figure 15b. Failure mode of clay banded limestone under Seam 4

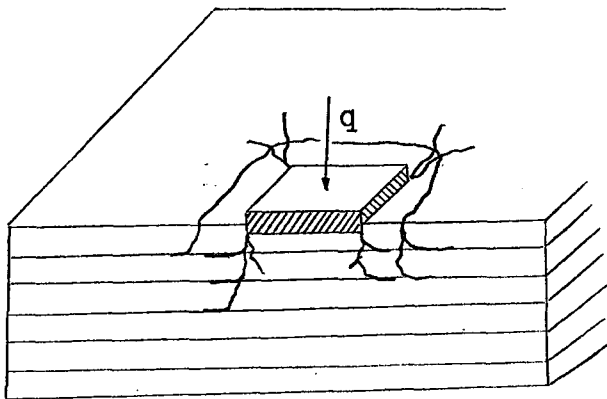


Figure 16. Failure mode of clay banded limestone under Seam 2

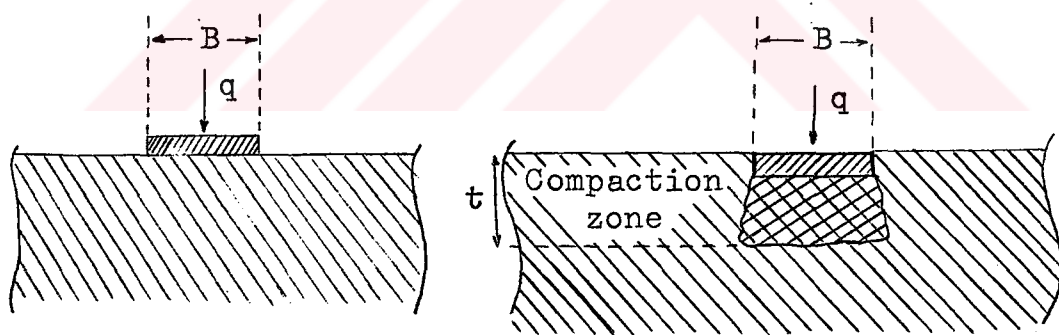


Figure 17. Punching failure mode for ulexite and colemanite.
($t = 2.B$)

4.5. Comparison of Results With Theoretical Estimation of Bearing Capacity

Barry and Nair (1970) used penetrometer and plate bearing tests to determine the in-situ bearing capacity of roof and floor strata. They concluded that the bearing capacities are independent of plate size if square or rectangular plates are used. They investigated the size effect for circular plates.

Rhodes et. al. (1978) compared the results from plate bearing tests with the results of laboratory triaxial tests, concluding that the in-situ tests are effective in determining the bearing capacity of the floor and assessing its time-dependent behaviour.

The effect of base plate's width vary with rock types. For the soft and plastic rock the bearing capacity increases with the base width or diameter. But for the brittle and elastic rock, it depends on the base type. For flexible bases with uniform pressure distribution, the bearing capacity is independent of the base size whereas for rigid base it varies inversely with the base width.

Several investigators (Afrouz (1975), Peng and Chiang (1984)) performed bearing capacity tests on underground coal mine floors and they suggested the following size relationship for plate bearing capacity

$$P_b = k A^m \quad \text{or} \quad P_b = k(B^2)^m \quad \text{for square base} \quad (4.1)$$

Sometimes, results are expressed in terms of P_{max} and B as;

$$P_{max} = K.B^n \quad (4.2)$$

where; k, m, K, and n are constants which equalize the equations.

A is the area of the base plate.

B is the width of the plate or diameter of plate.

P_{max} is the maximum load applied when the floor fails.

For the expression in (4.2), when $n=2$, P_b is constant and there is no size effect. When $n < 2$ there is a size effect on P_b and plate bearing capacity decreases with increasing plate size. When $n > 2$, which happens in testing soft clays, P_b increases with increasing plate size.

Constants K and n which are given in Table 16 and show the relation between maximum failure load (P_{max}) and plate width (B). These coefficients were determined for different rocks by several investigators. When the results of field tests in Simav mine are compared with others, it is seen that changing the plate size effects rock types around Simav mine more than coal measure rocks.

Value of power n is small for colemanite, so size effect for this rock is more pronounced than other rocks. Clay banded limestone and ulexite have almost the same n value controlling the plate size changes.

Table 16_a. Bearing capacity coefficients (by various invest.)

$P_{max} = K \cdot B^n$, P_{max} = max load (ton) , B= plate width (cm)				
Investigator.	Rock Type	K	n	B
Bary (1970)	Shale	0.8603	1.28	2.54-30.48
Lee (1961)	Coal	0.4134-1.5340	1.0-1.15	2.54-15.24
	Sandy shale or fireclay	0.2026-0.4573	1.5-2.0	" "
	Soft clay	0.0012-0.0092	2.4-3.0	" "
Jenkins (1958)	Medium hard shale	0.3940-0.1550	1.0-2.0	" "

Table 16_b. Bearing capacity coefficients at Simav mine

$P_{max} = K \cdot B^n$, P_{max} = max load (ton) , B= plate width (cm)				
	Rock Type	K	n	B
Field Results in Simav Mine	Colemanite	1.580	0.932	10-25
	Ulexite	0.465	1.122	"
	Clay banded limestone	0.972	1.148	"

Table 17a. Coefficients of bearing capacity with respect to base area.

$P_b = k + m \cdot A$, $P_b = \text{max. bear. cap. MPa}$ $A = \text{base area cm}^2$				
Rock Type	k	m	A	cor. ratio
Colemanite	14.146	-0.017	100-625	0.99
Ulexite	6.416	-0.0071	"	0.95
Clay Banded Limestone	14.447	-0.016	"	0.97

Table 17b. Coefficients of bearing capacity with respect to base area by using Power Law.

$P_b = k \cdot A^m$, $P_b = \text{max. bearing cap. MPa}$ $A = \text{base area cm}^2$				
Rock Type	k	m	A	cor. ratio
Colemanite	158.24	-0.534	100-625	0.91
Ulexite	46.50	-0.439	"	0.89
Clay Banded Limestone	97.17	-0.426	"	0.89

Table 18. Coefficients for bearing capacity with respect to base periphery / base area.

$P_b = k + m \cdot (P/A)$, $P_b = \text{max. bearing capacity, MPa}$ $P/A = \text{ratio of Periphery/area, cm}^{-1}$				
	Rock Type	k	m	P/A
Afrouz(1975)	Floor coal (Thickness range ; 45.7-81.3 cm)	0.02	42.2	0.25-0.4
Field Test Results in Simav Mine	Colemanite	1.074	29.69	0.16-0.4
	Ulexite	0.986	12.61	"
	Clay Banded Limestone	2.996	25.29	"

When test results are analysed with power law for a particular rock type as seen in Table 17, and when power factor m is high, this means a stronger size effect for this rock. When the results of tests are interpreted with linear regression which gives a higher correlation factor, a better interpretation of size effect is possible. When multiplication factor m is close to zero, this means a very weak size effect, and $m=0$ means there is no size effect, m values for the linear regression showed that ulexite has a smaller size effect compared with colemanite and clay banded limestone which have almost similar coefficients for changing plate size.

Table 18 shows the relation between P/A ratio to the maximum bearing capacity and this give an opportunity to compare the field test results with the result of Afrouz (1975). This table also shows that ulexite is the least effected rock from the size effect.

4.6. Comparison of Field Results With Theoretical Estimations

After determining the strength parameter of rocks; Bearing capacity formulas given in the beginning can be used to estimate the bearing capacity of related strata. Then, the estimated values can be compared with the field data.

Internal friction angles from triaxial tests for clay banded limestone, colemanite, and ulexite are 24.5° , 41° ,

and 31 respectively and these used in calculations. Calculations have been conducted by using Table 1. and results are tabulated in Table 19. Skempton's approach is the best between three of them.

According to Bieniawski (1967) , and Singh (1980) uniaxial compressive strength of rocks is effected by the specimen size. If the spesimen sizes used in the laboratory and size corresponding to the volume of rock under the loading plate are correlated with each other, a reasonable ratio could be estimated by using results of Bieniawski (1967) and Singh (1980). This ratio was estimated to vary between 0.2 - 0.3 for field tests performed in Simav Mine. Field compressive strength values were estimated by using a reduction ratio of 0.2 . When the laboratory strength values are reduced to the field values by using the related ratio, calculated bearing capacity values are close to in-situ field test results. However, modified Terzaghi and Brich & Hansen's approaches give higher bearing capacity values with respect to field results. Modified Terzaghi approach gives approximately 6 times higher value and Brich & Hansen approach gives 2 times higher values. These emprical formulas fully depend on internal friction angle of rock. A little change of internal friction angle causes a large change in bearing capacity.

Table 20 shows results of Goodman, (with Mohr and Coulomb failure criteria), and Hoek & Brown approaches. Generally, average values of Hoek & Brown approach fit well

with in-situ test results. In fact limit results of this approach are in the range of in-situ results considering the standard deviations. Results of Goodman's approach are similar with field tests if the reduced field compressive strength values are used during calculations. Average value of this approach also fits well with the field test results. As a result, provided that m , s , m_r , and s_r values of rock can be determined or in-situ compressive strength value of the same rock is known; Goodman and Hoek & Brown's failure formulas give close estimates of real bearing capacity values for that rock.

Approaches from foundation engineering give higher bearing capacity values with respect to field values. If the cohesion, internal friction angle and density of rock were determined from field tests they could give close estimates of real field bearing capacity.

Table 19. Calculated bearing capacity values by using analytical approaches of Foundation Engineering

Reduction Ratio for Comp. Streng.	Rock Type	Modified Compressive Strength Co MPa	Measured Av. Bear. Capacity MPa	Calculated Bear. Cap. STEMPTON Approach MPa	Calculated Bear. Cap. Mod. TERZAGHI Approach MPa	Calculated Bear. Cap. BRICH-HANSEN Approach MPa
1.0	Clay Banded Limestone	19.43	9.26	37.90	158.73	64.01
0.2	"	3.88	"	7.56	31.64	12.01
1.0	Colemanite	17.33	9.14	23.52	427.35	108.79
0.2	"	3.46	"	4.69	85.03	21.64
1.0	Ulexite	14.78	4.18	25.02	177.10	62.49
0.2	"	2.95	"	5.00	35.25	12.44

Table 20. Calculated bearing capacity values by using Mohr-Coulomb and Hoek-Brown Failure Criteria.

Reduction Ratio	For Comp. Stress	Rock Type	Modified Comp. Strength Co MPa	Calculated Bearing Capacity MOHR-COULOMB Failure Criterion MPa			Calculated Bearing Capacity HOEK-BROWN Failure Criterion MPa			Measured Average Bearing Capacity MPa
				Min.	Ave.	Max.	Min.	Ave.	Max.	
1.0		Clay Banded Limestone	19.43	42.13	65.38	3.88	7.77	12.99	9.26	
0.2		"	3.88	8.01	13.05	"	"	"	"	
1.0		Colemanite	17.33	38.60	102.07	3.46	6.93	11.59	9.14	
0.2		"	3.46	7.40	20.38	"	"	"	"	
1.0		Ulexite	14.78	47.71	61.04	2.95	5.91	9.89	4.18	
0.2		"	2.95	9.29	12.18	"	"	"	"	

5. FLOOR PENETRATION OF HYDRAULIC PROPS

5.1. Design of Base Plates With Respect To the Penetration Load

After determining the bearing capacity of strata and determining the design load density in the longwall face, further work should go on for analysing the penetration and failure load of hydraulic supports. In this chapter, penetration load will be calculated for circular base plates with diameters 20, 25, 30 cm. During calculations, size effect, and standard deviations will be examined and estimated penetration loads will be given with calculated standard deviations. Then, calculated penetration loads will be compared with the measured and predicted load values for the individual hydraulic props to find out if the proposed base plate size is sufficient to prevent the penetration of the hydraulic props under these load levels.

General results of load measurements on the existing timber support members, Pasamehmetoglu et. al.(1987), in longwalls of Seam 2 and Seam 4 varied from about 12 to 25 tons with spacing of timber members changing between 0.5 to 1 m. These values were taken into account in evaluating a proposed base plate.

Bearing capacities of the strata were obtained for square base plates, however penetration load will be calculated for circular base plates. In fact, square base plate creates more (about 1.1 times) stress concentration

especially at the corners, with respect to circular base plate. Therefore, calculation of penetration loads based on the results with square section plates has already a safety factor which is about 1.1 times.

5.1.1. Failure Loads for Clay Banded Limestone

During calculation; three different plate diameters will be examined. Firstly bearing capacity values for three plate sizes will be obtained from size effect figure, (Figure 10) . Then failure load will be calculated by multiplying these capacities by the related plate area

$$P_{\max} = P_b \cdot A \quad , \quad P_{\max} = P_b \cdot (d^2/4)$$

where; P_{\max} is the failure load. P_b is the bearing capacity value and A is the plate's base area. Failure loads which were calculated from above formula are tabulated in Table 21. According to that result, lower limit of failure load for plate which has 25 cm diameter is about 28 tons. Therefore with a 25 cm base plate, possibility of penetration is small according to this precalculation based on the measured loads. When hydraulic supports are used in longwall, load distribution along the longwall is expected to be better with respect to conventional timber prop-packs support's condition. In addition, increasing face advance rate decreases the maximum load which comes on props and it also decreases floor heaving in longwalls. When the floor strata are

subjected to heaving due to slow rate of advance, floor strata's bearing capacity decreased because of cracking perpendicular to bedding and separation parallel to bedding. Failure loads or penetration loads, which are given in Table 21 are results of tests performed on heaved floors. Therefore, if the rate of longwall face advance is expected to be high, average failure loads given in Table 21 can be used safely.

Bearing capacity tests performed at the starter raise of Panel III showed that average capacity was about $P_b = 6.0$ MPa for 15×15 cm plate size. But after several weeks; face advanced towards the mid-point of Panel III, and extra tests were performed. These tests gave a little higher values but if that weak floor condition under the colemanite seams will exist in future penetration load approach should be checked for 25 cm plate diameter again. If bearing capacity value for this weak floor strata is taken around $P_b = 4.2$ MPa keeping the size effect in mind, maximum load for clay banded limestone under colemanite seam will be $P = 20.6$ tons for 25 cm plate diameter. According to this result, if load coming on hydraulic props in colemanite longwalls is smaller than 20 tons then failure will not occur. Support load measurements showed that maximum measured load on timber members was 15 tons in colemanite of Seam 2. However, in order to be on the safe side plate with a 30 cm diameter should be used, or a special plate design which is

illustrated in Figure 18_d might be used in such a weak strata condition.

Another alternative for weak strata condition is to leave colemanite with a certain thickness to create artificial floor strata. This subject will be interpreted in the next section of this chapter.

5.1.2. Failure Loads for Colemanite

As it was explained before Seam 2 is mined with downward slicing. If the colemanite is the floor strata of the longwall, failure load for three different plate sizes can be obtained from Table 22. These failure loads are calculated according to average bearing capacity of colemanite determined as $P_b = 9.14 \pm 4.17$ MPa. This average capacity was determined from tests which were performed when the colemanite was at the roof. Further tests were carried out while colemanite was at the floor, and it was observed that their results were similar to each other. Bearing capacity of colemanite as the floor strata unit was measured averagely as $P_b = 7.44 \pm 2.0$ MPa. So, bearing capacity values which were obtain from the roof testing can be used during failure load determination of the floor.

The results of calculation show that plate dimension $d = 25$ cm suggested for clay banded limestone is expected to give good working condition without giving any failure.

Table 21. Penetration loads for clay banded limestone
(under Seam 4 and Seam 2)

Plate Dia. (cm)	Plate Area (cm ²)	Bearing Capacity (MPa)	Penetration Load (ton)		
			Minimum	Average	Maximum
20	314	10.4 ± 4.2	20.0	35.5	46.0
25	491	8.8 ± 3.1	28.0	43.2	58.4
30	707	8.2 ± 2.0	43.8	58.0	72.1

Table 22. Penetration loads for colemanite

Plate Dia. (cm)	Plate Area (cm ²)	Penetration Load (ton)		
		Minimum	Average	Maximum
15	177	8.79	16.17	23.56
20	314	15.60	28.70	41.79
25	491	24.40	44.87	65.35
30	707	35.14	64.62	94.10

5.1.3. Failure Loads for Ulexite

As seen in Table 15 the highest bearing capacity values around the seams were determined for ulexite. Mining method in Seam 4 was retreat longwall with sublevel caving, so that ulexite will not be the floor strata unit in Seam 4. In addition, floor strata of the Seam 4 are strong. So, there is no need to leave ulexite under Seam 4 for obtaining a good floor condition. Whereas ulexite will be floor strata during Seam 3 's upper part slicing. Results of failure load analysis are given in Table 23 . These results were found from average in-situ bearing capacity of ulexite which is equal to $P_b = 4.18 \pm 1.3$ MPa. One thing not to be forgotten that, these failure loads were found from the tests which were performed while ulexite was at the roof. Therefore, it might have contained cracks, crushed and weakness zones. These types of discontinuities may not developed if the ulexite is left as the floor strata. Rapid advance of longwall faces and uniformly distributed prop loads will prevent any failure problems when ulexite is left as the floor. Moreover, if any difficulties are created during Seam 3 's upper slice mining a layer of colemanite will be left to act as an artificial floor, since colemanite has higher failure loads with respect to ulexite.

Table 23. Penetration loads for ulexite

Plate Dia. (cm)	Plate Area (cm ²)	Penetration Load (ton)		
		Minimum	Average	Maximum
15	177	5.10	7.40	9.70
20	314	9.04	13.12	17.20
25	491	14.14	20.52	26.90
30	707	20.36	29.55	38.74

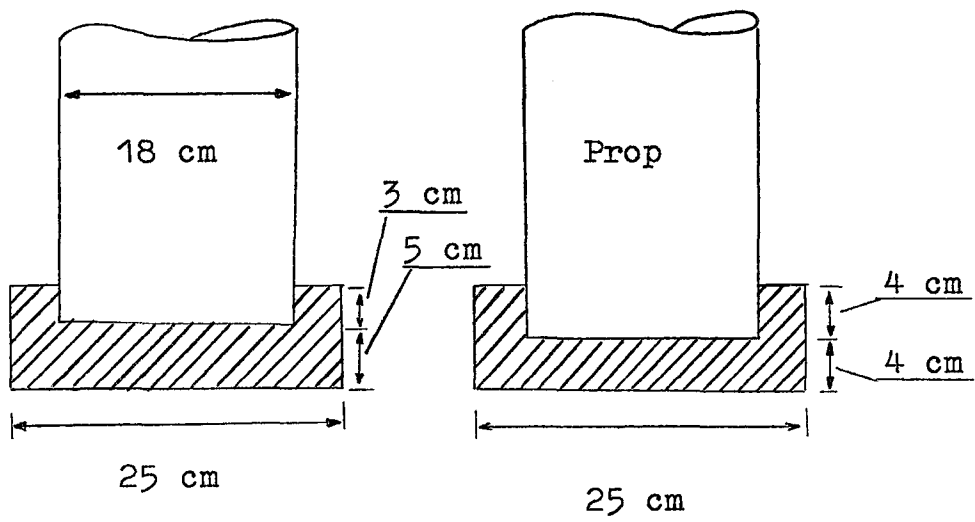
5.1.4. Suggested Base Plate Design for Hydraulic Props

Figure 18 shows suggested plate shapes, their dimensions and their weights. Plate thickness were chosen around 8 cm, so if load on the face prop increased to failure and penetration started, it would take time to penetrate through all the thickness of the base plate. It was measured that convergence rate in longwalls supported with timber was about 2.5-3.0 mm per hour. Moreover, it should be borne in mind that setting load of timber was always lower than required value due to lack of good setting operation. When hydraulic supports were started to be use, convergence rate would decrease up to about 0.5 mm per hour due to uniformly distributed load over the props in the longwall and sufficient setting load. After setting the hydraulic supports near the face line, it would take about 10 hours for reaching the failure load of strata and it would take an additional 120 hours for penetration of all the base plate. However hydraulic props would be moved in this time interval due to the advance of the face, and hydraulic props would not be subjected to that maximum load too long.

Difference between Figure 18_a and Figure 18_b is, as seen in figures; the depth of hole machined for hydraulic prop's base. This is 1 cm deeper in Figure 18_b. This deeper hole decreases the weight of base plate about 2 kg. However thickness under the prop is more in Figure 18_a, which supplies a uniform stress distribution over the

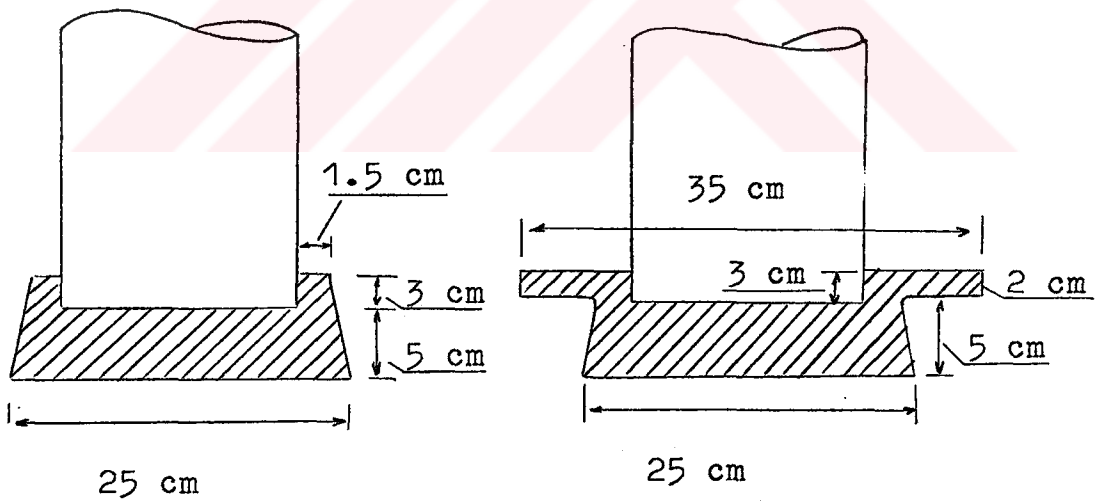
loaded area on the plate-rock contact. Therefore, effective area of load transfer at this contact will be higher for the plate of Figure 18_a. As a result of this, plate in Figure 18_a is suggested for safer working. In order to get better stress distribution in the rock and decrease the weight of plate, conical base plate is suggested, as seen in Figure 18_c. It has same advantages over plate designs suggested before : it's weight is smaller, but, the depth under the prop is enough to give a uniform stress distribution.

Figure 18_d shows another base plate design. In spite of it's heavier mass and difficulties during shaping, it has additional advantages over other plate designs. In order to explain these advantages, firstly failure mechanism of under that plate as seen in Figure 19 will be discussed, If the penetration of lower base starts along the diameter rock under the plate will fail and start to dilate due to cracking and crushing. Then this crushed zone apply a force to the rock surrounding the broken zone due to a volume increase (dilatation), and rock surrounding the broken zone moves upward. Further upward motion of the side rock will be restricted and confined when the expanding surface reaches the upper large plate above. Therefore, side rock heaving will be constrained. As a result of this effect, penetration rate of bottom plate decreases significantly. Moreover, upper plate also starts to distribute load over side rocks of bottom part.



a) $W=24.7$ kg

b) $W=22.7$ kg



c) $W=20$ kg

d) $W=27$ kg

Figure 18 . Typical suggested base plate and their weight.

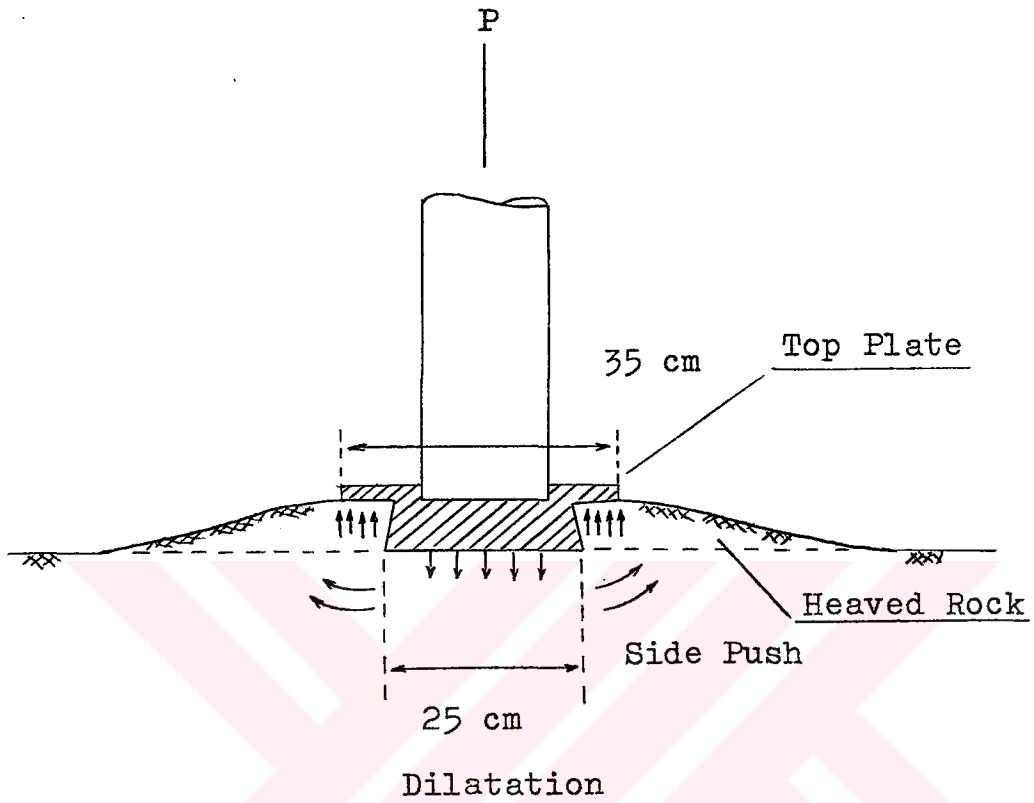


Figure 19. Penetration and failure mode under hydraulic prop with the special expanding cross-section base plate.

This confining effect increases rock strength, and thus bearing capacity is increased. Therefore, if this plate is used in longwalls, failure load of rock under this plate will increase up to 60 tons if minimum values were given in Table 21 for clay banded limestone are used. Another advantage of this plate is the resistance against any eccentricity of the loading.

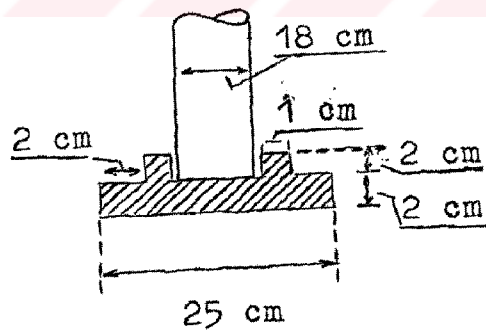
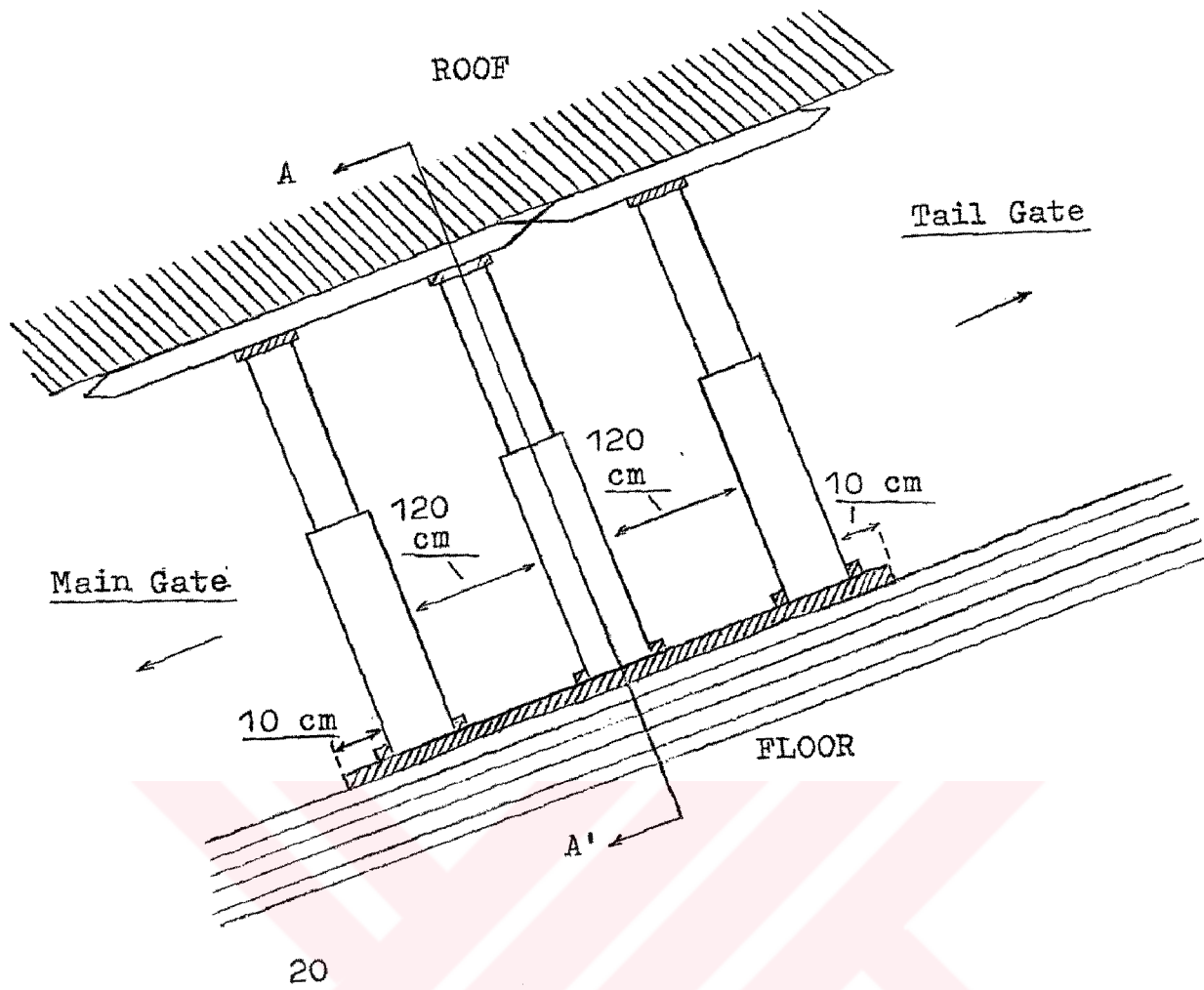
5.1.5. Alternative Precautions for Exceptionally Weak Floors

Test showed that weak strata conditions usually continued during the first 5-7 m advance from the starting point of panels. This weak strata condition was observed especially under Seam 2. Calculations were carried out according to tests performed at the starter raise of Panel III of Seam 2. According to the calculations this weakness zone is only able to carry about 20 tons when the largest design plate, 35 cm in diameter is used. Therefore, in situations like this, a thin colemanite layer should be left to resist prop loads until this zone disappears.

Thickness of colemanite layer proposed to be left during mining of Seam 3's upper slice and during mining of the panel starting zones, and other weakness zones, can be determined as follows ; colemanite layer should uniformly distribute prop's base load over the weak strata below suggested depth is equal to half of the base plate width. Therefore, in order to get stability,

thickness of colemanite layer should be about 20 cm for using a plate dimension of 25 cm in diameter. ($t=25/2$, $t=12.5$ cm ; for safety $t=20$ cm)

Design plates which were planned to be put under the prop have higher weight for practical operations. In order to eliminate this disadvantage and get higher contact area for better stability, steel bar is suggested to be placed under 3 props as a common plate,(Figure 20). This bar has a larger base area than prop's base plates. Therefore, loads coming from these 3 props will be distributed over a larger area which eliminates penetration of props. This steel bar is especially suggested for heaved strata and weak strata zones with this application, seams can be mined without leaving any layer as an artificial floor.



A-A' Cross-section

Figure 20. U-Shaped steel bar (common plate for three face props.)

6. ANALYSIS OF STRESSES AND FAILURE FOR LAYERED ROCK UNDER THE LOADING PLATE

6.1. Introduction

This chapter covers the theoretical analysis conducted to investigate the influence of discontinuities on the plate loading behaviour of the rock type tested during the field work.

The purposes of this analysis are;

a) Studying the effect of discontinuity spacing on the stress distribution in region underneath the plate.

b) studying the effect of stiffness parameters of the discontinuities on the stresses in the rock underneath the loading plate.

c) Investigating the effect of discontinuities on the bearing capacity failure of the bedded rock subjected to plate bearing test discussed in the previous chapters.

6.2. General Approach and Assumptions

Stress analysis is done by using the solutions given by C.M.Gerrard and W.J.Harrison (1970). These solutions involve simple loads of circular plan area applied to a homogeneous, linearly elastic and cross-anisotropic half space in which at any point, the axis of symmetry in the elastic properties is vertical. Formulas given in Appendix A are used in this section. Loads considered in

these formulas are applied uniformly over a circular plan area, although field tests have been conducted with loads applied to the rock by square-section load plates. With the exception of regions around corners for square plates, stress distribution in the rock under the plate is not expected to differ too much for circular and square loading plates, relatively simple solutions for circular plates are readily available. Since the major purpose here is to study the effect of discontinuities on the stresses and failure mechanisms of layered rock under the loading plate, it is decided to adopt solutions developed for circular loading plates on cross-anisotropic rock.

The existing solutions for axi-symmetric problems involving a cross-anisotropic half space are summarized in Table 24. All symbols related to elastic constants of cross-anisotropic rock are defined in the Appendix A, such as α , β . Among the solutions in the Table 24, the ones given by Gerrard and Harrison (1970) are more comprehensive than previous works in the following ways.

- i) Range of load types considered
- ii) Range of stresses and displacements solved
- iii) Range of cross-anisotropic material response considered

Cross-anisotropic concept here is assumed to involve a single joint set with a certain spacing S or a bedded rock with a spacing S again between the individual clay beds. Loading is assumed to be applied perpendicular to

Table 24. Summary of existing solutions (after Gerrard and Harrison, 1970)

Author	Type of Loading	Determined Stresses and Displacements
Michell (1900)	Vertical point load	w on surface of half space; stresses throughout half space
Barden (1963)	Uniform vertical pressure	σ_z on load axis w on surface
Wolf (1935)	Vertical point load	Stresses and displacement in half space
Quinlan (1949)	Vertical point load	Stresses and displacement in half space
Koning (1957)	Vertical point load & Uniform vertical displace.	All stresses and displacements in half space
Anon (1960)	Uniform vertical pressure	w on surface at centre and edge of load σ_z down load axis
Lekhnitskii (1963)	Vertical point load	All stresses throughout half space
Gerrard (1968)	Uniform vertical pressure Uniform vertical displacement Linear radial shear stress Torsional loads	All stresses, strains, and displacements in half space

the joint or bedding planes. The presence of joints increases the void ratio of the rock mass and causes its modulus of deformation to be less than that of the rock substance. Deformation properties of a single joint plane in a set can be represented by a unit normal stiffness coefficient, k_n and unit shear stiffness coefficient, k_s defined by :

$$\sigma = k_n \cdot A_n \quad , \quad \tau = k_s \cdot A_s \quad (6.1)$$

where ; σ : The average normal stress on the joint, (MPa)

τ : The average shear stress, (MPa)

A_n : Normal deformation or closure of the joint, (m)

A_s : Shear deformation parallel to the joint, (m)

k_n : Normal stiffness coefficient, (MPa/m)

k_s : Shear stiffness coefficient, (MPa/m)

If the joints are spaced apart with a spacing S as in the cross-anisotropic rock mass, total normal deformation, A_n , consists of the contribution by the rock substance and by the joints.

$$A_n = \sigma \cdot \left(\frac{S}{E} + \frac{1}{k_n} \right) \quad (6.2)$$

The composite modulus of deformation of the rock mass, E_n can be found by equating the total normal deformation, A_n

$$A_n = (\sigma \cdot s) / E_n \quad (6.3)$$

of the rock mass to the A_n in equation (6.2), and from here ;

$$E_n = \left(\frac{1}{E} + \frac{1}{s \cdot k_n} \right)^{-1} \quad (6.4)$$

After Kulhawy (1978), and Goodman (1980)

Similarly, the composite shear modulus of the rock mass is as follows :

$$G_{ns} = \left(\frac{1}{E} + \frac{1}{s \cdot k_s} \right)^{-1} \quad (6.5)$$

where first subscript n denotes normal to the discontinuity plane and s corresponds to the tangential direction. Altogether, G_{ns} , corresponds to a shearing in n - s plane. By using these approaches and simplifications, laminated and bedded rock under the loading plate can be represented by an "equivalent" homogeneous rock and "equivalent" material properties of this rock can be used in computations to study the stress-distributions and the failure mechanisms.

Typical bedding planes in the region were subjected to shear testing in the laboratory and the results including average values of k_n and k_s were previously given with the laboratory results in chapter 2. Results of deformability tests on major rock types and values of k_n and k_s from shear tests are generally used in the following analysis.

6.3. Solution Technique and Input Parameters

Stress and displacement formulation of Gerrard and Harrison (1970) given in Appendix A were adopted into a specially prepared computer program. This program for isotropic and cross-anisotropic half space under a circular loading area give stresses and displacements along vertical z-axis where $r=0$ and along horizontal r-axis where $z=0$.

As seen in Appendix A, for bedded (cross-anisotropic rock) rock, five elastic constants a,b,c,d, and f are used in stress-strain relations. For relating strains to stresses for the coordinate system of Figure 21.

(Goodman (1980))

$$\begin{bmatrix} \epsilon_z \\ \epsilon_y \\ \epsilon_x \\ \gamma_{zy} \\ \gamma_{zx} \\ \gamma_{xy} \end{bmatrix} = \begin{bmatrix} 1/E_z & -\nu_{zx}/E_x & -\nu_{zx}/E_x & 0 & 0 & 0 \\ -\nu_{zx}/E_x & 1/E_x & -\nu_{xy}/E_x & 0 & 0 & 0 \\ -\nu_{zx}/E_x & -\nu_{xy}/E_x & 1/E_x & 0 & 0 & 0 \\ 0 & 0 & 0 & 1/G_{zx} & 0 & 0 \\ 0 & 0 & 0 & 0 & 1/G_{zx} & 0 \\ 0 & 0 & 0 & 0 & 0 & R \end{bmatrix} \begin{bmatrix} \sigma_z \\ \sigma_y \\ \sigma_x \\ \tau_{zy} \\ \tau_{zx} \\ \tau_{xy} \end{bmatrix}$$

$$\text{where ; } R = \frac{2 \cdot (1 + \nu_{xy})}{E_x}$$

(6.6)

$\epsilon_z, \epsilon_y, \epsilon_x, \sigma_z, \sigma_y, \sigma_x$ are normal strain and stress components.

$\gamma_{zy}, \gamma_{zx}, \gamma_{xy}, \tau_{zy}, \tau_{zx}, \tau_{xy}$ are shear strain and stress components.

E_x, E_z are moduli of elasticity in horizontal and vertical directions.

ν_{zx}, ν_{xy} are Poisson's Ratios and first subscripts corresponding to the direction of loading and second subscripts showing strain " or expansion direction" perpendicular to the loading axis.

This matrix notation was temporarily introduced here to explain the input procedure for material properties of the bedded rock. As seen in relation (6.6) there are again five independent elastic constants for strain-stress relation of bedded rock. In the program, to be consistent with Gerrard and Harrison formulation, z, x, and y axes are also labeled as h and v denoting horizontal and vertical directions. Finally, using the equivalent isotropic medium approach and using v and h subscripts for vertical and horizontal directions input values of material constants in terms of $E, \nu, k_n, k_s,$ and s are calculated in the beginning of the program as :

$$\begin{aligned}
 \nu_h = \nu_{xy} = \nu & \quad , \quad \nu_{vh} = \nu_{zx} = \frac{E_v}{E} \cdot \nu \\
 \nu_{hv} = \nu_{xz} = \nu & \quad , \quad E_v = \left((1/E) + (1/k_n \cdot s) \right)^{-1} \\
 E_h = E & \quad , \quad G = G_{xy} = \frac{E}{2 \cdot (1 + \nu)} \\
 F = G_{zx} = \left((1/G) + (1/s \cdot k_s) \right)^{-1} & \quad (6.7)
 \end{aligned}$$

Then the program carries out the calculations by using the method of solution and formulations in the Appendix A .

6.4. Results of Stress Analysis

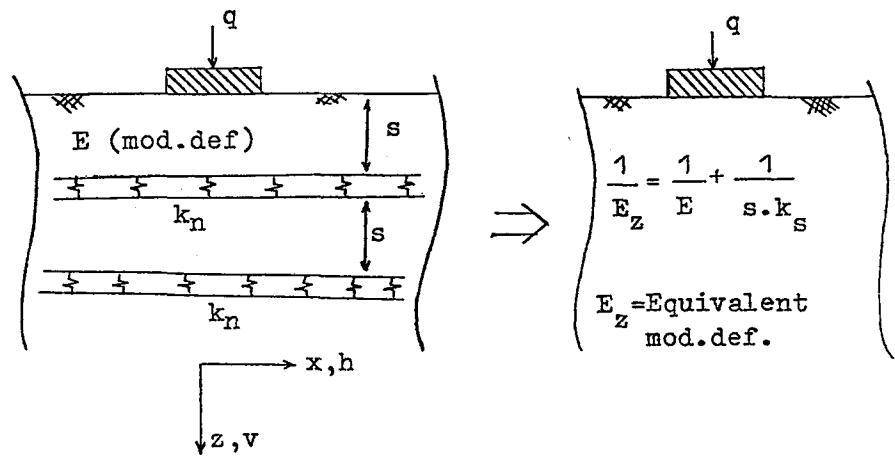
6.4.1. General Interpretation of Results

In order to show differences between stress distributions in cross-anisotropic rocks and isotropic rocks , results determined from the computer analysis, a series of curves was plotted in the next section.

Input data of the program was changed to investigate the influence of bed spacing and stiffness parameters of discontinuities. In order to study the effect of spacing on the stresses and displacements, elastic constants were defined in terms of stiffness and spacing as explained in the preceeding section.

Analyses were carried out to obtain stresses σ_z , σ_r , σ_θ under the loading plate, and the displacements under the plate; w, u . These were computed along two lines, $r=0$ and $Z=0$, as seen in Figure 22.

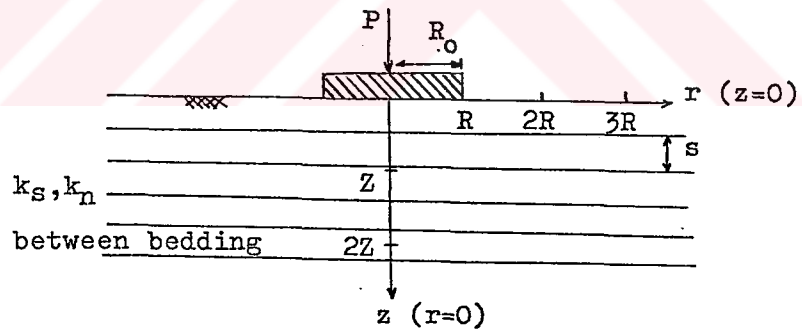
Curves for stress distribution and displacements will be presented in two sets. First set includes curves that show the effect of discontinuity spacing (s) and stiffness ratio (k_s/k_n) on radial stress (σ_r), tangential stress (σ_θ), vertical displacement (w), and radial displacement (u), at the surface ($Z=0$) around the edge of the plate for varying radial distance (r). Second set of curves includes



i) Layered cross-anisotropic rock mass.

ii) Equivalent homogeneous rock mass.

Figure 21. Representation of layered rock as homogeneous equivalent rock mass.



- σ_z = vertical stress at a point (MPa)
- σ_r = Radial " " "
- σ_θ = Tangential " " "
- W = Vertical displacement (m)
- U = Radial "

Figure 22. Coordinate system and the geometry of the problem.

variation of σ_z and $\sigma_r = \sigma_\theta$ with depth (Z) along $r=0$ line under the plate, again for different values of spacing (s) and the stiffness ratio (k_s/k_n).

Input parameters used in these analyses are given in Table 25. These parameters are chosen in such a way that the material behaviour represented by these parameters is very close to the behaviour of bedded rock tested in the field. Initial values of k_s and k_n in the table are the results of shear testing on typical bedding planes, and together with the initial value of spacing in the table they provide a good representation of the bedded rock tested in the field.

6.4.2. Discussion of Results of Stress Analysis

In Figures 23 and 24, σ_θ and σ_r are seen to approach infinity as $r/R_0 \rightarrow 1$ i.e. the edge of the loading plate. Tangential stress around the edge is compressive whereas radial stress, σ_r is tensile. Since $\sigma_z = 0$ and there is no shearing at the surface, this makes the radial stress minimum principal stress ($\sigma_3 = \sigma_r$) and the tangential stress maximum principal stress, ($\sigma_1 = \sigma_\theta$). Since the rock can not withstand infinite stresses, with the application of the load on the bearing plate there will be failure around the edge of the plate. Rocks are weak under tension. Therefore, failure possibly starts with a radial tensile crack around the edge perpendicular to the direction of $\sigma_3 = \sigma_r$. This mechanism has been used before for Mohr-Coulomb failure

Table 25. Input parameters of computer program

	Cross-anisotropic rock mass	Isotropic rock mass
Elastic Moduli (E)	3000 MPa	3000 MPa
Poisson's Ratio (ν) (for isotropic case)	0.25	0.25
Poisson's Ratio (ν_h) (effect of horizontal strain on complementary horizontal strain)	0.20	-
Applied Pressure (P)	8.0 MPa	8.0 MPa
Radius of Plate (R _o)	0.1 m	0.1 m
Internal Friction Angle (ϕ)	20°	20°
Normal Stiffness (k_n)	1000 MPa/m	-
Shear Stiffness (k_s)	3500 MPa/m	-
Spacing (s)	0.025 m	-

analysis in chapter 4. Stress concentrations at the surface that is the magnitudes of σ_r/P and σ_θ/P along $Z=0$ are seen to increase significantly for cross-anisotropic material. Much higher stress concentrations are observed for having closely spaced discontinuities with low values of k_n , i.e. increasing ratios of k_s/k_n . These results show that discontinuities and variations in their mechanical properties strongly influence the stress distribution, and thus the bearing capacity under plate loading.

Figure 25 shows that vertical displacement at the surface also increases dramatically with increasing spacing of discontinuities and either increasing k_s or decreasing k_n . This situation leads to high displacement gradients, i.e. surface strains, at the surface. Figure 26 shows dramatic increases for cross-anisotropic case the radial displacement at the surface compared with the isotropic case.

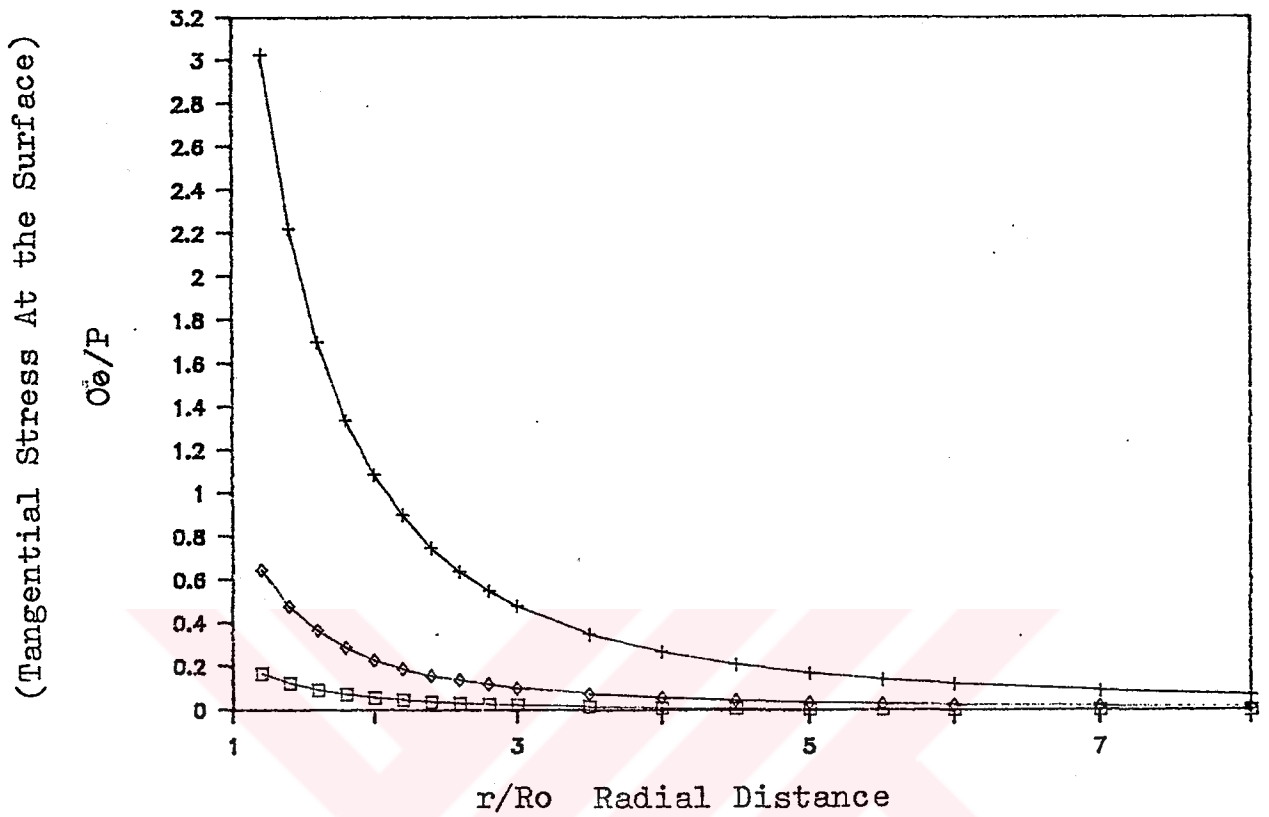
Figures 27 and 28 show the distribution of vertical stress σ_z and radial stress σ_r along the vertical symmetry axis $r=0$, since this is an axisymmetric problem and $r=0$ is the symmetry axis, $\sigma_r = \sigma_\theta$ and shear stress components $\tau_{r\theta} = \tau_{rz} = \tau_{\theta z} = 0$ along this axis. This means σ_z and $\sigma_r = \sigma_\theta$ are the principal stresses along Z at $r=0$. This is important in a failure analysis, since failure criteria are given mostly in terms of principal stresses. It is seen in these figures that stresses for isotropic case are hydrostatic, i.e. $\sigma_r = \sigma_z = \sigma_\theta$ right under the loading plate at the point $r=Z=0$. However, at the same point for cross-anisotropic

rock $\sigma_r = \sigma_\theta$ are different from σ_z . This means that anisotropy introduces large stress differences under the loaded area, and stress differences in general is what causes the failure of rocks. During a compressive Mohr-Coulomb failure analysis in the next section, this point will be seen in detail. An interesting point in Figure 28 is the existence of tensile stresses under the loaded area. It is seen in the figure that radial stress becomes tensile after a certain point along Z-axis. These tensile stresses increase with increasing discontinuity spacing and k_s/k_n ratio. Again, since rocks are weak under tension, this situation will also lead to increased cracking and reduced bearing capacities with increasing anisotropy.

6.5. Failure Analysis

Stress distributions presented in the previous section will be used here to investigate the failure of the bedded rock in a plate bearing test.

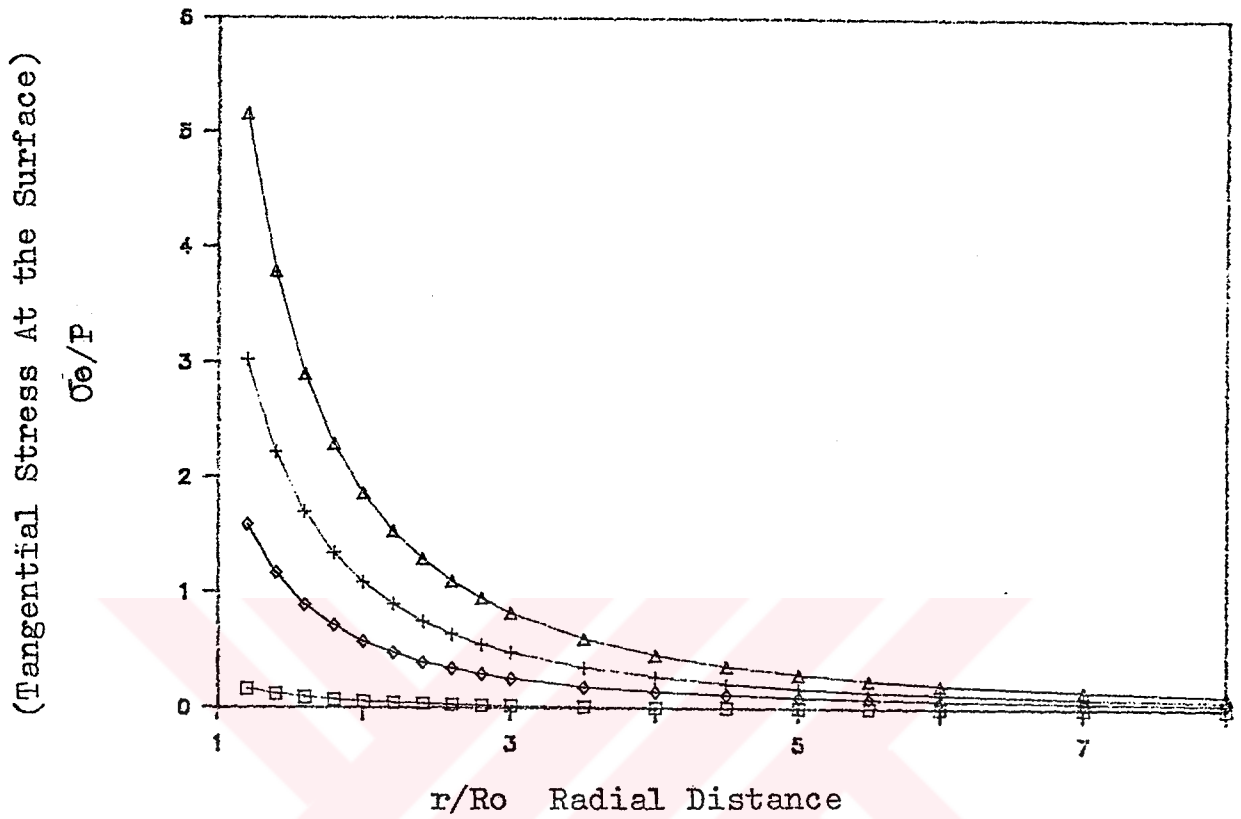
It has been stated before that failure possibly starts as radial cracking the edge of the loaded area. As the crack which develops perpendicular to the radial tensile stress at the edge, propagates into the rock, another failure process at a point along the Z-axis is usually in progress due to the stress difference between σ_z and $\sigma_r = \sigma_\theta$. This failure is a compressive Mohr-Coulomb type failure, and it has been discussed by Jaeger and



where ; + : For $s = 0.025$ m
 ◇ : For $s = 0.05$ m
 □ : For isotropic case

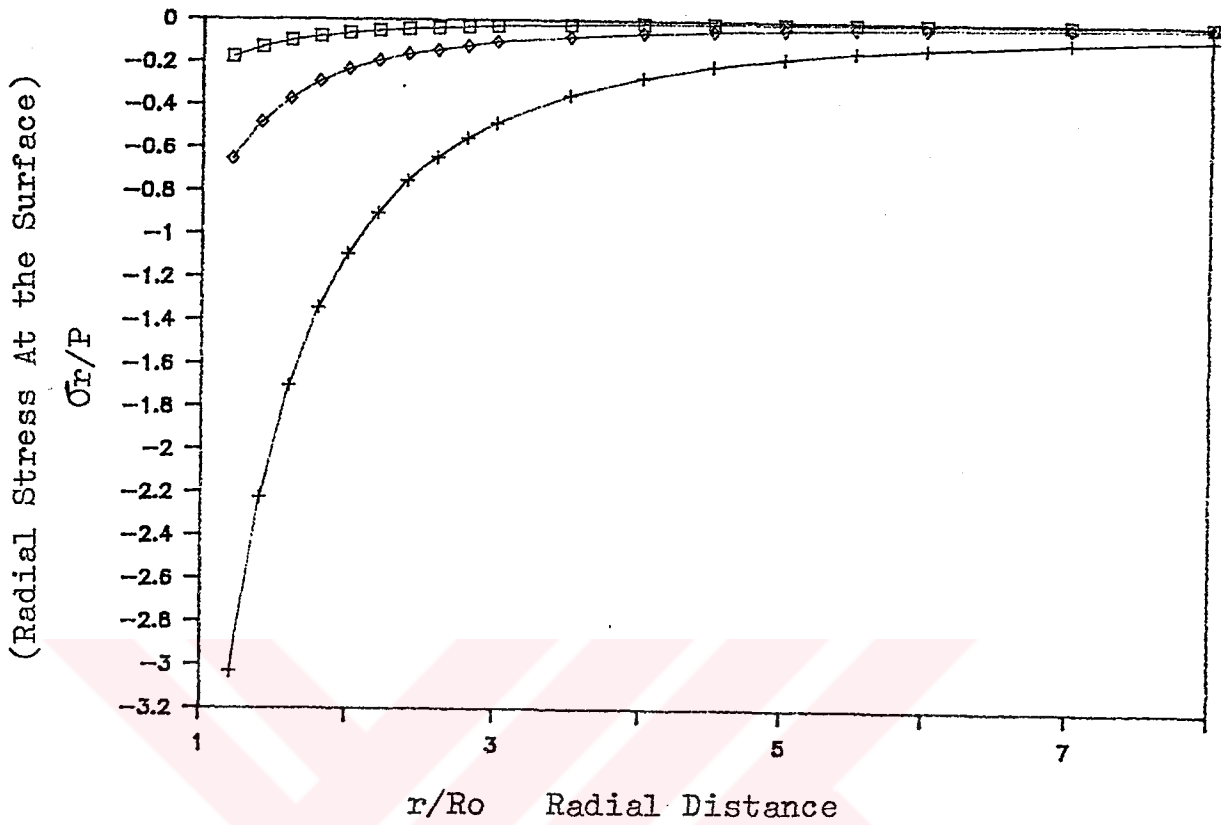
$$k_s/k_n = 3.5$$

- Figure 23a. Tangential stress distribution at the edge of the loading plate along a radial line at the surface: Different discontinuity spacing.



where ; Δ : For $k_s/k_n=10$
 $+$: For $k_s/k_n=3.5$
 \diamond : For $k_s/k_n=1.0$
 \square : For isotropic case
 $s=0.025$ m

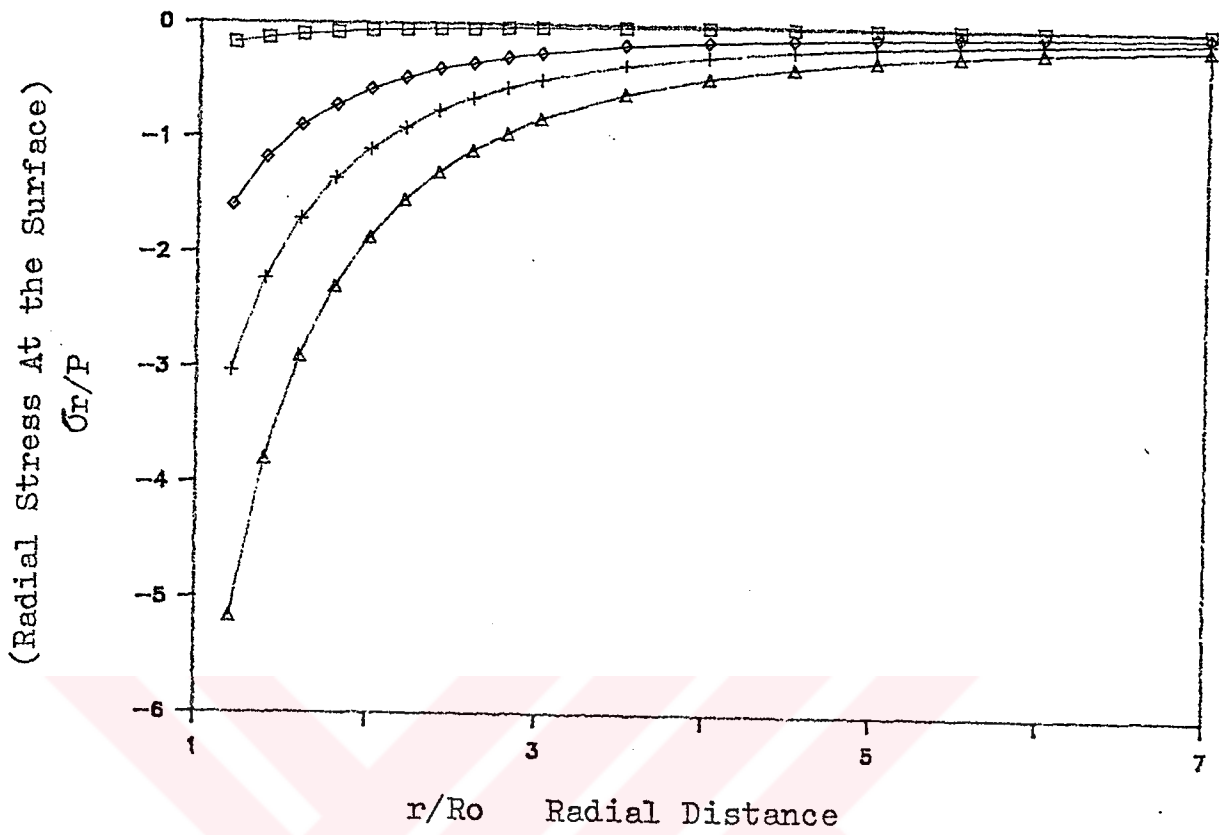
Figure 23b. Tangential stress distribution at the edge of the loading plate along a radial line at the surface : Different k_s/k_n ratios.



where ; $+$: For $s=0.025$ m
 \diamond : For $s=0.05$ m
 \square : For isotropic case

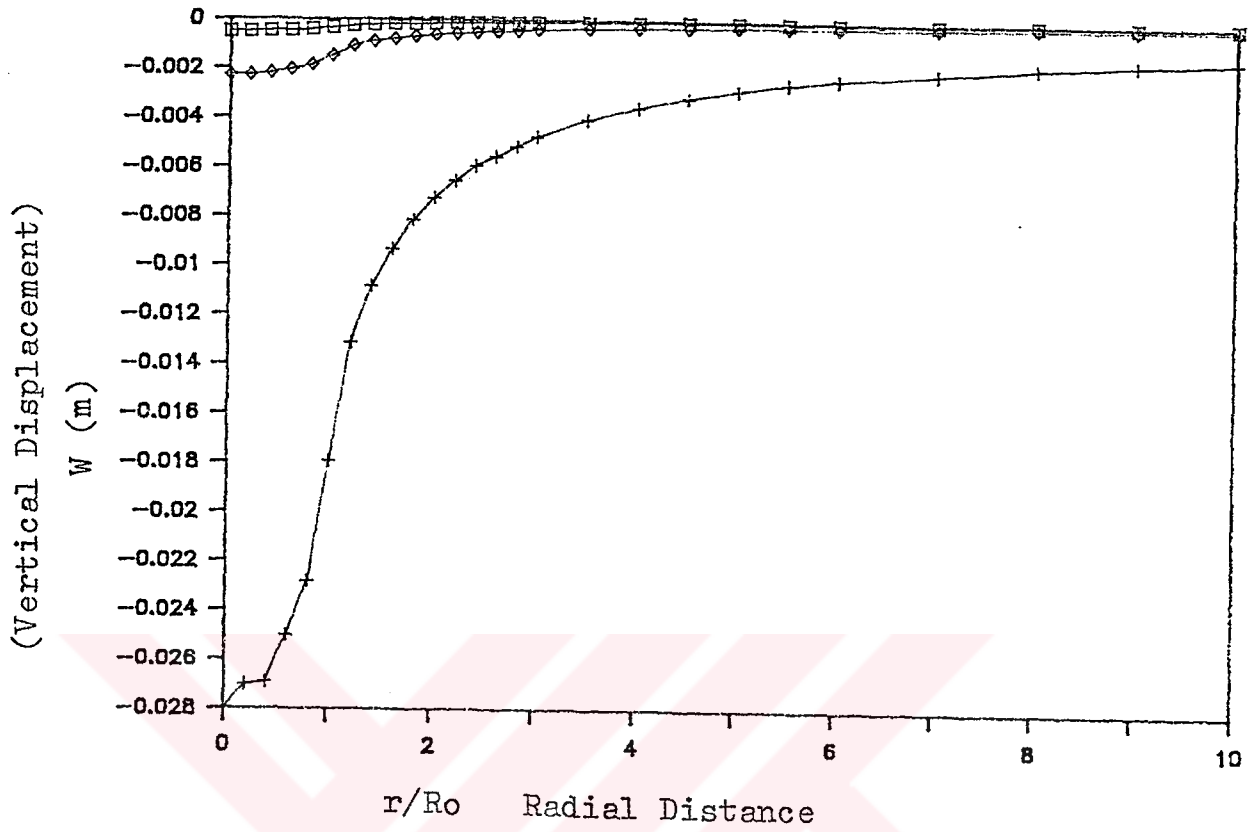
$$k_s/k_n = 3.5$$

Figure 24a. Radial stress distribution along the radial distance on surface : Different bedding space.



where ; Δ : For $k_s/k_n=10$
 + : For $k_s/k_n=3.5$
 \diamond : For $k_s/k_n=1.0$
 \square : For isotropic case

Figure 24b. Radial stress distribution along a radial line at the surface : Different k_s/k_n ratios.



where ;

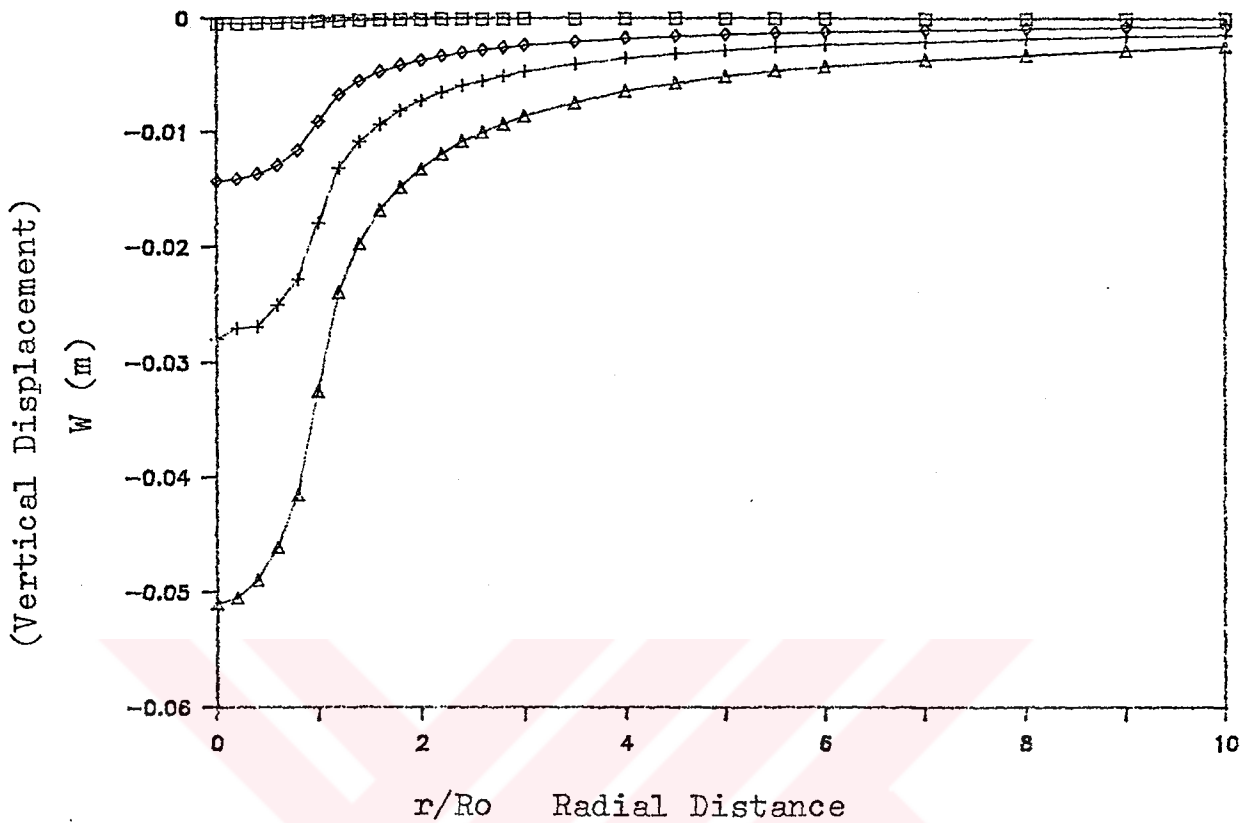
+ : For $s=0.025$ m

◇ : For $s=0.05$ m

□ : For isotropic case

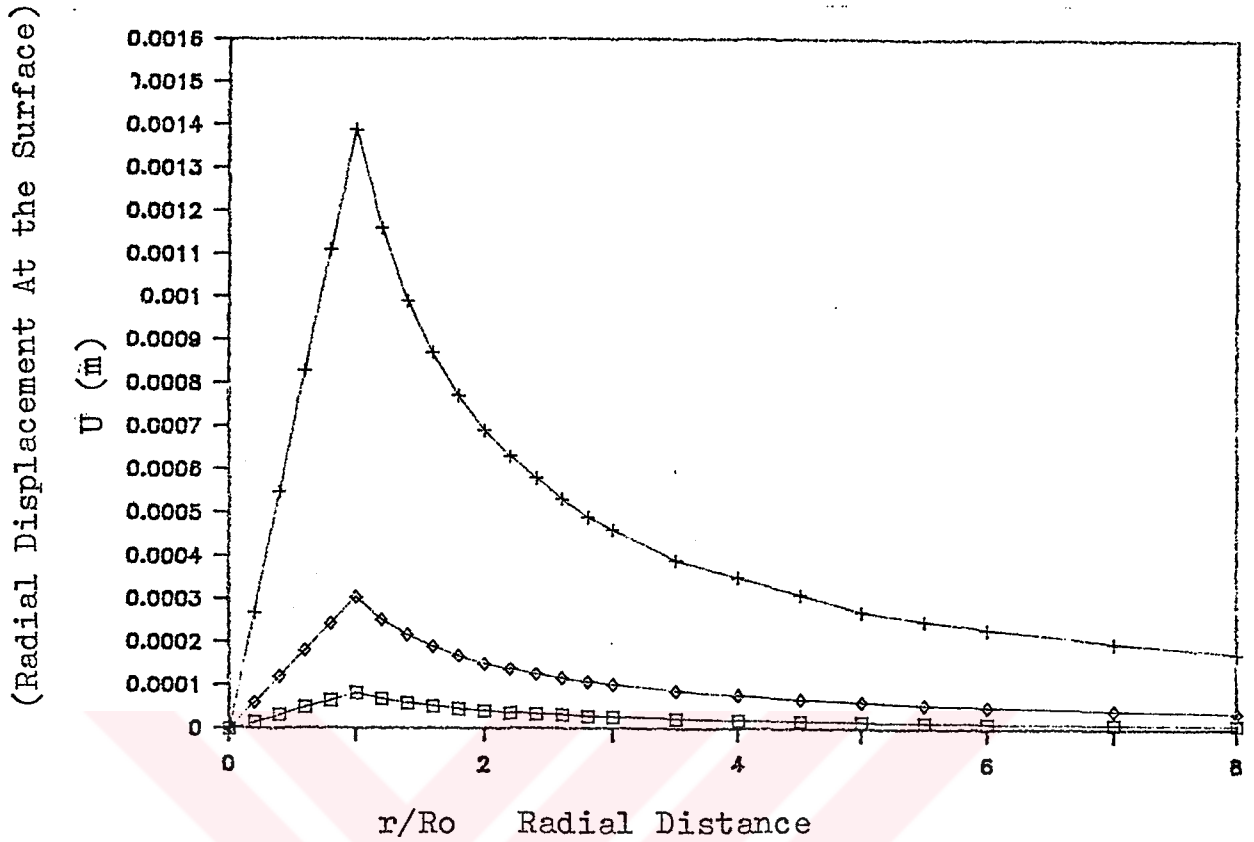
$$k_s/k_n = 3.5$$

Figure 25a. Vertical displacement along a radial line at the surface for different bed spacing.



Δ : For $k_s/k_n = 10$
 $+$: For $k_s/k_n = 3.5$
 \diamond : For $k_s/k_n = 1.0$
 \square : For isotropic case
 $s = 0.025$ m

Figure 25b. Vertical displacement along a radial line at the surface for different k_s/k_n ratios.

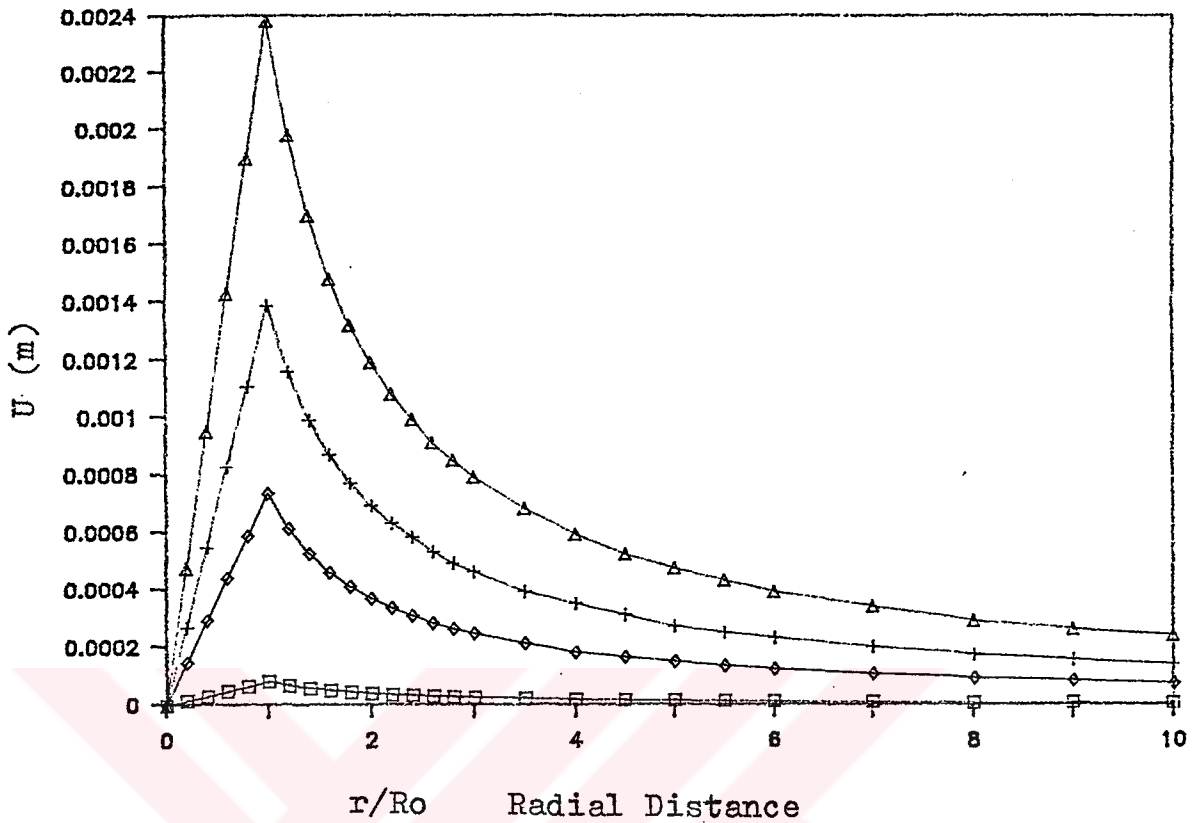


where; + : For $s=0.025$ m
 ◇ : For $s=0.05$ m
 □ : For isotropic case

$$k_s/k_n = 3.5$$

Figure 26a. Radial displacement distribution at the surface for different bed spacing.

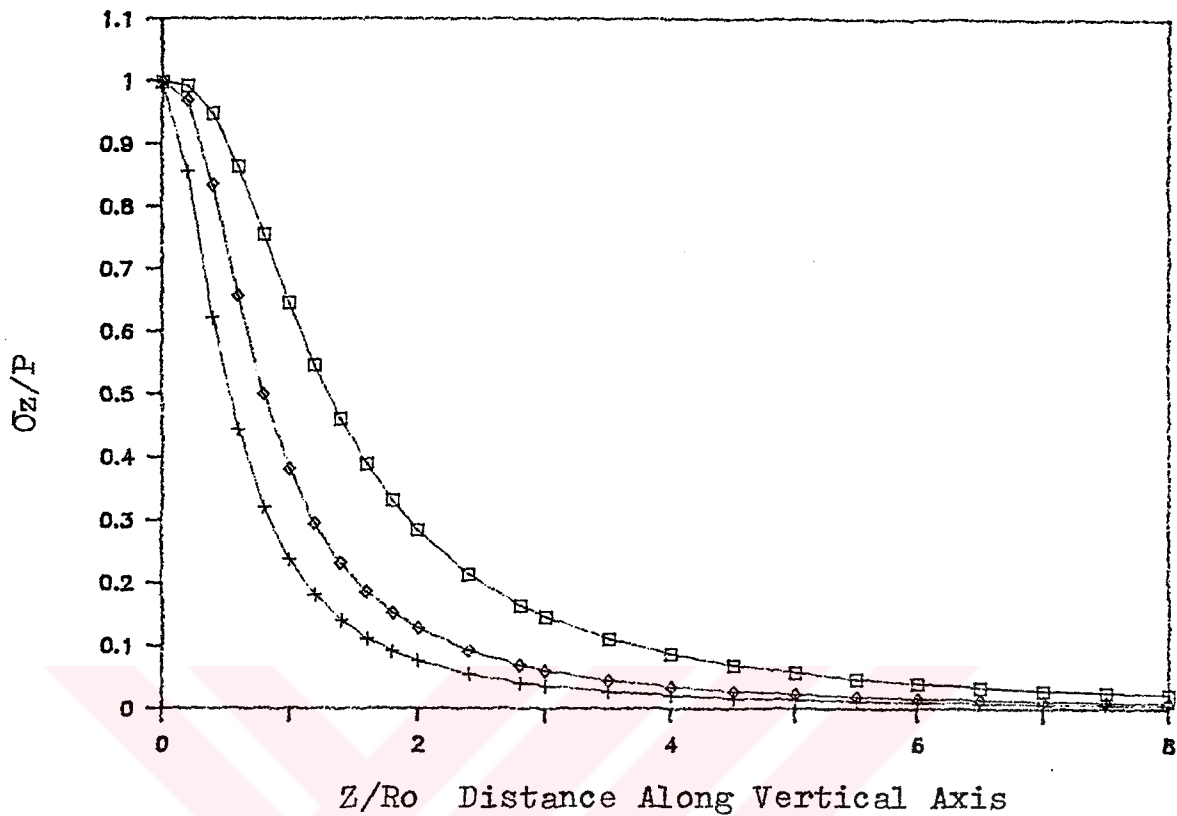
(Radial Displacement At the Surface)



where ; Δ : For $k_s/k_n = 10$
 $+$: For $k_s/k_n = 3.5$
 \diamond : For $k_s/k_n = 1.0$
 \square : For isotropic case
 $s = 0.025$ m

Figure 26b. Radial displacement distribution at the surface for different k_s/k_n ratios.

(Vertical Stress Along Vertical Axis)



where;

+ : For $s=0.025$ m

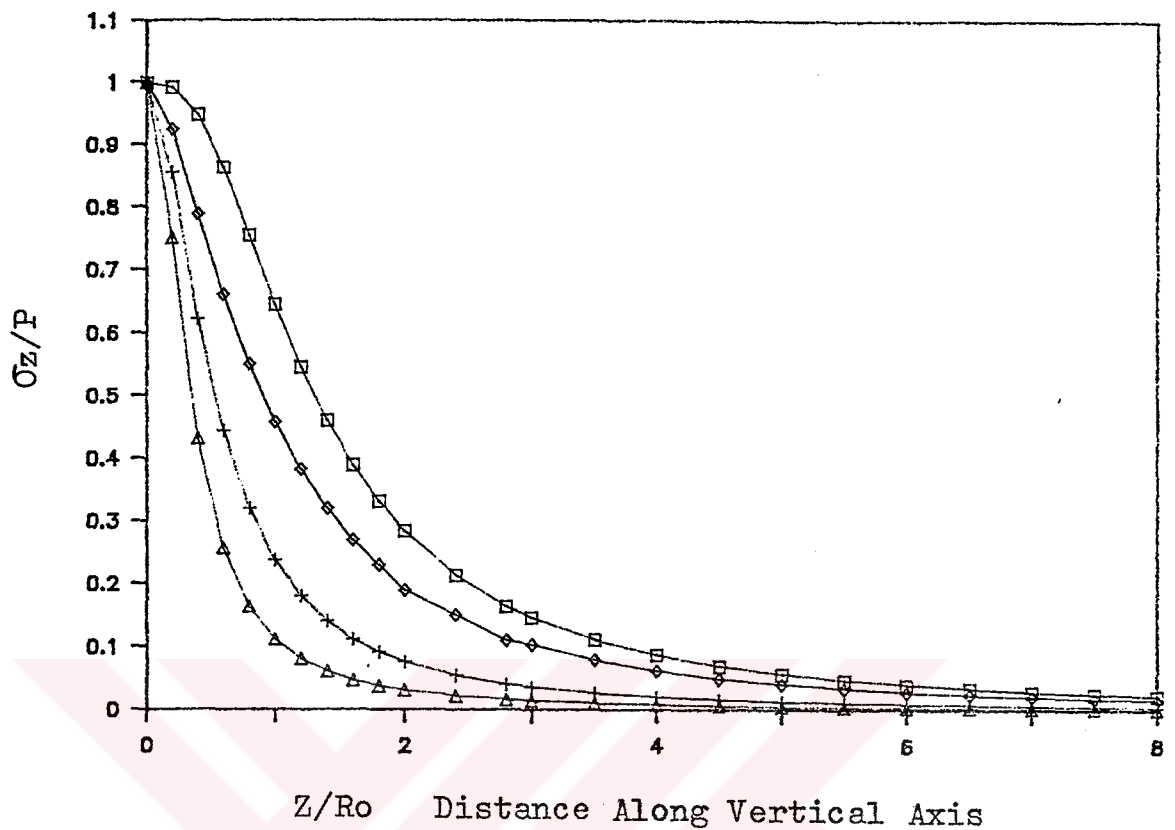
◇ : For $s=0.05$ m

□ : For isotropic case

$$k_s/k_n = 3.5$$

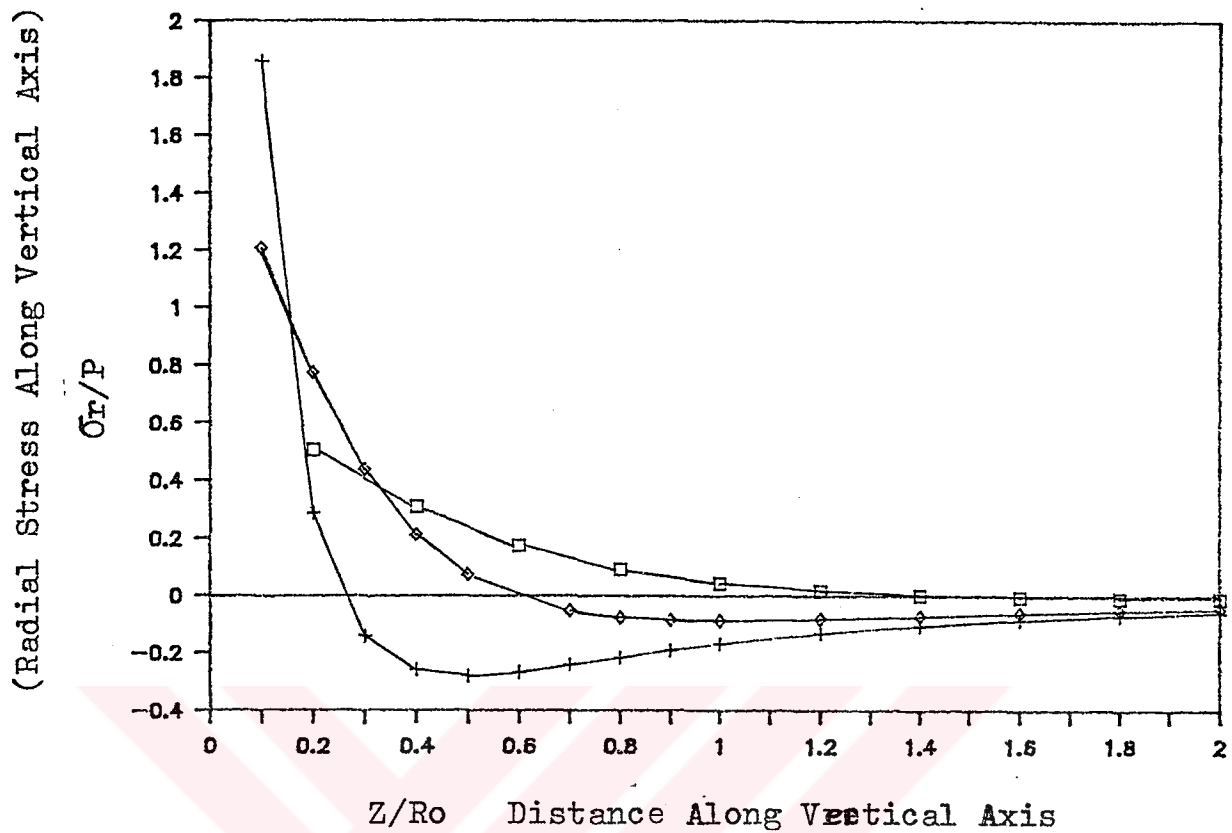
Figure 27a. Vertical stress distribution underneath the plate along $r=0$ line for different bed spacing.

(Vertical Stress Along Vertical Axis)



where ; Δ : For $k_s/k_n=10$
+ : For $k_s/k_n=3.5$
 \diamond : For $k_s/k_n=1.0$
 \square : For isotropic case
 $s=0.025$ m

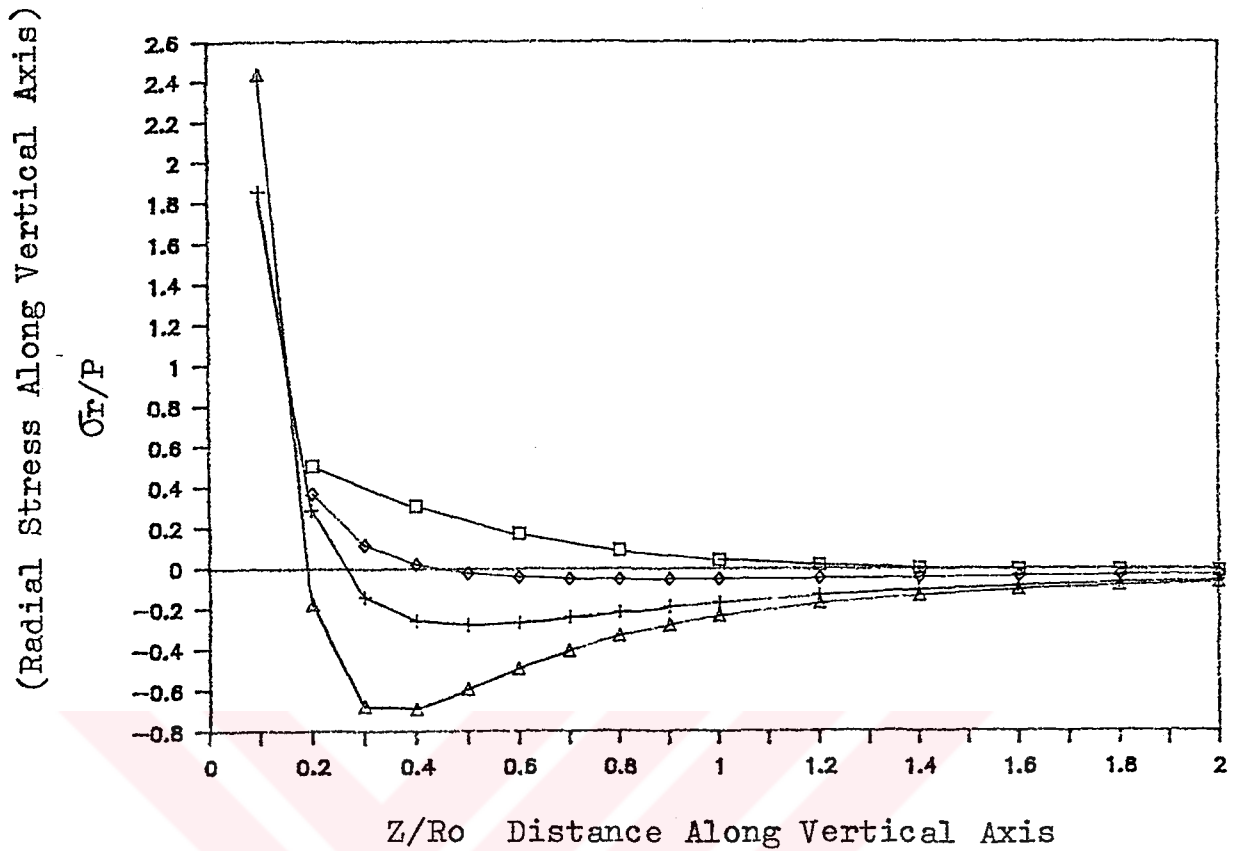
Figure 27b. Vertical stress distribution underneath the plate along $r=0$ for different k_s/k_n ratios.



where ; + : For $s=0.025$ m
 ◇ : For $s=0.05$ m
 □ : For isotropic case

$$k_s/k_n = 3.5$$

Figure 28a. Radial stress distribution along Z-axis beneath the center of the plate ($r=0$) for different bed spacing.



where ; Δ : For $k_s/k_n = 10$
 + : For $k_s/k_n = 3.5$
 ◇ : For $k_s/k_n = 1.0$
 □ : For isotropic case
 $s = 0.025$ m

Figure 28b. Radial stress distribution along Z-axis beneath the center of the plate for different k_s/k_n ratios.

Cook (1979) for the isotropic case. With increasing load, size of the region subjected to this type of failure increases, and broken rock in the region, if it is elastic brittle, due to dilatation and applies a side pressure to the surrounding rock. At the final failure stage, rock surrounding the dilatation zone fails under applied side pressure. This failure mechanism, in a simplified form, has been used in section 4 in order to develop the bearing capacity formulas in terms of known strength parameters.

Although the real bearing capacity is higher than the bearing pressure at which initiation of failure occurs along Z-axis a failure analysis based on this pressure level is still helpful in the sense that it provides us a lower bound estimate of bearing capacity, and it allows us to investigate the effects of discontinuity properties on the initiation of bearing capacity failures with such an investigation, variation of critical depth, Z_{cr} , at which the failure is initiated, can also be studied for different discontinuity parameters.

6.5.1. Failure Analysis For Isotropic Rock Under a Circular Loading Area

General approach used here is given by Jaeger and Cook (1979). The stresses parallel and radial to the symmetry (Z-axis) are expressed in the following form;

$$\sigma_z = P \cdot (1 - b^3) \quad (6.8)$$

$$\sigma_r = \sigma_\theta = P \cdot ((1 + 2\nu) + b^3 - 2 \cdot (1 + \nu)b) / 2$$

where; $b = Z / (R_o + Z^2)^{1/2}$, since $\sigma_r = \sigma_\theta$ and σ_z are principal stresses along Z-axis, Mohr-Coulomb failure criterion using these principal stresses :

$$\sigma_z = C_o + q \cdot \sigma_r \quad (6.9)$$

then, the bearing pressure p_{cr} at the initiation of failure is;

$$P_{cr} = 2 \cdot C_o / (2 \cdot (1 - b^3) - q \cdot (1 + 2\nu) - q \cdot b^3 + 2 \cdot q \cdot (1 + \nu)b) \quad (6.10)$$

Making the denominator a maximum by a differentiation ($\partial/\partial z$) with respect to Z gives the critical value of b, and thus Z_{cr} which makes applied bearing pressure P a minimum. This is the smallest pressure at which the failure is initiated at a depth $Z = Z_{cr}$ along Z-axis. Following expression found as explained

$$b_{cr} = (2 \cdot (1 + \nu)q / 3 \cdot (q + 2))^{1/2} \quad (6.11)$$

makes the minimum value of P fall in the range from one to two times the uniaxial compressive strength. For most rocks, maximum value of b is likely to range between a half and unity, indicating that failure occurs at a depth of the order of the radius of the bearing plate.

6.5.2. Failure Analysis For Cross-Anisotropic Rock Under a Circular Loading Area

The same approaches described for isotropic case will be adopted into the formulas for cross-anisotropic rock in the Appendix A.

Procedure for determination of critical depth will be illustrated for $B^2=0$ case. Then the results showing Z_{cr} for the other case ($B^2 > 0$) will be given together with $B^2 = 0$ case. $B^2 < 0$ case is not considered here, since this is not practically applicable for our bedded rock.

Stresses along Z-axis are :

$$\begin{aligned}\sigma_r = \sigma_\theta &= P. (S_5 - S_5 (Z / (Z^2 + \alpha^2)^{1/2}) - (S_6 / \alpha^3) (Z / (Z^2 + \alpha^2)^{3/2})) \\ \sigma_z &= P. (1 - (Z / (Z^2 + \alpha^2)^{1/2}) + (1 / \alpha^2) (Z / ((Z^2 + \alpha^2)^{3/2}))\end{aligned}\tag{6.12}$$

where B , S_5 , S_6 , and α depend on the elastic properties of the half space and they are defined in the Appendix A. It has been stated before that all these constants are expressed in terms of discontinuity properties k_s , k_n , s , and rock properties ν , and E in the computer program using the equivalent isotropic medium approach.

Expressing equation (6.12) in a more compact form by using K_1 , K_2 which are functions of Z

$$\begin{aligned}\sigma_r = \sigma_\theta &= P. K_1(Z) \\ \sigma_z &= P. K_2(Z)\end{aligned}\tag{6.13}$$

Application of Mohr-Coulomb failure criterion in equation (6.9) gives ;

$$P=P/C_0=1/(K_2-q \cdot K_1) \quad (6.14)$$

Differentiating the denominator with respect to Z again to get the minimum P that initiates failure

$$\frac{P}{Z} = (q \cdot S_5 - 1) \frac{\partial}{\partial Z} \left(\frac{Z}{(Z^2 + \frac{-2}{\alpha})^{1/2}} \right) + \left(\frac{S_6 \cdot q}{\alpha^3} + \frac{1}{\alpha^2} \right) \frac{\partial}{\partial Z} \left(\frac{Z}{(Z^2 + \frac{-2}{\alpha})^{3/2}} \right) \quad (6.15)$$

This yields the following quadratic equation in Z :

$$Z^4 - \frac{m_1}{m_3} Z^2 + \frac{m_1 + m_2}{m_3 \cdot \alpha^4} = 0 \quad (6.16)$$

where ;

$$m_1 = q \cdot S_5 - 1$$

$$m_2 = (q \cdot S_6 / \alpha^3) + (1 / \alpha^2)$$

$$m_3 = m_1 (1 + 2 / \alpha^2) + m_2 \cdot ((1 / \alpha^2) - 2)$$

In this equation, if $(m_1 + m_2) / (m_3 \cdot \alpha^4) = 0$ then the repeated roots are :

$$Z = 0 \quad , \quad Z = \pm (m_1 / m_3)^{1/2}$$

In general , the roots for $\beta^2 = 0$ are :

$$Z = \left[\frac{((m_1 / m_3) \pm ((m_1 / m_3)^2 - 4 \cdot (m_1 + m_2) / (\alpha^4 \cdot m_3))^{1/2})}{2} \right]^{1/2}$$

(6.17)

For $B^2 > 0$;

$$Z^2 = \left[\begin{array}{c} \frac{(n_3)^{2/3}}{\rho^{4/3} \cdot \rho^2} - \frac{(n_2)^{2/3}}{\rho^{4/3} \cdot \phi^2} \\ \frac{(n_2)^{2/3}}{\rho^{4/3}} - \frac{(n_3)^{2/3}}{\phi^{4/3}} \end{array} \right]$$

(6.17)

where ;

$$n_1 = ((\rho/(\rho-\phi)) + G_5 \cdot q) - ((\phi/(\rho-\phi)) + G_6 \cdot q)$$

$$n_2 = ((\phi/(\rho-\phi)) + (G_6 \cdot q))$$

$$n_3 = ((\rho/(\rho-\phi)) + G_5 \cdot q)$$

Note that only the positive values of Z are chosen as Z_{cr} since negative values are not physically applicable for this problem.

By substituting this critical depth, Z_{cr} , into the general expression for P, bearing pressure at which failure is initiated can be found in terms of the compressive strength, C_0 , constants m_1 , m_2 , m_3 , and α^4 in equation (6.17) and constants in equation (6.18) depend on the discontinuity properties (k_n , k_s , and s) elastic properties of the rock, and triaxial factor q for the rock. Therefore, effect of all these properties on the critical depth can be studied by using these equations (6.16), (6.17).

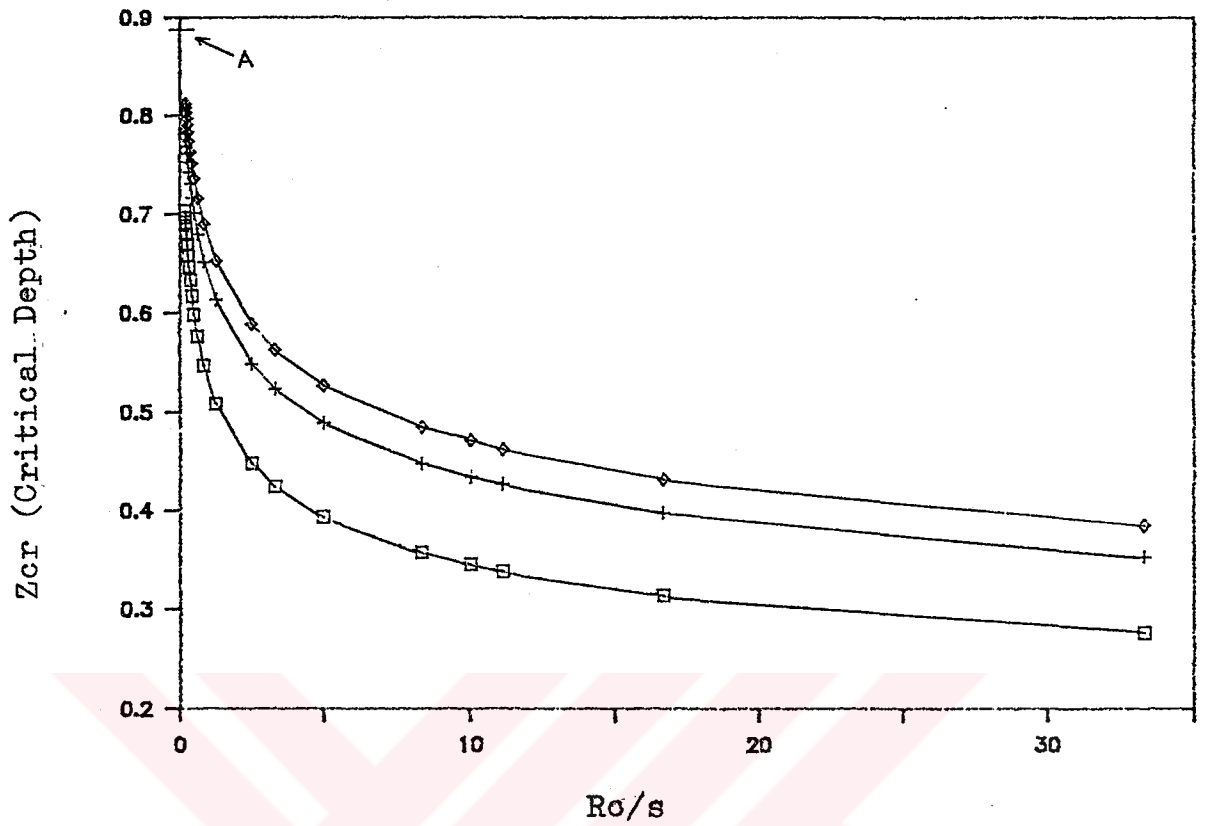
6.6. Effect of Spacing on Critical Depth

Curves showing the effect of spacing on the critical depth at which the failure initiates are given in Figure 29. As seen in Figure 29 with increasing bed spacing, the critical depth is positioned deeper along the Z-axis, and as spacing (s) goes to infinity it reaches a value which is equal to the value for isotropic case. Curves show that if the size or width of the loaded area is increased with respect to the spacing, or if beds are thin and very close closely spaced critical depth approaches to the surface, and it is almost half of the critical depth for isotropic case. With a decreasing k_s/k_n ratio, i.e. normal stiffness of the layers is lower and they are more open effect of spacing, and size effect are more pronounced.

In addition to the Z_{cr} values, failure loads in terms of compressive strength are calculated at these critical depths, and results, are plotted in Figure 30. Generally, p/Co ratios are smaller than unity for small spacings, and they approach the value for isotropic case for very large spacing or smaller plate sizes. For very closely spaced bedding or very large plate sizes compared to spacing, \bar{P} values tend to constant values. For increasing k_s/k_n ratios size effect becomes more pronounced, and values to which \bar{P} tends for very close spacing decrease significantly. Among these curves, the one which represents the field testing condition is the lowermost curve with $k_s/k_n=3.5$. In this case, a reduction of three times is predicted in

the failure initiation pressure of thinly bedded or laminated rock compared to approximately isotropic rock with very widely spaced beds. Therefore these results show that bearing capacity values for thinly bedded rock can be much smaller than bearing capacities for rocks containing widely spaced beds. Predictions based on the laboratory compressive strength tests might be misleading and bed spacing or discontinuity spacing must be taken into account in the determination of field bearing capacity values.

In-situ bearing capacity of clay banded limestone is equal to about 8.29 MPa, average value, and it's compressive strength is determined as about 19.43 MPa. Then, P/C_o ratio for this rock is 0.43 . This result and results obtained by the theoretical approach considering the size effect are close to each other. Therefore, emprical approaches given in chapter 4 are not always applicable to all cases, especially for rocks with open and closely spaced discontinuities, and formulations to predict the in-situ bearing capacities must also include properties of bedding and other discontinuities.



where ; \square : For $k_s/k_n=3.5$

$+$: For $k_s/k_n=1.0$

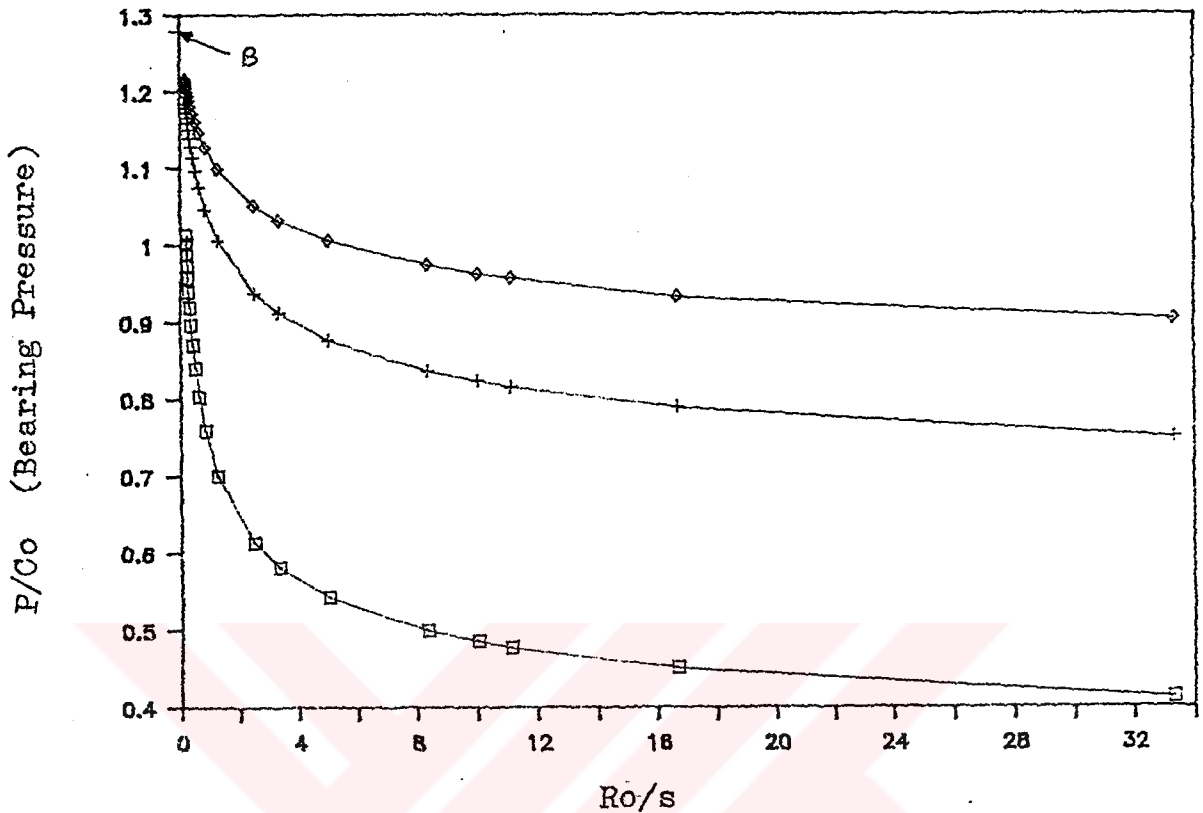
\diamond : For $k_s/k_n=0.5$

R_o : Radius of plate (m)

s : Bed spacing (m)

Point A : Critical depth for isotropic rock mass

Figure 29. Effect of spacing, plate size, and k_s/k_n ratios on the critical depth.



where; : For $k_s/k_n = 3.5$
 : For $k_s/k_n = 1.0$
 : For $k_s/k_n = 0.5$

R_o : Radius of plate (m)

s : Bedding spacing (m)

Point B : P/Co value for isotropic rock mass

Figure 30. Effect of spacing, plate size, and k_s/k_n ratios on the P/Co, i.e. the bearing pressure at which failure initiates along the vertical axis.

7. CONCLUSIONS

The major conclusions derived from this study are summarized as follows.

The rock mass encountered at Simav underground mine test site, is sedimentary in origin and they are classified as poor and very poor rock according to RMR and Q systems.

Plate loading test results show that bearing capacity of major strata around the seams, are determined as 9.14 MPa for colemanite, 4.18 MPa for ulexite, 9.26 MPa for clay banded limestone.

It was observed that ulexite and colemanite had punching type failure mechanisms. Clay banded limestone had brittle, and sometimes punching type failure mechanism which depended on the thickness of the stratum.

It was found that when the plate size increased bearing capacity of the same rock decreased and the magnitude of this decrease depended on the rock type.

In order to calculate in-situ bearing capacity from laboratory test results, several approaches, given in Foundation Engineering, were used. It was found that these approaches gived about 3-6 times higher values with respect to field results.

Mohr-Coulomb and Hoek-Brown's theoretical approaches were also used to estimate field bearing capacity from laboratory results and it was observed that they gived similar results with field data.

Several base plates to be used under the hydraulic props were suggested to prevent bearing capacity failure under the props. Failure loads for these plate size were determined. Consequently plate which had 25 cm in diameter was found to be safe in general for use on strata around the seams. However, a base plate with 35 cm diameter was also suggested for use in extreme cases of weaker strata in Simav Mine.

In order to investigate the failure mechanism under the base plate, stress distribution under the plate was calculated with a specially prepared computer program, and it was observed that stiffness of bedding planes and distance between them dramatically effected the failure loads and failure initiation depths, critical depth.

LIST OF REFERENCES

- Afrouz, A. 1975. "Yield and Bearing Capacity of Coal Mine Floors.", Int. J. Rock Mech. Min. Sci. 12, pp241-253
- Barry, A. J. & Nair, O. 1970. "In-situ Tests of Bearing Capacity of Roof and Floor in Selected Bituminous Coal Mines." A Progress Report in Longwall Mining. USBM RI 7406.
- Bieniawski, Z. T. 1980. Practical Rock Mechanics, Lecture Notes, The College of Earth and Mineral Sciences, The Pennsylvania State University.
- Bieniawski, Z. T. 1987. Strata Control in Mineral Engineering A. A. Balkema/Rotterdam 1987.
- Brinch, H. J. 1970. "Bearing Capacity." Danish Geotech. Inst. Bull. 28:pp5-11
- Brown, E. T. 1981. Rock Characterization Testing & Monitoring ISRM Suggested Methods. Pergamon Press.
- Dulaney, R. 1960. The Structural Strength of Coal Mine Floors. M.S. thesis Virginia Polytech. Inst. Blacksburg, VA.
- Gerrard, C. M. & Harrison, W. J. 1970. Circular Loads Applied to a Cross Anisotropic Half Space. Tech. Paper No:8 of the Division of Applied Geomech. CSIRO, Australia.
- Hoek, E. & Brown, E. T. 1980. Underground Excavations in Rock The Inst. of Min. and Metal. London.
- Goodman, R. 1980. Introduction to Rock Mechanics. Mc Graw Hill, New York.
- Jenkins, J. 1957-1958. "The Bearing Capacity of Mine Floors" Colliery Guardian, 195 pp 397-400

- Jeager, J.C. & Cook, N.G. 1971. Fundamentals of Rock Mechanics
Chapman and Hall Ltd. London.
- Kulhawy, F.H. 1978. "Geomechanical Model for Rock Foundation
Settlement" ASCE J. Geotech. Eng. Div. Feb. GT 2.
- Lee, R. 1961. "Testing Mine Floors." Colliery Engng. 38,
pp 255-261
- Meyerhof, G. 1955. "Influence of Roughness of Base and
Groundwater Conditions on the Ultimate Bearing
capacity of Foundations." Geotech. 5, pp 227-242
- Pasamehmetoglu, G.A. et.al. 1987. Second Progress Report
about Simav Underground Mine, Agudos 86.03.05.01.06
M.E.T.U. , Ankara.
- Skempton, A. 1942. "An Investigation of the Bearing Capacity
of Soft Clay Soil." J. Inst. Civil Eng. V18 p307
- Terzaghi, K. 1943. Theoretical Soil Mechanics . New York,
Wiley
- Terzaghi, K. & Peck, R. 1966. Soil Mechanics in Engineering
Practice. New York, Wiley

APPENDIX A

CIRCULAR LOADS APPLIED TO A
CROSS ANISOTROPIC HALF SPACE

by

C.M. Gerrard

W.J. Harrison

I. Notations

- R_0 Loaded radius.
- r, θ, z Cylindrical coordinates expressed in units of the loaded radius.
- U, W, V Displacement in the respective coordinate directions.
- $\sigma_r, \sigma_z, \sigma_\theta$ Direct stresses.
- a, b, c, d, f ... Components of the elasticity tensor.
- E_h Modulus of elasticity in the horizontal direction.
- E_v Modulus of elasticity in the vertical direction.
- ν_h Poisson's ratio (effect of horizontal strain on complementary horizontal strain).
- ν_{vh} Poisson's ratio (effect of vertical strain on horizontal strain).
- ν_{hv} Poisson's ratio (effect of horizontal strain on vertical strain).
- E Modulus of elasticity (isotropic material).
..... Poisson's ratio (isotropic material).
- P Uniform vertical pressure.

II. The Interrelationship Between the Elastic Constants

$$a = E_h \cdot (1 - \nu_{hv} \cdot \nu_{vh}) \cdot (1 + \nu_h)^{-1} \cdot (1 - \nu_h - 2 \cdot \nu_{hv} \cdot \nu_{vh})^{-1}$$

$$b = E_h \cdot (\nu_h + \nu_{hv} \cdot \nu_{vh}) \cdot (1 + \nu_h)^{-1} \cdot (1 - \nu_h - 2 \cdot \nu_{hv} \cdot \nu_{vh})^{-1}$$

$$c = E_h \cdot \nu_{vh} \cdot (1 - \nu_h - 2 \cdot \nu_{hv} \cdot \nu_{vh})^{-1}$$

$$d = E_h \cdot \nu_{vh} \cdot (1 - \nu_h) \cdot (\nu_{hv})^{-1} \cdot (1 - \nu_h - 2 \cdot \nu_{hv} \cdot \nu_{vh})^{-1}$$

III. Derived Elastic Quantities

$$\alpha^2 = (a \cdot d - c^2 - c \cdot f + f \cdot (a \cdot d)^{1/2}) / (2 \cdot f \cdot d)$$

$$\beta^2 = (a \cdot d - c^2 - c \cdot f - f \cdot (a \cdot d)^{1/2}) / (2 \cdot f \cdot d)$$

$$\emptyset = \alpha - \beta$$

$$\rho = \alpha + \beta$$

IV. Values of Coefficients G_n , and S_n

$$G1 = (2 \cdot c + f) \cdot \rho \cdot \emptyset \cdot f^{-1} \cdot (\rho - \emptyset)^{-1} \cdot (c + d \cdot \emptyset^2)^{-1}$$

$$G2 = (2 \cdot c + f) \cdot \rho \cdot \emptyset \cdot f^{-1} \cdot (\rho - \emptyset)^{-1} \cdot (c + d \cdot \rho^2)^{-1}$$

$$G3 = \rho \cdot (2 \cdot d \cdot \emptyset^2 - f) \cdot (\rho - \emptyset)^{-1} \cdot (c + d \cdot \emptyset^2)^{-1}$$

$$G4 = \emptyset \cdot (2 \cdot d \cdot \rho^2 - f) \cdot f^{-1} \cdot (\rho - \emptyset)^{-1} \cdot (c + d \cdot \rho^2)^{-1}$$

$$G5 = a \cdot G3 - c \cdot \emptyset \cdot G1$$

$$G6 = a \cdot G4 - c \cdot \rho \cdot G2$$

$$G7 = b \cdot G3 - c \cdot \emptyset \cdot G1$$

$$G8 = b.G4 - c.\beta.G2$$

$$G9 = \beta.\phi.(\beta-\phi)^{-1}$$

$$S1 = (2.c+f).2.d.\alpha^3.f^{-1}.(c+d.\alpha^2)^{-2}$$

$$S2 = (2.c+f).\alpha^2.f^{-1}.(c+d.\alpha^2)^{-1}$$

$$S3 = ((2.c+3.f-2.d.\alpha^2).d.\alpha^2+c.f).f^{-1}.(c+d.\alpha^2)^{-2}$$

$$S4 = (2.d.\alpha^2-f).a.f^{-1}.(c+d.\alpha^2)^{-1}$$

$$S5 = a.S3+c.S9$$

$$S6 = a.S4-c.\alpha.S2$$

$$S7 = b.S3+c.S9$$

$$S8 = b.S4-c.\alpha.S2$$

$$S9 = (2.c+f).\alpha^2.(d.\alpha^2-c).f^{-1}.(c+d.\alpha^2)^{-2}$$

V. When $r=0$ the Integrals Are Given By

$$I200(\xi) = (\xi^2+1)^{1/2} - \xi$$

$$I202(\xi) = 1 - \xi.(\xi^2+1)^{-1/2}$$

$$I204(\xi) = (\xi^2+1)^{-3/2}$$

$$I220(\xi) = I222(\xi) = I224(\xi) = 0$$

$$r^{-1}.I220(\xi) = I202(\xi)/2$$

$$r^{-1}.I222(\xi) = I204(\xi)/2$$

VI. When $Z=0$ the Relevant Integrals Are Given By

$$I_{200}(0) = \begin{cases} {}_2F_1(1/2, -1/2; 1; r^2) & \text{for } r < 1 \\ 2^{-1} & \text{for } r = 1 \\ (2 \cdot r)^{-1} \cdot {}_2F_1(1/2, 1/2; 2; r^{-2}) & \text{for } r > 1 \end{cases}$$

$$I_{202}(0) = \begin{cases} 1 & \text{for } r < 1 \\ 2^{-1} & \text{for } r = 1 \\ 0 & \text{for } r > 1 \end{cases}$$

$$I_{220}(0) = \begin{cases} 2^{-1} \cdot r & \text{for } r < 1 \\ 2^{-1} & \text{for } r = 1 \\ (2 \cdot r)^{-1} & \text{for } r > 1 \end{cases}$$

VII. Stresses and Displacements Under the Loading Plate

It can be seen that the sign of β^2 is not restricted by the strain energy conditions. Hence, for each loading condition, separate cases are considered as follows

- A. Cross-anisotropic ; α^2 positive, β^2 positive
- B. Cross-anisotropic ; α^2 positive, β^2 zero
- C. Isotropic (This is a special case of B ($\beta^2=0$) in which $\nu=1$)

A. Cross-anisotropic ; β^2 Positive, Solutions of Stresses and Displacements.

$$W = P.Ro.(-G1.I200(\emptyset Z)+G2.I200(\rho Z))$$

$$U = P.Ro.(-G3.I220(\emptyset Z)+G4.I220(\rho Z))$$

$$M = r^{-1}.(G3.I220(\emptyset Z)-G4.I220(\rho Z))$$

$$\sigma_r = P.(-G5.I202(\emptyset Z)+G6.I202(\rho Z)+(a-b).M)$$

$$\sigma_\theta = P.(-G7.I202(\emptyset Z)+G8.I202(\rho Z)-(a-b).M)$$

$$\sigma_z = P.G9.(\emptyset^{-1}.I202(\emptyset Z)-\rho^{-1}.I202(\rho Z))$$

B. Cross-anisotropic ; β^2 Zero, Solutions of Stresses and Displacements

$$W = P.Ro.(-S1.I200(\alpha Z)-S2.Z.I202(\alpha Z))$$

$$U = P.Ro.(S3.I220(\alpha Z)-S4.Z.I222(\alpha Z))$$

$$N = r^{-1}.(S3.I220(\alpha Z)-S4.Z.I222(\alpha Z))$$

$$\sigma_r = P.(S5.I202(\alpha Z)-S6.Z.I204(\alpha Z)-(a-b).N)$$

$$\sigma_\theta = P.(S7.I202(\alpha Z)-S8.Z.I204(\alpha Z)+(a-b).N)$$

$$\sigma_z = P.(I202(\alpha Z)+\alpha.Z.I204(\alpha Z))$$

C. Isotropic Case

The stresses, displacements are as for the case of cross-anisotropic; β^2 zero but with the following simplifications

$$S1 = 2 \cdot (1 - \nu^2) \cdot E^{-1}$$

$$S2 = (1 + \nu) \cdot E^{-1}$$

$$S3 = (1 + \nu) \cdot (1 - 2 \cdot \nu) \cdot E^{-1}$$

$$S4 = (1 + \nu) \cdot E^{-1}$$

$$S5 = 1$$

$$S6 = 1$$

$$S7 = 1$$

$$S8 = 0$$

$$S9 = (1 + \nu) \cdot (1 - 2 \cdot \nu) \cdot E^{-1}$$

$$\alpha = 1$$

$$f = E \cdot (1 + \nu)^{-1}$$